

Modeling recession flow and tracking the fate and transport of nitrate and water from  
hillslope to stream

Raymond Mark Lee

Dissertation submitted to the faculty of the Virginia Polytechnic Institute and State  
University in partial fulfillment of the requirements for the degree of

Doctor of Philosophy

In

Department of Forest Resources and Environmental Conservation

Kevin J. McGuire, Co-Chair

Brian D. Strahm, Co-Chair

Jennifer D. Knoepp

Ryan D. Stewart

Durelle T. Scott

October 19, 2018

Blacksburg, VA

Keywords: hillslope hydrology; nitrate transport; nutrient cycling; tracer experiment

Copyright © 2018 Raymond M. Lee

# Modeling recession flow and tracking the fate and transport of nitrate and water from hillslope to stream

Raymond Mark Lee

## ABSTRACT

Nitrate ( $\text{NO}_3^-$ ) export can vary widely among forested watersheds with similar nitrogen loading, geology, and vegetation, which suggests the importance of understanding differing internal retention mechanisms. Transport should be studied at the hillslope scale because the hillslope is the smallest unit with spatial and temporal resolution to reflect many relevant  $\text{NO}_3^-$  retention and transport (flow-generation) processes, and headwater forested watersheds are largely comprised of sections of hillslopes. I conducted two experiments to elucidate subsurface flow dynamics and  $\text{NO}_3^-$  transport and retention mechanisms on a constructed experimental hillslope model.

In the first experiment, I tested whether decadal pedogenetic changes in soil properties in the experimental hillslope used by Hewlett and Hibbert (1963) would lead to changes in recession flow. I repeated (twice) their seminal experiment, whose results led to the development of the Variable Source Area paradigm, by also saturating, covering, and allowing the experimental hillslope to drain until it no longer yielded water. In the historical experiment there was fast drainage for 1.5 d, followed by slow drainage for ~140 d, which led the authors to conclude that recession flow in unsaturated soil could sustain baseflow throughout droughts. This long, slow drainage period was not reproduced in my experiments. Shapes of the drainage curves in my experiments were similar to the historical curve, but slow drainage was truncated, ending after 17 and 12 d, due likely to a leak in the boundary conditions, rather than to pedogenetic changes since the historical experiment. Leakage to bedrock, analogous to the leak in the hillslope model, is a commonly observed phenomenon and this study highlights how that can reduce drainage duration and the contribution of moisture from soils to support baseflow.

In the second experiment, I tested whether movement of  $\text{NO}_3^-$ , which is considered a mobile ion, would be delayed relative to movement of water through a hillslope. I added concentrated pulses of  $^{15}\text{NO}_3^-$  and a conservative tracer ( $^2\text{H}_2\text{O}$ ) on the same experimental hillslope, which was devegetated and irrigated at hydrologic steady state. Retention of the  $^{15}\text{NO}_3^-$  tracer was high in the soil surface (0–10 cm) layer directly where the tracer was added. The portion of the  $^{15}\text{NO}_3^-$  tracer that passed through this surface layer was further retained/removed in deeper soil. The reduction in the peaks in  $\delta^{15}\text{N}$  breakthrough was an order of magnitude larger than in  $\delta^2\text{H}$  breakthrough at the outlet 5 m downslope of the tracer addition. The peaks in  $\delta^{15}\text{N}$  were also delayed relative to the peaks in  $\delta^2\text{H}$  by 1, 6, 9 and 18.5 d for slope distances of 0, 2, 4, and 5 m, respectively, from tracer addition to the outlet. The excess mass of  $^{15}\text{NO}_3^-$  recovered at the outlet was less than 3% of the original tracer mass injected. Nitrification and denitrification were estimated to be roughly 1:1 and were large fluxes relative to lateral transport into and out of the riparian zone. This tracer experiment shows that bedrock leakage, coupled with multiple retention/removal mechanisms can significantly delay export of added  $\text{NO}_3^-$  with implications of additional  $\text{NO}_3^-$  sink strength at the watershed scale.

# Modeling recession flow and tracking the fate and transport of nitrate and water from hillslope to stream

Raymond Mark Lee

## ABSTRACT (PUBLIC)

Nitrate ( $\text{NO}_3^-$ ) export can vary widely among forested watersheds with similar nitrogen loading, geology, and vegetation, which suggests the importance of understanding differing internal process mechanisms. I conducted two experiments to illustrate how water and  $\text{NO}_3^-$  moved on a constructed hillslope model.

In the first experiment, I quantified differences in soil properties in the hillslope model used by Hewlett and Hibbert (1963). Then I repeated (twice) the seminal drainage experiment described in Hewlett and Hibbert (1963). The same hillslope ( $21.8^\circ$ ; 40%) was wetted up, covered, and allowed to drain until water stopped exiting at the outlet. In the historical experiment there was fast drainage for 1.5 d, followed by slow drainage for  $\sim 140$  d, which led the authors to hypothesize that slow drainage in surface soil could continually contribute water to streams even during droughts. This long, slow drainage period was not reproduced in my experiments. Drainage was similar at the beginning of drainage between my experiments and the historical experiment, but in my experiment the slow drainage ended earlier (after 17 and 12 d) due likely to a leak in the constructed hillslope model, rather than to significant changes that occurred in the soil itself since the original experiment. This leak in the hillslope model is similar to leakage to bedrock, which is commonly observed in natural hillslopes.

In the second experiment, I tested whether  $\text{NO}_3^-$  and water would move through a hillslope at the same rate. I added concentrated pulses of  $\text{NO}_3^-$  (as  $^{15}\text{NO}_3^-$ ) and water (as  $^2\text{H}_2\text{O}$ ) on the same devegetated experimental hillslope. Retention of the  $^{15}\text{NO}_3^-$  tracer was high in the surface (0–10 cm) where the tracer was added, with little change in the immediately surrounding soil, despite high rates of water input immediately after tracer addition and throughout the experiment. The portion of the  $^{15}\text{NO}_3^-$  tracer that passed through the surface layer was further processed by microbes in deeper soil as it traveled downslope. This body of work shows that bedrock leakage, coupled with multiple retention mechanisms throughout the soil profile, can significantly delay export of added  $\text{NO}_3^-$  at the watershed scale.

To Lupita, Martha, and Vicki.

## ACKNOWLEDGEMENTS

First and foremost, I thank my co-advisors, Kevin McGuire and Brian Strahm, who believed in me since they hired me. They have led by example and always gave me invaluable scholarly and career advice, whether in the classroom, in work meetings in their offices, at coffee meetings at the pub, while driving out to and back from the study site (Coweeta), or over dinners at out-of-town conferences. I thank Jennifer Knoepp for her hospitality and guidance when I was setting up and running my experiments at Coweeta. I also thank Ryan Stewart for advising me when I built my computer model and Durelle Scott when I analyzed water samples in his lab. My committee has spent time with me in both official and unofficial capacities over the years, which has strengthened the product of my work and clarified to me the role and responsibilities of a career scientist. For this, I am very grateful.

I also thank the many people who have helped me in the field and lab. At Coweeta, I thank Jason Love, Carol Harper, Cindi Brown, Randy Fowler, Dave Hawthorne, and Brian Herndon for their hospitality in both the dormitory and the lab while I was there. I especially thank Brian for suggesting and then setting up the antenna connected to my data logger so I could access my data remotely from Virginia Tech—this was a real boon. At Virginia Tech, I thank Dave Mitchem for running several clean and efficient labs. Dave's guidance with lab protocol and his clear instruction on using many analytical instruments made my time in the labs profitable and enjoyable. I thank Kelly Peeler whose assistance in her lab on the other side of campus also helped me turn my water into numbers. I also thank my labmates, colleagues, and friends for their assistance and support during all of the time we spent together. Namely, I thank Andrés Peralta, Stephanie Duston, Tyler Weiglein, Jake Diamond, Carrie Jensen, Amy Gondran, J.P. Gannon, Glenia Pena Lugo, and Captain Harry Lineback.

Finally, I thank the people who worked deftly and tirelessly, but whom I was never fortunate enough to meet. In Autumn 2016, scores of fires scorched western North Carolina and north Georgia, burning tens of thousands of acres and threatening my study site and the Coweeta basin at large. Firemen quickly arrived from all corners of the country, from Alaska to Arizona to Florida to Virginia, and elsewhere in between. They extinguished the fires, preserving my work and the work of many others, for which I thank them. Furthermore, I thank the people in the Departments of Transportation who maintain the highways and rest stops in Virginia, Tennessee, and North Carolina. I used many of these rest stops, which are among the finest in the country, and napped in their parking lots. Their work made it possible to drive smoothly to Coweeta from Virginia Tech and back at all hours of the day and night. Finally, I thank Lupita (Lupitas Restaurant), Martha (Martha's Kitchen), and Vicki (Vicki's Restaurant) for their tacos, southern buffets, and Friday Fish Fries that nourished me. This project would not be possible without them.

## TABLE OF CONTENTS

Acknowledgements .....	v
List of Figures .....	vii
List of Tables .....	x
Attribution .....	xi
Chapter 1: Introduction .....	1
Chapter 2: Revisiting the Hewlett and Hibbert (1963) soil drainage experiment and modeling the effects of long-term pedogenic processes and leaky boundary conditions.....	10
Chapter 3: Transport of a $^{15}\text{NO}_3^-$ tracer along an experimental hillslope and evidence for coupled nitrification-denitrification .....	54
Chapter 4: Lagged export of a $^{15}\text{NO}_3^-$ tracer relative to a conservative tracer on an experimental hillslope .....	90
Chapter 5: Conclusions .....	127
Appendix .....	131

## LIST OF FIGURES

Figure 2.1. (a) Top view of the soil model with locations of monitoring instruments and soil core sampling sites. The aspect ratio is 2:1. (b) Side view of the soil model with moisture sensors and tensiometers. The aspect ratio is 1:1. ....37

Figure 2.2. Bulk density profiles along the hillslope. The mean is shown in red and the original bulk density reported in the historical experiment (Hewlett and Hibbert 1963) is shown at the bottom. ....38

Figure 2.3. (a) Soil textural class in this study (silt loam) and reported in the historical experiment (sandy clay loam; Hewlett and Hibbert 1963) plotted on a USDA soil texture triangle. (b) Percent sand versus percent silt throughout the depth profile and across the hillslope. ....39

Figure 2.4. Observed and modeled soil water retention curves. Observed data include field data at a similar soil model (Hewlett 1961); paired tensiometer and soil moisture sensor data in the study hillslope (1.1 [down], 4.9 [mid], and 8.7 [up] m upslope; all 35 cm depth) for our first drainage experiment; and data from saturation experiments done in the lab to soil cores taken from the study hillslope (7.3 [mid], and 13 [up] m upslope; all 15 cm depth). Additional points placed on the x-axis show values of maximum soil moisture, when the soil model was saturated, for sensors that were in the same profile and deeper than the sensors paired with a tensiometer. ....40

Figure 2.5. Linearly interpolated volumetric soil moisture,  $\theta$ , for our first drainage experiment (Experiment 1) at 0, 2, 10, 20, and 60 d after drainage was initiated. Small circles in the soil profile indicate locations of moisture sensors. In the bottom panel the large circle indicates the location of the leak added to select modeling runs using HYDRUS. The aspect ratio is 1:1.....41

Figure 2.6. (a) Time series of outflow ( $L d^{-1}$ ) observed and modeled in this study compared to results from the historical experiment (Hewlett and Hibbert 1963). (b) Log transformed recession flow data ( $\log[Q]$  [ $L d^{-1}$ ] and  $\log[\frac{dQ}{dT}]$  [ $L d^{-2}$ ]) in this study compared to results from the historical experiment (Hewlett and Hibbert 1963). The average slope ( $b = 1.76$ ) of experiments in this study was only slightly higher than the slope ( $b = 1.65$ ) for the historical experiment, and the average slope of all three experiments ( $b = 1.90$ ) was higher than the current and historical experiments separately. Lines indicate a top envelope (slope  $b = 1$ ), two bottom envelopes (slopes  $b = 3/2$  and  $b = 3$ ), and maximum observed flow,  $Q$ . ....42

Figure 2.7. (a) Time series of pressure head (cm) at different elevations above the outlet pipe in this study compared to results from the historical experiment (Hewlett and Hibbert 1963). There were three elevations in this study and four from the historical experiment. (b) Time series of pressure head (cm) at different elevations above the outlet observed in this study compared to model results using HYDRUS (with inclusion of a leak). The observed and modeled elevations were the same. Circle symbols on the x-axis show the times when outflow ended in each scenario. ....43

Figure 3.1. (a) Top view of the soil model with locations of instruments, soil core sampling sites, and tracer addition. The aspect ratio is 2:1. (b) Side view of the soil model with locations of lysimeters and tracer addition. The aspect ratio is 1:1. (c) Zoomed-in side view of lysimeter pair and other instrumentation (field tensiometer and capacitance-based soil moisture sensor) in the soil from a concurrent experiment. Figure is not to scale. (d) Zoomed-in front view of lysimeter pair and other instrumentation. Figure is not to scale. ....77

Figure 3.2. Conceptual model of fate and transport of  $\text{NO}_3^-$  through the study hillslope, from  $\text{NO}_3^-$  addition at the hillslope surface to  $\text{NO}_3^-$  export at the outlet. An idealized water table and saturated zone are shown in blue; an idealized configuration of a separate sand fill is shown near the outlet. Mechanisms that make  $\text{NO}_3^-$  available are shown in black or green and include addition (black) and mobilization (green); the mechanism that transports  $\text{NO}_3^-$  is shown in blue and is subsurface lateral throughflow or outflow at the outlet; mechanisms that retain or remove  $\text{NO}_3^-$  are shown in red and include immobilization, denitrification, and loss to leakage. The width of arrows (not to scale) show relative significance of the respective mechanism. ....79

Figure 3.3. Time series of  $\delta^2\text{H}$  and  $\delta^{15}\text{N}$  at shallow lysimeters (25 cm depth) and outlet. A colored band shows the range of background composition taken before the addition of the tracer; the colored line inside the band indicates the median background value. Downslope distance away from the tracer addition is given in the middle of each panel. ....80

Figure 3.4. Time series of  $\delta^2\text{H}$  and  $\delta^{15}\text{N}$  at deep lysimeters (65 cm depth) and outlet. A colored band shows the range of background composition taken before the addition of the tracer; the colored line inside the band indicates the median background value. Downslope distance away from the tracer addition is given in the middle of each panel. ....81

Figure 3.5. Time series of  $\text{NO}_3^-$ ,  $\text{NH}_4^+$ , and DON concentrations at shallow lysimeters (25 cm depth) and outlet. The colored line indicates the median background value. Downslope distance away from the tracer addition is given in the middle of each panel. ....82

Figure 3.6. Time series of  $\text{NO}_3^-$ ,  $\text{NH}_4^+$ , and DON at deep lysimeters (65 cm depth) and outlet. The colored line indicates the median background value. Downslope distance away from the tracer addition is given in the middle of each panel. ....83

Figure 4.1. (a) Top view of the hillslope model with locations of instruments, soil core sampling sites, and tracer addition. The aspect ratio is 2:1. (b) Side view of the hillslope model with location of tracer addition. The aspect ratio is 1:1. ....114

Figure 4.2. (a) Time series of the water balance (points;  $Q_{\text{in}}$  and  $Q_{\text{out}}$ ) and cumulative volumetric recovery (black line) at the outlet. (b) Time series of isotopic signature of  $\delta^2\text{H}$  (points) and cumulative mass recovery (black line) at the outlet. Data are presented as the daily average isotopic composition weighted by volumetric flow at the time each sample was collected. The blue band indicates the range of background concentrations and the line inside the band indicates the median value. (c) Time series of isotopic signature of  $\delta^{15}\text{N}$  (points) and cumulative mass recovery (black line) at the outlet. The red band indicates the range of background concentrations

and the line inside the band indicates the median value. Monthly labels at the bottom indicate the first day of the month. .... 115

Figure 4.3. (a) Soil profiles of  $\delta^{15}\text{N}$  (‰) and (b) N (%) collected before and after the experiment. Data points for the samples collected inside the tracer addition area (Fig. 4.1a) are highlighted in red. .... 117

Figure 4.4. Topview of  $\delta^{15}\text{N}$  (‰) and N (%) at the surface (0–10 cm) and bottom (bottom 2 cm) of the soil model at the end of the experiment. The tracer addition area is highlighted in red. The aspect ratio is 1:1. .... 118

Figure 4.5. Heat maps of  $\delta^{15}\text{N}$  (‰) from the top view of the (a) O horizon and (b) 0–10 cm layer of the soil profile. The tracer addition area is overlaid by a  $5 \times 5$  grid in the center of each plot. A black contour line in (b) shows the highly enriched area inside which  $\delta^{15}\text{N}$  values were above background. This contour was determined by spatial linear interpolation of the data points. (c) Boxplots of  $\delta^{15}\text{N}$  (‰) for the background and label samples. Whiskers extend a distance equal to up to 1.5 times the inter-quartile range, and data beyond that distance are represented individually by asterisks. Points in the background boxplots correspond to data taken along the hillslope (O horizon samples were taken after tracer addition only outside of the tracer addition area; 0–10 cm layer samples were taken before tracer addition; see Fig. 4.1). Points in the label boxplot for the O horizon correspond to samples collected from two areas: yellow points correspond to the tracer addition area, and grey points correspond to the area (rectangles with grey borders in panel [a]) outside of the tracer addition area. .... 119

Appendix A1. Timeseries of pH at lysimeters and outlet. Numbers indicate the downslope distance (m) away from the tracer addition; “5” indicates the outlet. Samples are color-coded by depth (i.e., shallow lysimeters at 25 cm depth, deep lysimeters at 65 cm depth, and outlet). A colored band shows the range of background concentrations taken before the tracer addition; the colored line inside the band indicates the median concentration. .... 131

Appendix A2. Boxplots of DOC for shallow and deep soil lysimeters (brown) and outflow (blue). Background concentrations are in black. .... 132

Appendix A3. Timeseries of anion concentrations at lysimeters and outlet. Numbers indicate the downslope distance (m) away from the tracer addition; “5” indicates the outlet. Samples are color-coded by depth (i.e., shallow lysimeters at 25 cm depth, deep lysimeters at 65 cm depth, and outlet). A colored band shows the range of background concentrations taken before the tracer addition; the colored line inside the band indicates the median concentration. .... 133

Appendix A4. Timeseries of cation concentrations at lysimeters and outlet. Numbers indicate the downslope distance (m) away from the tracer addition; “5” indicates the outlet. Samples are color-coded by depth (i.e., shallow lysimeters at 25 cm depth, deep lysimeters at 65 cm depth, and outlet). A colored band shows the range of background concentrations taken before the tracer addition; the colored line inside the band indicates the median concentration. .... 134

## LIST OF TABLES

Table 2.1. Physical and hydraulic properties of the soil in the physical and numeric (HYDRUS) soil model. Subscripts (D, M, U) indicate slope position (downslope, midslope, upslope, respectively). Standard errors are given in parentheses.....	45
Table 2.2. Mass balances of water and conservative tracer ( $^2\text{H}_2\text{O}$ ).....	46
Table 3.1. Mass balance of $\text{NO}_3^-$ -N in the saturated riparian zone. Change in storage refers to aqueous-phase $\text{NO}_3^-$ -N in soil solution in the riparian zone.....	84
Table 4.1. Mass balance calculations of pools and fluxes of the $^2\text{H}$ and $^{15}\text{NO}_3^-$ -N tracers. ....	120

## ATTRIBUTION

### Chapter 2

Kevin J. McGuire, Ph.D., (Virginia Tech, Forest Resources and Environmental Conservation and Virginia Water Resources Research Center) helped with study design, site preparation, data interpretation, and editing of the manuscript.

Brian D. Strahm, Ph.D., (Virginia Tech, Forest Resources and Environmental Conservation) helped with with study design, site preparation, data interpretation, and editing of the manuscript.

Jennifer D. Knoepp, Ph.D., (Coweeta Hydrologic Laboratory, USDA Forest Service) helped with with study design and site preparation.

Rhett Jackson, Ph.D., (University of Georgia, Athens, Warnell School of Forestry and Natural Resources) helped with data interpretation and editing of the manuscript.

Ryan Stewart, Ph.D., (Virginia Tech, School of Plant and Environmental Science) helped with computer model setup and data interpretation.

### Chapter 3

Kevin J. McGuire, Ph.D., (Virginia Tech, Forest Resources and Environmental Conservation and Virginia Water Resources Research Center) helped with study design, site preparation, data interpretation, and editing of the manuscript.

Brian D. Strahm, Ph.D., (Virginia Tech, Forest Resources and Environmental Conservation) helped with study design, site preparation, data interpretation, and editing of the manuscript.

Jennifer D. Knoepp, Ph.D., (Coweeta Hydrologic Laboratory, USDA Forest Service) helped with study design and site preparation.

Durelle T. Scott, Ph.D., (Virginia Tech, Biological Systems Engineering) helped with data interpretation and editing of the manuscript.

### Chapter 4

Kevin J. McGuire, Ph.D., (Virginia Tech, Forest Resources and Environmental Conservation and Virginia Water Resources Research Center) helped with study design, site preparation, data interpretation, and editing of the manuscript.

Brian D. Strahm, Ph.D., (Virginia Tech, Forest Resources and Environmental Conservation) helped with study design, site preparation, data interpretation, and editing of the manuscript.

Jennifer D. Knoepp, Ph.D., (Coweeta Hydrologic Laboratory, USDA Forest Service) helped with study design and site preparation.

Durrelle T. Scott, Ph.D., (Virginia Tech, Biological Systems Engineering) helped with data interpretation and editing of the manuscript.

## Chapter 1: Introduction

### 1.0 Background

The fate and transport of nitrate ( $\text{NO}_3^-$ ) is a critical issue in forest ecosystem science. As a mobile and bioavailable form of nitrogen (N), one of the most common limiting nutrients for productivity worldwide (Vitousek and Howarth 1991),  $\text{NO}_3^-$  is simultaneously linked to plant productivity and water quality. Thus, understanding whether terrestrial ecosystems are net sources or sinks for N, and how those dynamics change from system to system, and over time within a system, has long been a focus of research (e.g., Aber et al. 2003). However, the net effect of varied mechanisms controlling fate and transport of  $\text{NO}_3^-$  are not easily predicted. This is partly true because few studies have experimentally tracked them all the way from the hillslope to the stream. Many studies investigate retention processes at the smaller core or plot scale, or measure stream water  $\text{NO}_3^-$  concentrations at larger scales, such as the watershed outlet, and then infer potential processes upslope (e.g., Adams et al. 2014). Such viewpoints can limit our predictive power of these dynamic systems because they often lack a coupled and mechanistic focus on N transformation and transport processes.

Given that we so often fail to quantify the combined effects of  $\text{NO}_3^-$  reaction and transport processes, watershed export of  $\text{NO}_3^-$  remains highly unpredictable (Sudduth et al. 2013). For example, there are no clear monotonic trends of N export in pristine reference forests (Argerich et al. 2013), and though stream water  $\text{NO}_3^-$  concentrations often show a temporary increase in disturbed forests (e.g., Watmough et al. 2005, Rhoades et al. 2017), there are often consistent, decadal decreases in stream water  $\text{NO}_3^-$  concentrations in other disturbed forests (Goodale et al.

2005; Lucas et al. 2016). The nuance of magnitude and timing of these observations of N export suggest we should focus on scales of observation that allow for better integration of coupled N cycling and transport processes.

In homeostatic mature forests, the unexpected decreases in  $\text{NO}_3^-$  export cannot be due only to biologically mediated mechanisms that store N in biologically active surface soils (immobilization) and vegetation. A proposed revision to the standard conceptual model in northeastern US forests highlights the role of the mineral soil horizons as an important retention sink (Lovett et al. 2018). Additionally, denitrification processes are important because they remove N from soils altogether (Goodale et al. 2005; Lucas et al. 2016). Ultimately, conversion of a headwater forest from a  $\text{NO}_3^-$  sink to source depends on the net effects of many competing and interacting processes that either retain or transport the  $\text{NO}_3^-$  at the hillslope scale (Burt and Pinay 2005). Cumulative export of  $\text{NO}_3^-$  from hillslopes to the stream can then be scaled up to express total export of  $\text{NO}_3^-$  from the watershed.

Different locations on the hillslope can play different roles in the formation of hot spots and hot moments (cf. McClain et al. 2003), where and when disproportionately large rates of reactions (e.g., nitrification, denitrification) can rapidly occur. There is additional variability in net  $\text{NO}_3^-$  processing because transport rates control mobilization of N that translocates N from upslope to initiate  $\text{NO}_3^-$  production/removal reactions or translocates N downslope for further processing. Nitrate becomes available in soil all along hillslopes, due either to addition from the atmosphere (e.g., deposition or fixation) or internal soil transformation processes (e.g., mineralization and nitrification). In N-limited forest ecosystems, much of the available  $\text{NO}_3^-$  is retained by microbes

in the biologically active soil surface (Aber et al. 1998; Qualls et al. 2000) or taken up by vegetation (Adams et al. 2014). Nitrate that passes through areas with strong retention sink potential is hydrologically transported to the subsurface environment where and when the rate of  $\text{NO}_3^-$  transport exceeds the rates of retention (e.g., immobilization) and removal (e.g., denitrification). Mobile  $\text{NO}_3^-$  can then adsorb onto colloidal surfaces of soil particles through abiotic geochemical interactions in soil (Kahl et al. 1999; Strahm and Harrison 2006; Strahm and Harrison 2007). Nitrate that is not biologically or geochemically retained and reaches the bottom of the hillslope can be denitrified in the riparian zone (Davidson and Swank 1986). Any  $\text{NO}_3^-$  that is not retained or denitrified is exported into the stream.

Transport of  $\text{NO}_3^-$  can vary due also to soil physical properties and hydrologic dynamics that control water movement. Variable lengths and hydraulic conductivities of flow paths can attenuate, delay, or accelerate flow, causing variations of water travel times associated with different flow paths in a hillslope (Kirkby 1988). As water moves into and out of neighboring soil layers or slope positions, the amount of time spent in any section of these is an important consideration for the quantity and timing of  $\text{NO}_3^-$  transport (Cirimo and McDonnell 1997; van der Velde et al. 2010). Antecedent moisture conditions on the hillslope affect processing rates and the transport efficiency that control the timing of  $\text{NO}_3^-$  response (Christopher et al. 2008). When water moves quickly through hillslope soils with high nitrification rates to the stream, there is often higher  $\text{NO}_3^-$  export because the  $\text{NO}_3^-$  can bypass biogeochemical retention processes (Welsch et al. 2001; Ross et al. 2012; Zhang et al. 2016). During storm periods of high discharge, a large proportion (e.g., 33% [Sebestyen et al. 2014]) of this stormflow  $\text{NO}_3^-$  can be unprocessed and atmospherically derived (Rose et al. 2015).

## 1.1. Objectives and layout of the dissertation

Fate and transport of  $\text{NO}_3^-$  through and out of a forest is controlled by transport and reaction processes that can be loosely categorized as hydrological, biological, and geochemical, all of which interact dynamically across multiple scales of time and space. This dissertation is an investigation of the net effect of those processes and is limited to the hillslope scale because the hillslope is the smallest unit with spatial and temporal resolution to reflect many relevant  $\text{NO}_3^-$  transport (flow-generation) and reaction processes, and headwater forests are largely comprised of sections of hillslopes. The overarching aim of this dissertation is to answer the question: *What is the fate of a pulse of  $\text{NO}_3^-$  introduced on a hillslope?*

I answer this question by combining field and lab experiments, statistical analyses, and computer modeling. I conducted two field experiments on an experimental hillslope soil model, and the experiments are described in three chapters of this dissertation. In the first field experiment (Chapter 2), soil development processes (e.g., root establishment, macropore development, organic matter accumulation, weathering, and particle migration) that have occurred in the soil model over ~50 y since its construction for a hydrological experiment (Hewlett and Hibbert 1963) were considered an experimental treatment. I quantified the changes to soil characteristics in field samples, which were then analyzed for other hydraulic descriptors, including the soil water retention curve, saturated hydraulic conductivity, and van Genuchten parameters (van Genuchten 1980). Then I repeated the original drainage experiment (Hewlett and Hibbert 1963) that helped form the foundational theory on subsurface recession flow on hillslopes (i.e., the Variable Source Area paradigm). This physical experiment was replicated numerically with a 2-

D finite element computer simulation model (HYDRUS; Šimůnek et al. 2012). Data gathered from the physical experiment were used to calibrate parameters in the simulations and results from the simulations in turn informed and supported the interpretation of results from the physical experiment. I answer the following research questions: Have soil properties changed over the past 53 years, and have those changes affected water retention and recession flow dynamics from the hillslope?

In the second field experiment, I conducted a controlled experiment in which the journey of a  $\text{NO}_3^-$  hot spot was directly monitored from hillslope to stream. I added an isotopically labeled  $\text{NO}_3^-$  tracer ( $^{15}\text{NO}_3^-$ ) on the experimental hillslope and used a series of lysimeters to track its course relative to a conservative water tracer ( $^2\text{H}_2\text{O}$ , later recovered as  $^2\text{H}-^{16}\text{O}-^2\text{H}$  and hereafter referred to as  $^2\text{H}$ ) along a 5 m stretch of hillslope down through a riparian zone with a permanent water table exiting into a stream. The soil model was devegetated and continually irrigated at steady state with unlabeled water that was volumetrically and chemically similar to local throughfall in the watershed. The dual tracer allowed me to make inferences about retention processes as the  $^2\text{H}$  was the control for conservative transport of a solute (Becker and Coplen 2001) and also elucidated water transport dynamics along the hillslope. Constituents in both soil solution along the hillslope and in outflow at the bottom of the model were monitored until the outflow returned to background concentrations. Soil samples were taken along the hillslope before and after the tracer addition and analyzed for chemistry.

Results from the dual tracer experiment are presented in two chapters, separating internal  $\text{NO}_3^-$  transport and retention dynamics along the hillslope from the  $^{15}\text{NO}_3^-$  tracer mass balance and

timing of  $^{15}\text{NO}_3^-$  export at the outlet. In Chapter 3, I answer the following research questions: What is the timing of a conservative tracer moving through the hillslope? Is there a delay in movement of the  $^{15}\text{NO}_3^-$  tracer compared to the conservative tracer? Where and why does it occur? What roles do nitrification and denitrification play? In Chapter 4, I answer the following research questions: Where (e.g., litter, soil, outflow) is the added  $^{15}\text{NO}_3^-$  recovered? What is the timing and quantity of export of a pulse of  $^{15}\text{NO}_3^-$  added on a hillslope? What implications does this have for  $\text{NO}_3^-$  export at the watershed scale?

In Chapter 5, the results from my experiments are summarized. Impacts of pedogenetic processes on recession flow, and impacts of internal  $\text{NO}_3^-$  retention mechanisms on timing and load of  $\text{NO}_3^-$  export are discussed, with attention to timing of  $\text{NO}_3^-$  export at the watershed scale.

## References

- Aber, J., W. McDowell, K. Nadelhoffer, A. Magill, G. Berntson, M. Kamakea, S. McNulty, W. Currie, L. Rustad, and I. Fernandez. 1998. Nitrogen saturation in temperate forest ecosystems. *BioScience*, 48: 921–934.
- Aber, J. D., C. L. Goodale, S. V. Ollinger, M.-L. Smith, A. H. Magill, M. E. Martin, R. A. Hallett, and J. L. Stoddard. 2003. Is nitrogen deposition altering the nitrogen status of northeastern forests? *BioScience*, 53: 375–389.
- Adams, M. B., J. D. Knoepp, and J. R. Webster. 2014. Inorganic nitrogen retention by watersheds at Fernow Experimental Forest and Coweeta Hydrologic Laboratory. *Soil Science Society of America Journal*, 78: S95–S104.
- Argerich, A., S. L. Johnson, S. D. Sebestyen, C. C. Rhoades, E. Greathouse, J. D. Knoepp, M. B. Adams, G. E. Likens, J. L. Campbell, W. H. McDowell, F. N. Scatena, and G. G. Ice. 2013. Trends in stream nitrogen concentrations for forested reference catchments across the USA. *Environmental Research Letters*, 8: 1–8.
- Becker, M. W., and T. B. Coplen. 2001. Use of deuterated water as a conservative artificial groundwater tracer. *Hydrogeology Journal*, 9: 512–516.
- Burt, T. P. and G. Pinay. 2005. Linking hydrology and biogeochemistry in complex landscapes. *Progress in Physical Geography*, 29: 297–316.
- Christopher, S. F., M. J. Mitchell, M. R. McHale, E. W. Boyer, D. A. Burns, and C. Kendall. 2008. Factors controlling nitrogen release from two forested catchments with contrasting hydrochemical responses. *Hydrological Processes*, 22: 46–62.
- Cirno, C. P. and J. J. McDonnell. 1997. Linking the hydrologic and biogeochemical controls of nitrogen transport in near-stream zones of temperate-forested catchments: a review. *Journal of Hydrology*, 199: 88–120.
- Davidson, E. A. and W. T. Swank. 1986. Environmental parameters regulating gaseous nitrogen losses from two forested ecosystems via nitrification and denitrification. *Applied and Environmental Microbiology*, 52: 1287–1292.
- Goodale, C. L., J. D. Aber, P. M. Vitousek, and W. H. McDowell. 2005. Long-term decreases in stream nitrate: Successional causes unlikely; Possible links to DOC? *Ecosystems*, 8: 334–337.
- Hewlett, J. D. and A. R. Hibbert. 1963. Moisture and energy conditions within a sloping soil mass during drainage. *Journal of Geophysical Research*, 68: 1081–1087.
- Kahl, J., S. Norton, I. Fernandez, L. Rustad, and M. Handley. 1999. Nitrogen and sulfur

- input-output budgets in the experimental and reference watersheds, Bear Brook watershed in Maine (BBWM). *Environmental Monitoring and Assessment*, 55: 113–131.
- Kirkby, M. 1988. Hillslope runoff processes and models. *Journal of Hydrology*, 100: 315–339.
- Lovett, G. M., C. L. Goodale, S. V. Ollinger, C. B. Fuss, A. P. Ouimette, and G. E. Likens. 2018. Nutrient retention during ecosystem succession: a revised conceptual model. *Frontiers in Ecology and the Environment*, 16: 1–7.
- Lucas, R. W., R. A. Sponseller, M. J. Gundale, J. Stendahl, J. Fridman, P. Högberg, and H. Laudon. 2016. Long-term declines in stream and river inorganic nitrogen (N) export correspond to forest change. *Ecological Applications*, 26: 545–556.
- McClain, M., E. W. Boyer, C. L. Dent, S. E. Gergel, N. B. Grimm, P. M. Groffman, S. C. Hart, J. W. Harvey, C. A. Johnston, E. Mayorga, W. H. McDowell, and G. Pinay. 2003. Biogeochemical hot spots and hot moments at the interface of terrestrial and aquatic ecosystems. *Ecosystems*, 6: 301–312.
- Qualls, R. G., B. L. Haines, W. T. Swank, and S. W. Tyler. 2000. Soluble organic and inorganic nutrient fluxes in clearcut and mature deciduous forests. *Soil Science Society of America Journal*, 64: 1068–1077.
- Rhoades, C. C., R. M. Hubbard, and K. Elder. 2017. A decade of streamwater nitrogen and forest dynamics after a mountain pine beetle outbreak at the Fraser Experimental Forest, Colorado. *Ecosystems*, 20: 380–392.
- Rose, L. A., S. D. Sebestyen, E. M. Elliott, and K. Koba. Drivers of atmospheric nitrate processing and export in forested catchments. *Water Resources Research*, 51: 1333–1352.
- Ross, D. S., J. B. Shanley, J. L. Campbell, G. B. Lawrence, S. W. Bailey, G. E. Likens, B. C. Wemple, G. Fredriksen, and A. E. Jamison. 2012. Spatial patterns of soil nitrification and nitrate export from forested headwaters in the northeastern United States. *Journal of Geophysical Research*, 117: G01009.
- Sebestyen, S. D., J. B. Shanley, E. W. Boyer, C. Kendall, and D. H. Doctor. 2014. Coupled hydrological and biogeochemical processes controlling variability of nitrogen species in streamflow during autumn in an upland forest. *Water Resources Research*, 50, doi: 10.1002/2013WR013670.
- Šimůnek, J., M. Th. Van Genuchten, and M. Šejna. 2012. The HYDRUS Software Package for Simulating Two- and Three-Dimensional Movement of Water, Heat, and Multiple Solutes in Variably-Saturated Porous Media, Technical Manual, Version 2.0, PC Progress, Prague, Czech Republic, pp. 258.

- Strahm, B. D. and R. B. Harrison. 2006. Nitrate sorption in a variable-charge forest soil of the Pacific Northwest. *Soil Science*, 171: 313–321.
- Strahm, B. D., and R. B. Harrison. 2007. Mineral and organic matter controls on the sorption of macronutrient anions in variable-charge soils. *Soil Science Society of America Journal*, 71: 1–8.
- Sudduth, E. B., S. S. Perakis, and E. S. Bernhardt. 2013. Nitrate in watersheds: Straight from soils to streams? *Journal of Geophysical Research: Biogeosciences*, 118: 291–302.
- van der Velde, Y., G. H. de Rooij, J. C. Rozemeijer, F. C. van Greer, and H. P. Broers. 2010. Nitrate response of a lowland catchment: On the relation between stream concentration and travel time distribution dynamics. *Water Resources Research*, 46: W11534. doi: 10.1029/2010WR009105.
- van Genuchten, M. T. 1980. A closed-form equation for predicting the hydraulic conductivity of unsaturated soils. *Soil Science Society of America Journal*, 44: 892–898.
- Vitousek, P. M. and R. W. Howarth. 1991. Nitrogen limitation on land and in the sea: How can it occur? *Biogeochemistry*, 13: 87–115.
- Watmough, S. A., J. Aherne, C. Alewell, P. Arp, S. Bailey, T. Clair, P. Dillon, L. Duchesne, C. Eimers, I. Fernandez, N. Foster, T. Larssen, E. Miller, M. Mitchell, and S. Page. 2005. Sulphate, nitrogen and base cation budgets at 21 forested catchments in Canada, the United States and Europe. *Environmental Monitoring and Assessment*, 109: 1–36.
- Welsch, D. L., C. N. Kroll, J. J. McDonnell, and D. A. Burns. 2001. Topographic controls on the chemistry of subsurface stormflow. *Hydrological Processes*, 15: 1925–1938.
- Zhang, J., P. Tian, J. Tang, L. Yuan, Y. Ke, Z. Cai, B. Zhu, and C. Müller. 2016. The characteristics of soil N transformations regulate the composition of hydrologic N export from terrestrial ecosystem. *Journal of Geophysical Research Biogeosciences*, 121.

## **Chapter 2: Revisiting the Hewlett and Hibbert (1963) soil drainage experiment and modeling the effects of long-term pedogenic processes and leaky boundary conditions**

**Authors:** Raymond M. Lee<sup>1</sup>, Kevin J. McGuire<sup>1,2</sup>, Brian D. Strahm<sup>1</sup>, Jennifer D. Knoepp<sup>3</sup>, Rhett Jackson<sup>4</sup>, and Ryan D. Stewart<sup>5</sup>

<sup>1</sup>Department of Forest Resources and Environmental Conservation, Virginia Tech, Blacksburg, VA 24061, USA

<sup>2</sup>Virginia Water Resources Research Center, Virginia Tech, Blacksburg, VA 24061, USA

<sup>3</sup>Coweeta Hydrologic Laboratory, USDA Forest Service, Otto, NC 28763, USA

<sup>4</sup>Warnell School of Forestry and Natural Resources, University of Georgia, Athens, GA 30602, USA

<sup>5</sup>School of Plant and Environmental Science, Virginia Tech, Blacksburg, VA 24061, USA

**Abstract:** Subsurface flow dominates the flow of water from the hillslope to the stream in forested headwater watersheds. Hewlett and Hibbert (1963) used a constructed experimental hillslope ( $0.91 \times 0.91 \times 15.0$  m;  $21.8^\circ$ ) filled with a reconstituted C horizon soil to investigate the potential importance of a particular type of subsurface flow, interflow, in mountain catchments. They saturated the experimental hillslope, covered it to prevent evapotranspiration, and allowed it to drain until it no longer yielded water. The resulting drainage recession curve suggested there were two modes of subsurface recession drainage: fast drainage of the saturated portion of the hillslope in the first 1.5 d, then slow drainage of unsaturated soil for the balance of the experiment (145 d). Hydrologists had inferred that the long, slow drainage was evidence that soil moisture from the unsaturated zone could sustain stream baseflow, even in periods of extended drought. Now that the experimental slope has grown vegetation and processed forest litter for 53 years, we twice repeated the experiment expecting that bioturbation and pedogenesis would have

changed the recession curve. Unexpectedly, the recession curves were unchanged for the first 9-10 days of drainage, indicating that biological processes and pedogenesis had not significantly altered bulk hydraulic conductivities or soil moisture release characteristics of the soil model. Furthermore, drainage ceased after 17 and 12 d, due to an apparent leak in the concrete walls possibly created by root growth. This leak is analogous to loss to bedrock, which is a commonly observed phenomenon. This study presents more natural recession behavior that highlights how such leakage can reduce drainage duration in drought periods and thereby reduce the contribution of moisture from soils to baseflow.

**Keywords:** hillslope hydrology; Variable Source Area; baseflow

## 2.0. Introduction

Water movement from the hillslope to the stream in forested headwater watersheds is dominated by subsurface processes. Shallow lateral subsurface flow over an impeding layer, sometimes called subsurface stormflow, interflow, or throughflow, is initiated when infiltrating precipitation raises the moisture content of topsoils above an impeding layer to near or above field capacity (Freeze 1972). Due to the hydraulic conductivity contrast between the topsoil and the impeding layer, lateral downslope flow can occur as unsaturated flow (Zaslavsky and Sinai 1981), saturated flow (Dunne and Black 1970), or saturated macropore flow (e.g. Beven and Germann 1982). Hewlett and Hibbert's experimental hillslope work (Hewlett 1961a; Hewlett and Hibbert 1963; hereafter collectively referred to as "H & H") indicated that after precipitation has ceased and the saturated zone has contracted, hydraulic head gradients can move soil moisture laterally from upslope soils in large volumes over an extended period, sustaining baseflow between storms.

Hewlett's interest in sustained baseflow support by unsaturated interflow was motivated by observations that streams in the mountainous terrain of the Coweeta Hydrologic Laboratory were not supported by large valley aquifers but still sustained baseflows during long periods without rain. To determine if unsaturated interflow could explain this paradox, H & H built experimental soil models composed of an inclined concrete structure filled with locally-sourced and reconstituted C horizon forest soil, then conducted drainage experiments. In the 1963 study, they saturated a covered, sloping (21.8°; 40%) 15 m trough of sandy loam soil that was homogenized and repacked to a depth of 0.91 m. After saturation, they allowed it to drain until it no longer yielded water (145 d). From this experiment, they developed a drainage recession curve used to

argue that there were two modes of drainage: fast drainage of the saturated portion of the hillslope, which lasted 1.5 days, then slow drainage of unsaturated soil for the balance of the experiment (see Fig. 2 in Hewlett and Hibbert 1963).

These observations of long-duration unsaturated drainage of sloping soils have been highly influential in shaping our understanding of the role of soil moisture, as opposed to groundwater aquifers, in supplying water to headwater streams even in periods of drought. For example, long-duration recession flow through unsaturated soil, as described in H & H, has been widely observed (Rothacher 1965; Weyman 1973; Mosley 1979; Moore 1997; Post and Jones 2001; McGuire and McDonnell 2010) and accepted to inform conceptual models (Scholl and Hibbert 1973; Harr 1977; Dunne 1983; Genereux and Hemond 1990; Kirkby 1988; Bonell 1998; Torres et al. 1998; McGlynn and McDonnell 2003; Nippgen et al. 2015). Furthermore, H & H suggest that the area supplying baseflow is not constant but expands or shrinks in response to the interactions among precipitation, recharge, and soil moisture, which led to the development of the Variable Source Area concept (VSA; Hewlett 1961b, Hewlett and Hibbert 1967). The VSA concept, which is the foundation for commonly used physically-based watershed models (e.g., TOPMODEL [Beven and Kirkby 1979; Wolock and McCabe 1995; Golden et al. 2014]; Soil Moisture Routing model [Frankenberger et al. 1999]; CN-VSA [Lyon et al. 2004]), informed numerous studies and continued to be refined for decades after the concept was conceived (Dunne 1983; Ward 1984; Bernier 1985; Ambroise 2004; Weiler et al. 2005; Nippgen et al. 2015).

However, several limitations of the controlled experiment in Hewlett and Hibbert (1963) may distinguish the recession flow curve produced from their idealized hillslope compared to recession flow observed from hillslopes with intact and heterogeneous natural soil. The primary limitation was that the hillslope soil profile was texturally and structurally homogenous, a simplification that could not account for the distribution of hydraulic conductivities with the soil profile found in natural hillslopes (e.g., Beven 1982; Elsenbeer 2001). There is often an exponential decline in saturated hydraulic conductivity and porosity with soil depth that can significantly influence transit time of water (Ameli et al. 2016). Another limitation was that vegetation and organic matter were negligible or absent from their hillslope. Naturally present organic matter in the soil surface would increase soil water retention, as organic matter is strongly correlated with soil moisture content at saturation (Ankenbauer and Loheide 2016). Not incorporating organic matter provided more control for isolating mechanisms affecting drainage but, again, did not replicate natural conditions. Furthermore, the lower boundary of the soil model, representing the soil-bedrock interface, was flat and impermeable, which was uncharacteristic of natural bedrock in many systems that may have bedrock fractures (Freer et al. 2002; Appels et al. 2015; Hale and McDonnell 2016; Pfister et al. 2017, Gabrielli et al. 2018; Klaus and Jackson 2018). These artifacts in the flow domain and boundary conditions likely impacted the movement of water into, through, and out of the soil model. Analytical and numerical models have replicated the experiment and adequately estimated outflow, though these simplifications were also incorporated in those models (Sloan and Moore 1984; Stagnitti et al. 1986; Zecharias and Brutsaert 1988; Steenhuis et al. 1999). Thus, what is truly needed to further advance our understanding of the relationship between hillslope soil moisture and baseflow is a

more realistic set of field observations and modeling exercises that more accurately represent the physical properties regulating the subsurface environment.

More than 50 years had passed since the Hewlett and Hibbert (1963) experiment was conducted, and pedogenetic processes (e.g., weathering, aggregate formation, organic matter incorporation, settling, erosion) visibly changed the soil properties in the soil model from the original experiment to a condition that was closer to those in adjacent natural forest soils. For example, trees (up to 40 cm ground line diameter) grew inside the soil model, a thin A horizon developed, and invertebrates (e.g., ants and worms) colonized the soil, all of which would be expected to alter the pore structure and drainage dynamics (Beven and Germann 1982; Hendrickx and Flurry 2001; Clothier et al. 2008). We were interested in how such changes may impact recession flow compared to the original observations of H & H and the subsequent broadscale interpretations of hillslope subsurface flow dynamics that have built off of their work.

Here we characterized the soil in the original hillslope model for changes in properties, including horizonation, texture, bulk density, carbon content, saturated hydraulic conductivity, and water retention. Furthermore, we report on two repetitions of the H & H drainage experiments (using the same hillslope model as in Hewlett and Hibbert [1963]), which were complemented by investigations with a 2-D dynamic numerical model. We also conducted irrigation and tracer experiments to examine drainage and hydrologic mass balance. We aimed to answer the following research questions: Have soil properties changed over the past 53 years, and have those changes affected water retention and recession flow dynamics from the hillslope?

## **2.1. Methods**

### **2.1.1. Physical experiment**

#### ***2.1.1.1. Physical soil model***

The study site at Coweeta Hydrologic Laboratory (hereafter Coweeta) in southwestern North Carolina was a concrete-lined planar trough ( $0.91 \times 0.91 \times 15.0$  m) that represented a hillslope with a water table maintained by an outlet pipe (i.e., seepage face) at a height of 0.46 m above the ground at the base (Hewlett and Hibbert 1963; Fig. 2.1). The toeslope segment was level, extending 0.3 m. The soil model was packed with  $10.85 \text{ m}^3$  of sieved (6.4 mm) soil that was excavated near the soil model from the C horizon of a locally sourced Saunook (formerly known as Halewood) sandy loam, averaging 60% sand, 18% silt, and 22% clay, that graded to sand and gravel at the toe of the slope to simulate gravelly stream bank conditions (Hewlett and Hibbert 1963). The fill material was homogenous and packed to a bulk density of  $1.3 \text{ g cm}^{-3}$ . Total pore space in the packed soil was ~50% by volume.

In 2012 all (four) trees were cut at the base and removed from the soil model, leaving the root structure intact in the soil. In 2015, the soil model was covered by a curved shelter, ~2 m above the ground surface at its peak, which was open at the top and bottom ends of the soil model, allowing airflow across the soil surface and gas exchange between the soil and atmosphere. The shelter cover was made of laminated reinforced polyethylene film, which prevented meteoric water input while allowing transmission of 83% of incoming diffuse visible light. Seasonal leaf litterfall was collected continuously near the soil model over an equal surface area and added back onto the soil surface. The soil model was maintained in a devegetated state with herbicide (glyphosate).

### **2.1.1.2. Physical and hydraulic properties of soil**

Soil samples were collected before and after the drainage experiments to be analyzed for physical and hydraulic properties (Fig. 2.1a). When installing instruments (described below), three cores were collected from capacitance-based moisture sensor locations and three cores were collected from tensiometer locations; 10 additional cores (Fig. 2.1a) were collected after the drainage experiments. All cores were separated into 10 cm depth increments (after correcting for compaction during excavation). Cores collected from instrument locations were extracted using a soil probe (2 cm diameter), and the additional cores were extracted using a soil auger (2.2 cm diameter). A mean depth of the soil model was calculated with the hole depths from which soil cores were removed. The mean depth, which was less than what was reported in the historical experiment, was used to calculate a new volume and mass in the soil model. We used this volume (9.4 m<sup>3</sup> of soil, a decrease of 1.5 m<sup>3</sup> [or 14%] across the hillslope) and volumetric soil water content point measurements, linearly interpolated across the soil model, to estimate total volumetric water content in the hillslope.

Samples were air dried, then oven dried at 65 °C to remove moisture, then weighed to calculate bulk density and porosity. Subsamples were analyzed for soil texture using the laser diffraction method on a particle size analyzer (Model CILAS 1190, CPS US, Fitchburg, WI). Other subsamples were ball-milled and analyzed for carbon content (Model Vario MAX CNS, Elementar, Ronkonkoma, NY).

Three additional cores (5.1 cm depth; 5.1 cm diameter) were collected from the surface in the 10–15 cm depth layer at locations 1.6, 7.3, and 13.0 m upslope and then analyzed for both water

retention in a range of soil moisture conditions and for saturated hydraulic conductivity ( $K_s$ ; Fig. 2.1). Water retention was measured on a HYPROP (Meter, Pullman, WA) using the Schindler (1980) evaporation method (Peters and Durner 2008). Then soil cores were saturated in the laboratory and  $K_s$  values were measured on a KSAT automated constant head device (Meter, Pullman, WA) using the falling head test method (Reynolds et al. 2002).

### **2.1.1.3. Drainage and irrigation experimental setup**

The drainage experiment as described in Hewlett and Hibbert (1963) was repeated twice to confirm reproducibility. To initialize the hillslope for each experiment, we irrigated the soil model for several weeks using sprinklers (Fig. 2.1) to hydrologic steady state and then added water by hand to near-saturation in one event just before drainage, when intensive measurements commenced. In these events, we added 1,500 L of water continuously and evenly across the surface for 7 h ( $1.6 \text{ cm h}^{-1}$ ) in the first experiment and 9 h ( $1.2 \text{ cm h}^{-1}$ ) in the second, until volumetric soil moisture was 43.0 and 43.6%, respectively, and the rate of outflow ( $Q$ ) plateaued. These were similar initial conditions for the start of the historical experiment (Hewlett and Hibbert 1963). Immediately after the water additions, a plastic tarp was placed directly on the soil to prevent evaporation and free drainage was allowed to occur for 60 and 48 d, respectively (by which time  $Q$  had ceased).

### **2.1.1.4. Additional mass balance experiments**

After the drainage experiments, we confirmed the presence and magnitude of a leak from the soil model by calculating a water mass balance while irrigating the soil model at steady state for 141 d. The daily irrigation rate ( $6.1 \text{ mm d}^{-1}$ ;  $86 \text{ L d}^{-1}$ ) was similar to the mean daily average gross

precipitation rate ( $6.5 \text{ mm d}^{-1}$ ;  $89 \text{ L d}^{-1}$ ) in the wettest year on record at low elevation in the Coweeta basin, which is also equal to the mean daily average precipitation rate at high elevation (Laseter et al. 2012). We assumed evapotranspiration during this period was negligible because the soil was irrigated only once daily, minimizing exposure of wet soil to the atmosphere, and at 08:00, when temperature was cool; the soil model was protected from wind by the shelter, further minimizing atmospheric influence; and there was no live vegetation in the soil model to transpire water from the soil.

Additionally, we applied a conservative deuterium tracer (a mixture of 10 mL of  $^2\text{H}_2\text{O}$  [99.9 atom %  $^2\text{H}$ ] and 90 mL of deionized water) onto the hillslope at 5 m above the outlet at the beginning of this steady-state irrigation period. We sampled water at the outlet to measure total recovery of the mass of the tracer until the  $^2\text{H}$  signature returned to the pre-tracer background level. Isotopic analysis of  $^2\text{H}$  was done on an isotopic liquid water and water vapor analyzer (Model L1102-i, Picarro, Santa Clara, CA) using a modified sampling protocol and post-processing correction and normalization procedures, all of which maximized precision, accuracy, and efficiency (van Geldern and Barth 2012). The precision of the method was  $\leq 0.5 \text{ ‰}$ , which was within the generally accepted values (1–2 ‰) for traditional isotope ratio mass spectrometry.

#### ***2.1.1.5. Water monitoring***

Outflow was measured by a tipping bucket (Snowmetrics, Fort Collins, CO; Elder et al. 2014; 500 mL increments) at the outlet (Fig. 2.1). Soil moisture was measured across the hillslope by capacitance-based sensors (Model Drill & Drop, Sentek, Stepney, South Australia; point measurements every 10 cm depth at 1.1, 4.9, and 8.7 m upslope from the outlet) and time-

domain reflectometry (TDR)-based sensors (Model CS615, Campbell Scientific, Logan, UT; integrated measurements over 30 cm depth increments at 3.0, 6.8, and 12.5 m upslope).

Capacitance-based sensors were installed to the maximum depth (~85 cm), and TDR-based sensors were installed in clusters of three at depths 0–30, 30–60, and 55–85 cm. A correction (Campbell Scientific 1996) supplied by the manufacturer was applied to the soil moisture data collected from TDR-based sensors to remove bias from air and soil temperature and then the data were further smoothed with a 24 h moving window average. The capacitance-based sensors were corrected to the TDR-based sensors during periods of soil saturation when sensor values plateaued.

Soil matric potential was measured by field tensiometers (Model T4, UMS, Pullman, WA) at three locations, 0.6, 4.4, and 8.2 m upslope. Tensiometers were installed to 35 cm depth and a slurry of silica flour and water was emplaced around the porous cups to ensure good contact around the base of each tensiometer with surrounding soil.

## **2.1.2. Numerical modeling experiment**

### ***2.1.2.1. Numerical model selection***

Drainage and hydrologic mass balance experiments were also done using a numerical model (HYDRUS-2D, hereafter HYDRUS; Šimůnek et al. 2012). HYDRUS is a two-dimensional finite element model that simulates transport of water, heat, and solutes through variably saturated porous media by numerically solving the Richards equation for saturated-unsaturated water flow and convection-dispersion transport (Šimůnek et al. 2012). It has been used to successfully model subsurface saturated and unsaturated flow through hillslopes (e.g., Keim et al. 2006; Hopp

and McDonnell 2009; Pangle et al. 2017). Model performance of HYDRUS was evaluated by the Nash-Sutcliffe Efficiency (NSE; Nash and Sutcliffe 1970).

### **2.1.2.2. Model parameterization and calibration and hydraulic properties of soil**

We assumed there were two soil materials: the soil model was filled primarily with a homogeneous sandy loam soil across most of the hillslope and secondarily with a pure sand just beneath the elevation of the outlet pipe at the base of the hillslope, as described in the historical experiment (Hewlett and Hibbert 1963). Default model parameters in HYDRUS were used for the sand.

For the hillslope soil, the volumetric soil water content ( $\theta$ ;  $\text{cm}^3 \text{cm}^{-3}$ ) as a function of the water pressure head ( $h$ ; cm) was estimated using the van Genuchten-Mualem model (van Genuchten 1980):

$$\theta(h) = \theta_r + \frac{(\theta_s - \theta_r)}{[1 + (\alpha h)^n]^m} \quad (1)$$

where  $\theta_r$  is the residual water content,  $\theta_s$  is the saturated water content,  $h$  is positive,  $m = 1 - 1/n$ , and  $\alpha$  and  $n$  are curve shape parameters. Four independent parameters ( $\theta_r$ ,  $\theta_s$ ,  $\alpha$ , and  $n$ ) were estimated from observed soil water retention data measured at a similar soil model that was packed with the similar soil (Hewlett 1961a). The residual ( $\theta_r$ ) and saturated water content ( $\theta_s$ ) were assumed to be 0 (Hewlett 1961a) and 53% (Experiment 1, below), respectively. Constants  $\alpha$  and  $n$  were then estimated to be  $3.44 \text{ (m}^{-1}\text{)}$  and  $1.25$  (unitless), respectively, using nonlinear least squares curve fitting. Saturated hydraulic conductivity ( $K_s$ ;  $\text{m d}^{-1}$ ) was assumed to be 2.1

(Steenhuis et al. 1999), and pore-connectivity ( $l$ ; unitless) was assumed to be 0.5 (Mualem 1976). Hysteresis was not considered in the numerical model because the soil model was wetted to near-saturation before being allowed to drain and, therefore, only the drying curve was used.

## **2.2. Results**

### **2.2.1. Changes in soil properties**

There were salient changes in volume and characteristics of the soil in the soil model since the historical experiment, which suggested some combination of weathering, settling and/or compaction, and erosional loss (particulate or soluble) processes (Table 2.2). Soil depth ranged from 71.0–87.5 cm, with depth generally decreasing toward the lower hillslope position, and the mean decreased from 91.4 in the historical experiment to 80.0 ( $\pm 2.3$ ) cm. Bulk densities ranged from 0.75–1.69 and averaged 1.23 ( $\pm 0.02$ ) g cm<sup>-3</sup>, as compared to the originally reported uniform bulk density of 1.3 g cm<sup>-3</sup> (Fig. 2.2). Particle size analysis determined that the soil we collected was silt loam (19% sand, 73% silt, and 8% clay averaged across the hillslope; Fig. 2.3), though soil was originally reported to be sandy clay loam (60% sand, 18% silt, and 22% clay). In the surface (0–10 and 10–20 cm depth) layers, mean bulk density was low (0.96  $\pm$  0.04 and 1.14  $\pm$  0.03 g cm<sup>-3</sup>, respectively; Fig. 2.2) and the mean proportion of silt was high (77.4  $\pm$  0.5 and 73.5  $\pm$  0.6 %, respectively; Fig. 2.3b) relative to the rest of the soil profile (bulk density = 1.29  $\pm$  0.02 g cm<sup>-3</sup>; proportion of silt = 72.0  $\pm$  0.3 %). Mean organic C content was high in the 0–10 cm depth layer (1.9  $\pm$  0.1%) and 10–20 cm depth layer (0.9  $\pm$  0.04%) compared to the rest of the soil profile (0.7  $\pm$  0.01%). Colonization of soil by invertebrates was visually observed, though the extent of their burrows was not quantified in order to reduce disturbance to the soil model.

Net changes in hydrologic properties appeared to be small. Lab core-based measurements of soil water retention were in near perfect agreement with historic soils, whereas in-situ measurements showed some variation due to larger water contents and concomitant higher pressure head (Fig. 2.4). Porosity, determined at multiple sensor locations by volumetric soil moisture values at saturation,  $\theta_s$  (mean  $\theta_s = 53.1 \pm 0.03\%$ ), was higher than  $\theta_s$  (49%) reported in the historical experiment (Fig. 2.4). As a reference, mean porosity, calculated from bulk density, was  $53.4 (\pm 0.01) \%$  across the hillslope in this study, an increase from the originally reported 50.9%. Analyses of soil cores taken from the surface showed  $K_s$  (geometric mean of  $11.3 \text{ cm h}^{-1}$  averaged across the hillslope in this study [Table 2.1]), which was within the range of  $8.6 \text{ cm h}^{-1}$  (Steenhuis et al. 1999) compared to  $16.8 \text{ cm h}^{-1}$  also averaged across the same hillslope in another study [Sloan and Moore 1984]).

### **2.2.2. Outflow in drainage experiments**

In the first drainage experiment (Experiment 1; Fig. 2.5), the drainage pattern for the majority of drainage was similar to that of the historical experiment for the first 10 days, with fast drainage occurring in the first 1.5 d followed by a transition to slower drainage (Fig. 2.6a); however, unlike the observations of Hewlett and Hibbert (1963), we observed a second transition point after which  $Q$  stopped at 17 d (Fig. 2.6a). During the 17 d drainage period, we estimated from soil moisture data that 744 L were lost from the hillslope; of this, 570 L were recorded at the outlet and 174 L were unaccounted for (Table 2.2). We continued to monitor soil moisture for 43 d after the cessation of  $Q$ . In the time between cessation of  $Q$  (17 d) and when we terminated the experiment (60 d), there was a decrease in mean soil moisture ( $\theta$ ) from 35.0 to 33.7 %. This suggested additional water had been lost from the hillslope. Assuming that evaporative losses

through the plastic cover were negligible, and coupled with the observation that water did not pool at the toe of the slope (Fig. 2.5), this estimated non-negligible loss suggested a potential leak in the lower boundary of the soil model. In total, 867 L were lost from the soil model over 60 d and 123 L of that were lost after  $Q$  stopped exiting the outlet pipe at 17 d. Hewlett and Hibbert (1963) reported that 1,260 L drained from the hillslope over 145 d, and 960 L of that were drained in the first 5 d. In comparison, in the first 5 d in our experiment 619 L were estimated to have drained from the hillslope, but only 440 L exited the outflow pipe.

In the second drainage experiment (Experiment 2) the drainage pattern was similar to the first drainage experiment and  $Q$  stopped after 12 d (Fig. 2.6a), confirming the reproducibility of the first experiment and also further supporting the possibility of a leak in the soil model. During this drainage period (12 d), 763 L were lost from the hillslope; of this, 460 L exited the outlet pipe and 303 L were unaccounted for and possibly lost through leakage (Table 2.2). Again, water was lost from the entire soil in the time after  $Q$  stopped (12 d; mean  $\theta = 35.4\%$ ) until the end of the experiment (48 d; mean  $\theta = 32.8\%$ ). In total, 1,011 L of water were lost from the soil over 48 d. In the first 5 d, 687 L were estimated to have drained from the hillslope, but only 410 L exited the outlet pipe. In both of our drainage experiments, the size of the saturated wedge, which remained along the soil-bedrock interface at the toeslope position, continued to diminish even after  $Q$  had stopped (Fig. 2.5).

HYDRUS simulated  $Q$  well for the historical drainage experiment (NSE = 0.89; Fig. 2.6a) because it represented the physical soil model as a homogeneous, isotropic soil, and there were no data points early in the historical drainage curve ( $T < 0.1$  d) when macropores were likely

contributing to outflow. HYDRUS did not simulate outflow well for Experiments 1 (NSE = 0.15;) and 2 (NSE = 0.0), which had more data points early in the drainage curve when there were high rates of flow. There was better agreement when the simulation for the initial 0.1 d was excluded from the model performance criterion (NSE = 0.79 and 0.75 for Experiments 1 and 2, respectively). It was possible that a dual-domain porosity representation of the hillslope would improve our results in the first 0.1 d of drainage; however, we did not have enough information to parameterize HYDRUS in this way.

Outflow was examined also by plotting the logarithms of both rates of change in recession flow,  $\log(\frac{dQ}{dT})$ , and recession flow,  $(\log[Q])$ ; Fig. 2.6b). This presentation of recession flow was introduced by Brutsaert and Nieber (1977) and was based on solutions to the Boussinesq equation (Boussinesq 1904) to describe drainage from an ideal, unconfined rectangular aquifer bounded below by a horizontal impermeable layer, and flowing laterally into a fully penetrating stream. The theory has been applied successfully in humid, steep hillslopes such as the study hillslope for the historical drainage experiment (Zecharias and Brutsaert 1988).

Short- and long-time flow regimes visually manifest themselves in the shape of the ‘lower envelope’ of log-log plotted data, depending on the slope,  $b$ . Generally, a flow regime is categorized as short-time ( $b = 3$ ), long-time ( $b = 3/2$ ), or a combination of the two ( $b = 1$ ). In a short-time flow regime,  $Q$  occurs shortly after wetting, and there is relatively high  $Q$  and  $\frac{dQ}{dT}$ . In principle, the largest flow rate would be observed if the entire hillslope were initially and uniformly saturated, as in this study. A break in the slope of a line enveloping the lower boundary of the  $\log(\frac{dQ}{dT})$  vs.  $\log(Q)$  data indicates a transition point between short- and long-time

flow. A similar claim about a transition point between fast and slow drainage from larger pores and smaller pores, respectively, was made by Hewlett and Hibbert (1963) in analyzing their drainage curve.

Drainage was similar between the historical and our experiments at high and medium flows, but was different at low flows ( $\log[Q] < 2$ , likely due to a leak (Fig. 2.6b). The average slope ( $b = 1.76$ ) of our experiments was only slightly higher than the slope ( $b = 1.65$ ) for the historical experiment, due to the inclusion of faster flow rates in the first 0.1 d of drainage. The average slope of all three experiments ( $b = 1.90$ ) was higher than for our experiments alone because data points at low-flows ( $\log[Q]$ ) from the historical experiment outweighed the impact of the higher values of  $\log\left(\frac{dQ}{dT}\right)$  when there was a leak.

### **2.2.3. Soil water potential conditions during drainage**

Soil water potential data were generally similar in our drainage experiments compared to the historical experiment and corroborated the soil moisture and  $Q$  data (Fig. 2.7a). Soil water potential (cm) was positive at the sensor located at an elevation 5 cm below the outlet, indicating the existence of a water table at nearly the same elevation as in the historical experiment.

However, after  $Q$  stopped exiting the outlet in both of our experiments the positive pressure decreased rapidly and became negative almost immediately, suggesting the persistent loss of water in the soil model through another pathway that was below the elevation of this tensiometer.

Based on the above drainage curve and water potential observations, we repeated the HYDRUS simulations with the incorporation of a leak in the lower boundary. We added a one-node

(representative of 1 cm) crack to the bottom boundary at the joint of the two concrete floors (location shown in Fig. 2.5). Doing so improved the fit between modeled (with leak) and observed drainage curves (Fig. 2.6a) for Experiment 1 (for entire time series, NSE = 0.12; for  $T > 0.1$  d, NSE = 0.84) and 2 (for entire time series, NSE = 0.0; for time  $> 0.1$  d, NSE = 0.81). Observation nodes placed at the corresponding locations of the tensiometers in the hillslope model showed similar patterns of water potential. In the numerical model, water potential was ~10 cm higher (more positive) relative to the physical experiments at upslope sample locations (137 and 278 cm above the outlet) until  $T \approx 1$  d and at the sample location below the outlet until  $T \approx 3$  d. After these respective times, water potential was less positive relative to the physical experiments, indicating a different distribution of water content and water potential spatially and temporally in the numerical experiment relative to the physical experiments. However, these differences did not appear to largely affect drainage at the outlet. Outflow ( $Q$ ) ceased after 13.8 d in the numerical experiment, which was similar to when  $Q$  ceased in the physical experiments (17 and 12 d). At the sample location below the outlet, water potential became negative at the same time and decreased at similar rates in the numerical and physical experiments.

#### **2.2.4. Additional mass balance experiments**

When the soil model was irrigated at steady state, long-term  $Q$  was approximately 71.5% of inflow over a 141 d period (Table 2.2). Simulation of irrigation at steady state in the HYDRUS model with a leak in the boundary conditions showed that modeled outflow was similar (70.1% of inflow over a 141 d period). During this steady-state irrigation period total recovery of the mass of a conservative deuterium tracer at the outlet of the soil model was also similar (70.0% of the application), thus, independently corroborating the presence and magnitude of the leak

inferred from the observed and modeled water balances. The outflow was 71.2 % when averaged over the drainage experiments and these mass balance experiments (Table 2.2).

### **2.3. Discussion**

In this study we compared the flow mechanisms during recession drainage in an idealized hillslope (Hewlett and Hibbert 1963) and in that same hillslope after more than 50 y of pedogenesis, a period over which change in physical properties increased soil complexity to better approximate natural conditions. Our major finding was that the long, slow drainage observed in the historical and seminal study was not observed in repeated experiments. Though evidence of changes in soil was found (e.g., additions of biomass, tree root networks, and insect burrows; soil profile development; soil compaction; and lessivage), their resulting impacts on the drainage pattern, described by rates of outflow, soil moisture, and soil water potential, appeared to have been quite small relative to those imposed by a leak in the lower boundary of the hillslope.

#### **2.3.1. Implications of changes to soil on subsurface flow**

The loss of soil volume since the historical experiment was likely due to processes of both compaction within the model and physical particle migration through and out of the model. The deepest subsamples consistently had a higher bulk density (Fig. 2.2), supporting the former, and there was a higher proportion of silt versus sand for downslope cores (Fig. 2.3b), supporting the latter. We calculated the upper limit of erosional loss to be 1,829.5 kg of soil, given the loss of soil depth and increase in porosity, assuming that there was no compaction and that bulk density was the mean of the historical and current measurements throughout the profile. If, instead, we

assumed a conservation of mass and no erosional loss, then mean bulk density would have to be  $1.70 \text{ g cm}^{-3}$  (though it was  $1.20 \text{ g cm}^{-3}$ ) and porosity would have to decrease to 36 % (though it was 56 %), both of which were not observed. Therefore, we conclude there was likely some combination of compaction within the model and erosional loss of soil out of the model.

Large changes to the texture and structure of the soil possibly led to increased preferential flow in this study compared to the historical experiment. Fast nonlinear flow was observed early in our drainage curves (Fig. 2.6), which incorporated additional data points in the first 0.1 d of drainage that extend the drainage curve reported in the historical experiment. However, it was unclear how the fast flow rate has changed since the historical experiment due to the absence of data points in the historical experiment. It was likely that the volume of macropore flow increased because of erosional processes and additional changes in the surface of the soil, including heterograde bulk density profiles and visual observations of root and invertebrate burrow networks. All of these changes to the soil can in turn significantly modify the pore space in the soil matrix. Aggregate formation creates macropores, and roots and invertebrates push through soil, moving particles and creating large channels, all of which are favorable for preferential flow, especially during initial wetting and drainage (Torres et al. 1998). Preferential flow can occur even without presence of visually apparent macropores (Jackson et al. 2016).

It was unclear why the observed changes in soil largely did not impact the soil water retention and moisture relationship (Fig. 2.4) nor the general drainage pattern in the first 10 d (except for possible preferential flow described above; Fig. 2.6). We hypothesize that there were competing hydrologic effects from the multiple changes in soil properties. Reduction in particle size from

mostly sand to mostly silt indicated weathering of soil, especially at the surface. This led to an increase in total porosity and decrease in average pore size, which should have increased water retention. Less water would be partitioned as fast flow, which moves primarily due to gravity through channel networks, and more water would be partitioned as slow flow, which occurs primarily due to capillary tension through the soil matrix. This decreases the overall hydraulic conductivity of the soil and shifts the water retention curve so that for a given volumetric water content, there is a more negative water potential (higher tension). Coincidentally, there was an introduction of vegetation and invertebrate burrows, which could have introduced pore channels that had opposing effects on the soil hydrology.

### **2.3.2. Soil particle analyses methods**

It was possible, though unlikely, there was a discrepancy in soil texture results due to different methods in particle size analyses in the historical and current studies. Hewlett and Hibbert (1963) used a hydrometer method to measure the density of a solution in which the soil particles were assumed to settle according to assumptions of Stokes' law, namely that soil particles were rigid, spherical, and smooth, rather than irregular in shape; had similar densities; were separated from each other; and did not interact during settling (Wen et al. 2002). We used a laser diffraction method to measure the diffraction of a laser light source by the soil particles in soil-water suspension, which was based on the assumption that particles of a given sample diffract light through a given angle that depends on the particle diameter.

We accepted the laser diffraction method as favorable for several reasons. The laser diffraction method was independent of the density of the individual particles, as the calculated size

distribution was based on geometry and not mass, and reduced error from incorporating such assumptions. Furthermore, the largest change between the historical study and this study was in sand content, and the two methods have been demonstrated to measure sand content equally well, with discrepancies only in the clay content (Cheetham et al. 2008; Stefano et al. 2010). Moreover, discrepancies between results from the two methods are typically mis-classification from one textural class to an adjacent class on a soil texture triangle, and not large enough to change to a non-adjacent class (Miller and Schaetzl 2012), as in this study (Fig. 2.3a). The magnitude of change that we detected in particle size distribution was large enough to overwhelm potential differences between the two methods, suggesting that there was indeed a real shift from the soil being composed of mostly sand-sized particles to mostly silt-sized particles. Such large-scale weathering from sand to silt has been observed in other humid climate systems (Pye 1983).

### **2.3.3. Implications of a leaky soil boundary condition to baseflow**

Many modeling studies have been done to reproduce the results from the historical drainage experiment, but these studies did not use the same physical hillslope model after flow domain and boundary conditions had changed over time, and so they have come to conclusions not supported by this study. Other studies developed mathematical models (both simple and complex, and either analytic or finite element) predicting subsurface flow on the study hillslope (Sloan and Moore 1984) that were later improved (Stagnitti et al. 1986; Steenhuis et al. 1999). Drainage timing and volume predicted by such mathematical models using either Richards' or Boussinesq's equation agree well with the results of the historical experiment. Other work in a replicate physical model has shown that inferences about physical processes drawn from

graphical analysis of recession curves can be misleading because they present break points that possibly do not have physical meaning (Anderson and Burt 1977; Anderson and Burt 1980). The rate of diminution of the geometric dimensions of the saturated wedge, rather than the mathematical relationship between  $Q$  and time, was argued to be a better predictor of  $Q$ . Our drainage experiments do provide clear evidence that long-term drainage cannot be fully accounted for without considering the constant contribution of water from unsaturated soil upslope to the saturated wedge (Fig. 2.5). However, these modeling studies and discussion about the progressive diminution of the saturated wedge can lead to misleading conclusions about timing and volume of drainage to the outlet if water is siphoned off through a leak in the boundary conditions.

We concluded there was a leak from the following lines of evidence:

- 1)  $Q$  stopped abruptly, despite the drainage pattern being similar to the historical drainage pattern for most of drainage (Fig. 2.6a);
- 2) Soil water potential at depths below the position of the water table shifted from positive to negative after  $Q$  stopped (Fig. 2.7);
- 3) Soil moisture continually decreased across the entire hillslope after  $Q$  stopped (Fig. 2.5);
- 4) HYDRUS model simulations of the drainage experiment replicated the observed drainage pattern and water potential after a leak was added to the boundary conditions in the model (Fig. 2.6a, 2.7b).
- 5) Water mass balance during steady state, when evaporation was minimal, indicated that irrigation was not equal to outlet discharge (Table 2.2);

- 6) Applied conservative tracer mass was not completely recovered (Table 2.2);
- 7) There was significant loss of water from the hillslope during the wetting up of both drainage experiments (Table 2.2).

This leak in the study hillslope model was analogous to bedrock fractures found in many natural watersheds. The magnitude of our leak (28.8 %; Table 2.2) was within the range of values of water loss from the soil mantle to bedrock in the Akatsu and Obara catchments (Japan), where such loss accounted for at least 18 % and 30 % of precipitation, respectively, and the relative loss decreased with increasing watershed size (Terajima et al. 1993). There was a loss of 56 to 71% of applied irrigation that flowed through fractured bedrock (Anderson et al. 1997). The loss of water was higher, accounting for 91% of irrigation water, at an experimental hillslope in the Panola Mountain Research Watershed, where the rerouting of stormflow through bedrock fractures delayed its arrival downslope by 2 days relative to stormflow that drained through the soil (Tromp-van Meerveld et al. 2007). Delayed hydrologic responses over many months or even years at low-elevation watersheds at Coweeta were suspected to be due to long flowpaths through fractured bedrock (Post and Jones 2001).

This study showed, using the same hillslope model and experimental design that led to the development of the VSA concept, that a term for leakage from surface soil should be incorporated into future models. This leakage term in our study does not invalidate the VSA concept, but rather provides further support for it. Flow along the hillslope is still connected to the stream, but cracks and fractures in bedrock can either retard or accelerate subsurface flow substantially by retaining or rerouting water. The historical drainage experiment showed, through

the VSA concept, that the areas contributing water would contract in the recession period and cause nonlinear contributions from shallow soil baseflow for a long period of time (Hewlett and Hibbert 1963). Therefore, the outflow hydrography would likely be nonlinear, as well. Although surface soil contribution to baseflow can be much shorter than previously thought in natural hillslopes, the loss of water to bedrock leakage highlights the importance of bedrock flow paths in maintaining baseflow in humid mountain systems. The rerouting of water through bedrock fractures can further increase the nonlinearity of flow during the recession period.

Other studies have shown that drainage area, microtopography, and permeability of bedrock, rather than the soil surface, can be key variables to the timing and quantity of runoff (Tani 1997; Freer et al. 2002; McGlynn and McDonnell 2003; Tromp-van Meerveld and McDonnell 2006; Lehmann et al. 2007; Hopp and McDonnell 2009). This study provides additional evidence to show how the location and size of the leak in the study hillslope impacted timing and quantity of drainage from hillslope soils. The HYDRUS model results showed that only a small leak (representative of 1 cm) in the boundary conditions was required to decrease the recession drainage period by nearly an order of magnitude, from 145 d in the historical experiment to under 14 d (Fig. 2.6a). There was a large pressure head pushing water out of the leak when the leak was placed at the bottom corner of the soil model in HYDRUS (Fig. 2.5), so that an analogous bedrock fracture in the riparian zone can disconnect the hillslope from the outlet and impact the timing of water and solute movement to the stream. However, in preliminary model runs, a leak of the same size placed at 6 m upslope along the lower boundary conditions had a negligible impact on the shape of the recession curve due to the smaller pressure head.

Our results showed that a hillslope surface soil, despite having a leaky boundary, can still move water quickly to the outlet with little impact to the beginning of the recession curve (Fig. 2.6b). Given that our drainage curves did not deviate from the historical curve until 12–17 d after the initial wetup period, the impact of the leak on timing and volume of drainage would be larger between storms than during the storm. If there are repeated storms within 12–17 d of each other, then we suspect the leak will not largely change the characteristics of the recession flow. However, drought severity and frequency at Coweeta (Laseter et al. 2012) and elsewhere in the United States (Strzepek et al. 2010) and around the world (Vicente et al. 2014; Yu et al. 2014) have increased over time due to more extreme distribution of precipitation throughout the year. Forecast increased periods of drought could severely impact baseflow where loss of water in leaky bedrock has been observed to be a significant term in the water balance (Tromp-van Meerveld et al. 2007). This suggests that some catchments may actually be less resilient, with lower potential to store water in soils over long time periods and release water gradually (Carey et al. 2010), than previously thought.

## **2.4. Conclusion**

We expected that 53 years of tree growth, litter deposition and processing, invertebrate burrowing, and associated pedogenic processes would substantially alter drainage from Hewlett and Hibbert's 1963 inclined soil model. Soil sampling and analysis did reveal the development of an A horizon, stratification of bulk densities, and increases in soil carbon. Lab measurements of moisture release curves and  $K_s$  values, however, indicated little change in soil hydraulic properties. Two repetitions of the Hewlett and Hibbert drainage experiment revealed no significant changes in the recession curve for the first 10 days. Two-dimensional numerical

modeling informed by empirically-derived soil hydraulic parameters also did not predict a change in recession behavior. These experiments raise questions about how much pedogenesis is required to effect significant changes in lateral subsurface flow behavior.

The Hewlett (1961) and Hewlett and Hibbert (1963) experiments have led hydrologists to believe that lateral downslope unsaturated flow in mountain environments can sustain stream baseflows for long periods of time. However, when we repeated the experiment in the same experimental hillslope more than 50 years later, the long, slow drainage could not be reproduced. The creation of leakage in the boundary conditions of the soil model, analogous to soil leakage into bedrock fractures, had the largest impact to the duration of drainage, reducing it by nearly an order of magnitude in our experiments compared to the original, but with little impact to the shape of the rest of the drainage curve. This suggests that leakage to bedrock, which is common in many natural hillslopes, could have larger impacts on drainage in between precipitation events, rather than immediately after an event.

## **2.5. Acknowledgements**

This research was supported, in part, by the Virginia Agricultural Experiment Station and the McIntire-Stennis Program of the U.S. Department of Agriculture (USDA) National Institute of Food and Agriculture (NIFA). Additionally, this work was supported by grants from the Virginia Water Resources and Research Center, the Edna Bailey Sussman Foundation, the USDA Forest Service, and the Institute for Critical Technology and Applied Science at Virginia Tech. The authors are grateful to the staff at Coweeta Hydrologic Laboratory for assistance and hospitality while in the field.

## Figures and Tables

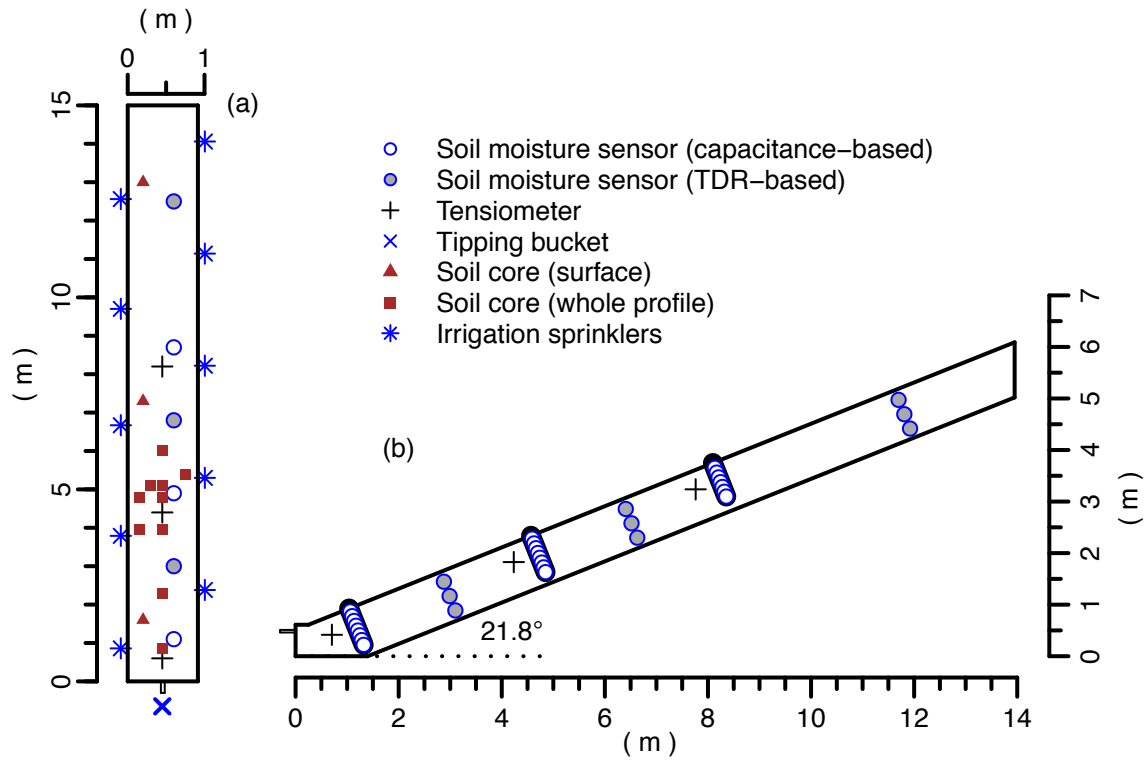


Figure 2.1. (a) Top view of the soil model with locations of monitoring instruments and soil core sampling sites. The aspect ratio is 2:1. (b) Side view of the soil model with moisture sensors and tensiometers. The aspect ratio is 1:1.

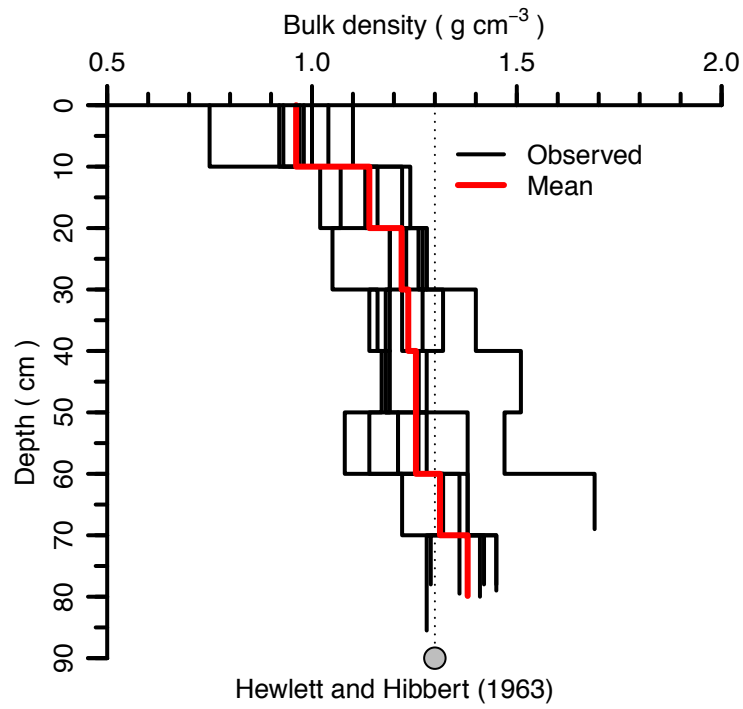


Figure 2.2. Bulk density profiles along the hillslope. The mean is shown in red and the original bulk density reported in the historical experiment (Hewlett and Hibbert 1963) is shown at the bottom.

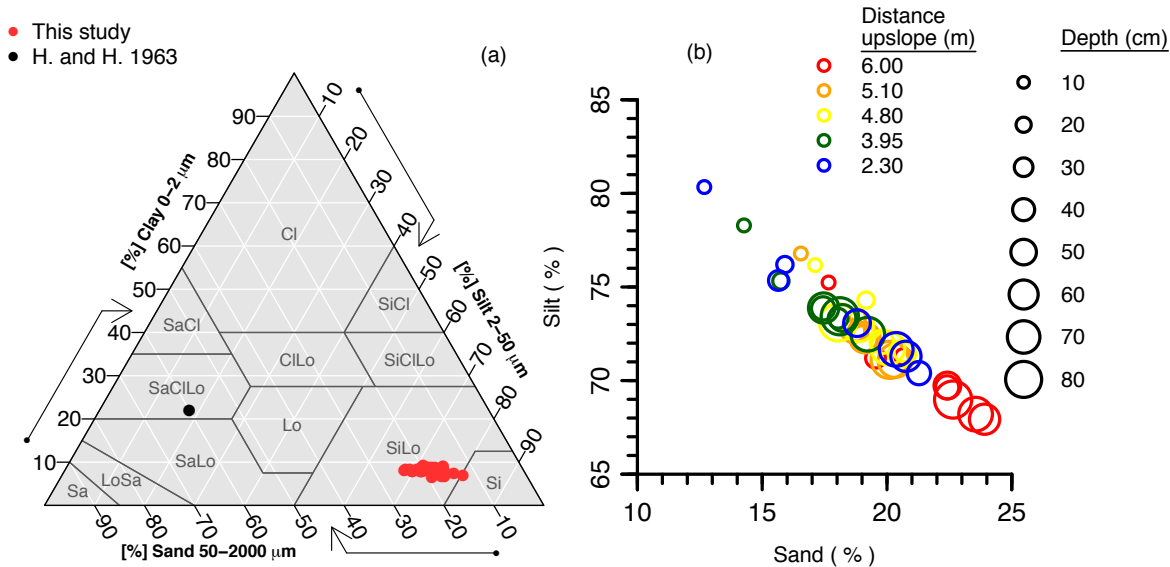


Figure 2.3. (a) Soil textural class in this study (silt loam) and reported in the historical experiment (sandy clay loam; Hewlett and Hibbert 1963) plotted on a USDA soil texture triangle. (b) Percent sand versus percent silt throughout the depth profile and across the hillslope.

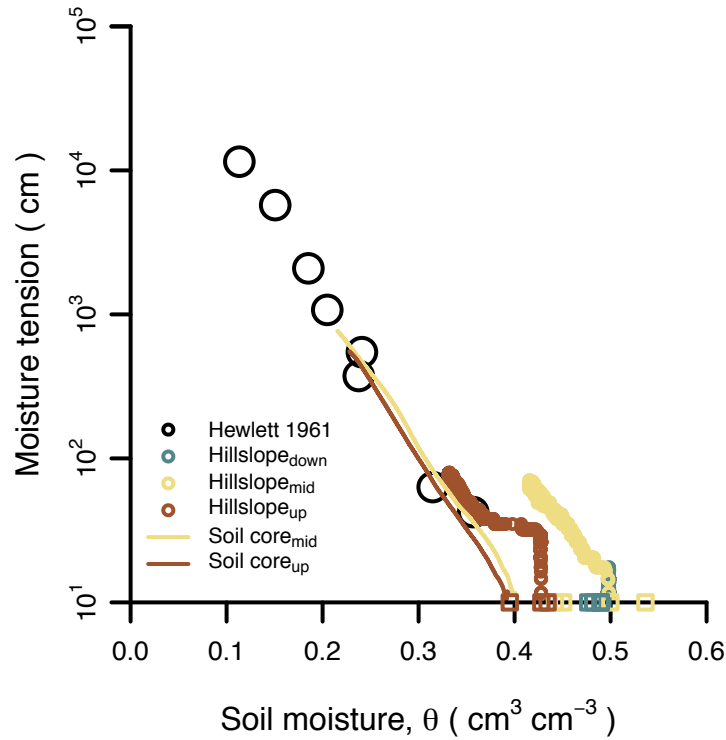


Figure 2.4. Observed and modeled soil water retention curves. Observed data include field data at a similar soil model (Hewlett 1961); paired tensiometer and soil moisture sensor data in the study hillslope (1.1 [down], 4.9 [mid], and 8.7 [up] m upslope; all 35 cm depth) for our first drainage experiment; and data from saturation experiments done in the lab to soil cores taken from the study hillslope (7.3 [mid], and 13 [up] m upslope; all 15 cm depth). Additional points placed on the x-axis show values of maximum soil moisture, when the soil model was saturated, for sensors that were in the same profile and deeper than the sensors paired with a tensiometer.

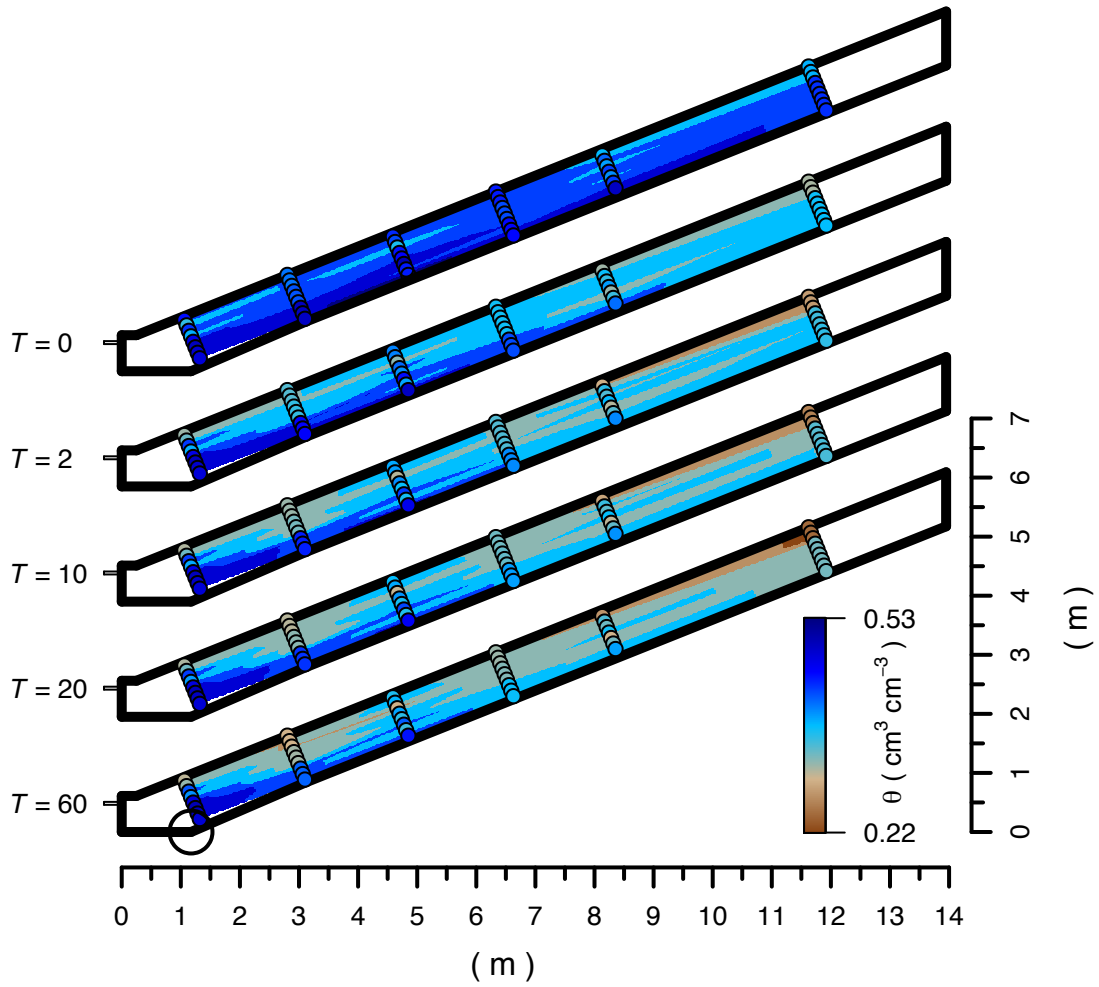


Figure 2.5. Linearly interpolated volumetric soil moisture,  $\theta$ , for our first drainage experiment (Experiment 1) at 0, 2, 10, 20, and 60 d after drainage was initiated. Small circles in the soil profile indicate locations of moisture sensors. In the bottom panel the large circle indicates the location of the leak added to select modeling runs using HYDRUS. The aspect ratio is 1:1.

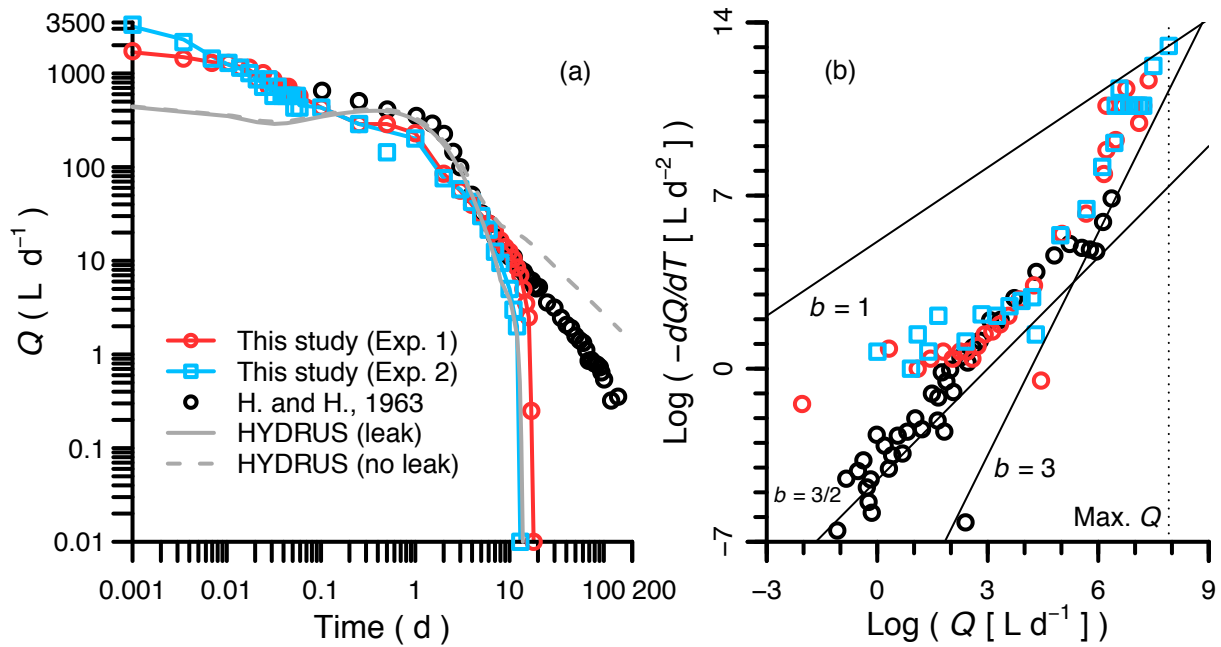


Figure 2.6. (a) Time series of outflow ( $L d^{-1}$ ) observed and modeled in this study compared to results from the historical experiment (Hewlett and Hibbert 1963). (b) Log transformed recession flow data ( $\log[Q]$  [ $L d^{-1}$ ] and  $\log[\frac{dQ}{dT}]$  [ $L d^{-2}$ ]) in this study compared to results from the historical experiment (Hewlett and Hibbert 1963). The average slope ( $b = 1.76$ ) of experiments in this study was only slightly higher than the slope ( $b = 1.65$ ) for the historical experiment, and the average slope of all three experiments ( $b = 1.90$ ) was higher than the current and historical experiments separately. Lines indicate a top envelope (slope  $b = 1$ ), two bottom envelopes (slopes  $b = 3/2$  and  $b = 3$ ), and maximum observed flow,  $Q$ .

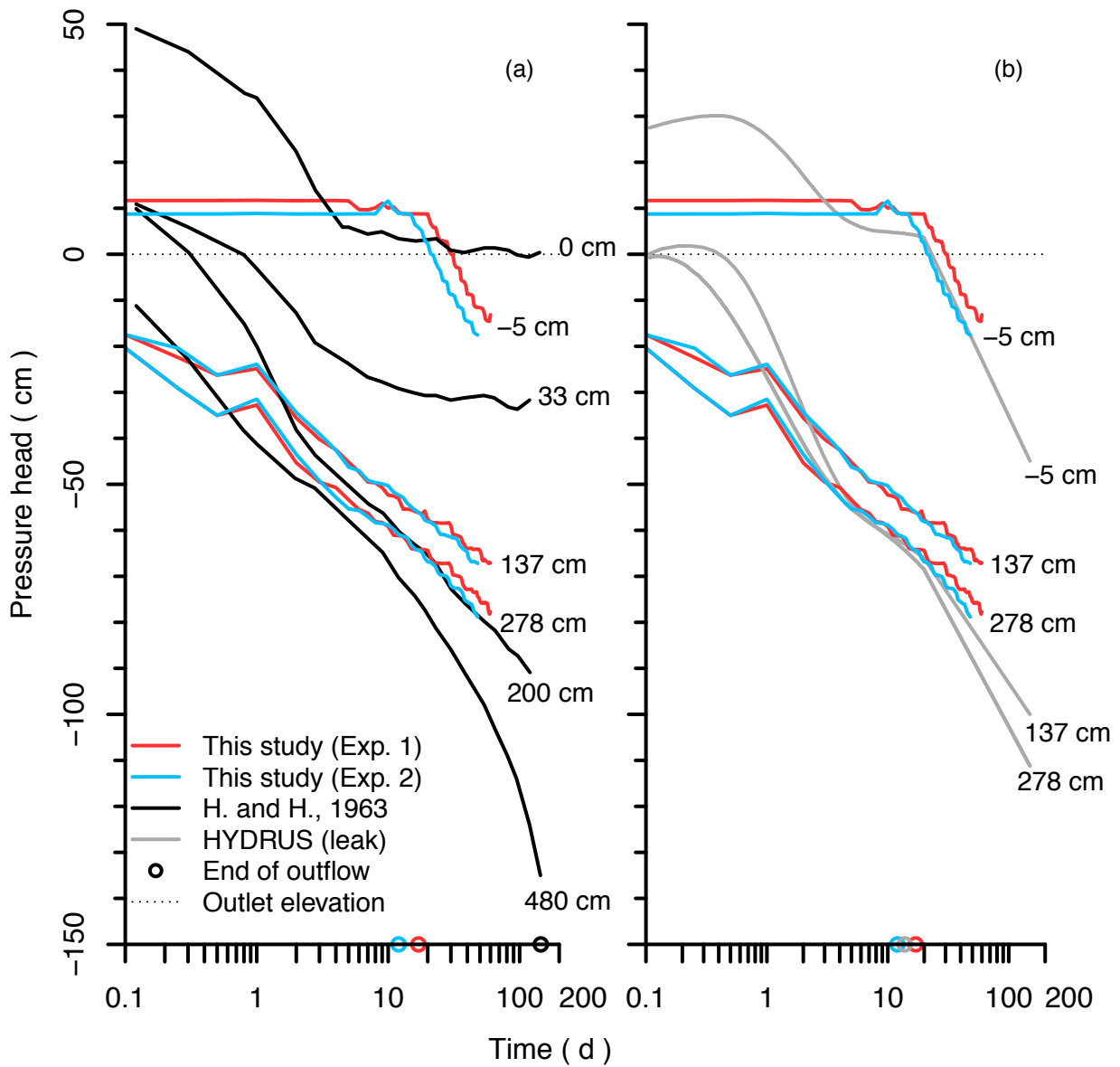


Figure 2.7. (a) Time series of pressure head (cm) at different elevations above the outlet pipe in this study compared to results from the historical experiment (Hewlett and Hibbert 1963). There were three elevations in this study and four from the historical experiment. (b) Time series of pressure head (cm) at different elevations above the outlet observed in this study compared to model results using HYDRUS (with inclusion of a leak). The observed and modeled elevations

were the same. Circle symbols on the x-axis show the times when outflow ended in each scenario.

Table 2.1. Physical and hydraulic properties of the soil in the physical and numeric (HYDRUS) soil model. Subscripts (D, M, U) indicate slope position (downslope, midslope, upslope, respectively). Standard errors are given in parentheses.

	Previous studies		This study	
	Physical	Physical	Physical	HYDRUS
Bulk density ( $\text{g cm}^{-3}$ )	1.3*	1.2 (0.02)		
Porosity (%)	50.9*	55.0 (0.01)		
Sand (%)	60*	19.0 (0.3)		
Silt (%)	18*	72.9 (0.3)		
Clay (%)	22*	8.1 (0.07)		
$\theta_r$ ( $\text{cm}^3 \text{cm}^{-3}$ )	0.0**	—		0.0
$\theta_s$ ( $\text{cm}^3 \text{cm}^{-3}$ )*	0.49**	0.49 <sub>D</sub> (0.003)		0.53
		0.50 <sub>M</sub> (0.02)		
		0.45 <sub>U</sub> (0.01)		
$K_s$ ( $\text{cm h}^{-1}$ )†	8.4‡; 8.6§	10.7 <sub>D</sub>		8.2
		19.7 <sub>M</sub>		
		6.9 <sub>U</sub>		
$a$ ( $\text{m}^{-1}$ )				3.44
$n$ (—)				1.25

\*Hewlett and Hibbert 1963. \*\*Lab values reported in Hewlett 1961. \*\*\*Values for the physical model in this study are means for in situ sensors in the bottom 30 cm of the soil profile at the time of initial drainage for both of our drainage experiments. Each slope location includes data from capacitance-based and TDR-based moisture sensors. †Values for the physical model in this study are results from cores taken from 10–15 cm depth in the soil model and then analyzed in the lab. The value for the HYDRUS model was slightly adjusted during calibration after taking initial estimates made for the whole hillslope in previous studies. ‡Zecharias and Brutsaert 1988. §Steenhuis et al. 1999.

Notes: Residual soil moisture,  $\theta_r$ , was not determined in this study because the hillslope and collected soil cores were not drained beyond permanent wilting point.

Table 2.2. Mass balances of water and conservative tracer ( $^2\text{H}_2\text{O}$ ).

Experiment	Initial storage (L)	Cumulative inflow (L)	Water removed during sampling (L)	Cumulative outflow during wetup (L)	Storage at beginning of drainage (L)	Cumulative outflow during drainage (L)	Total cumulative outflow (L)	Change in storage (L)	Residual (L)	1 – (Residual / Net inflow) × 100 (%)
Irrigation/drainage (1 <sup>st</sup> experiment)	3300	1500	0	(260)	4567	(570)	(830)	(157)	503	66.5
Irrigation/drainage (2 <sup>nd</sup> experiment)	3399	1500	0	(361.5)	4537.5	(460)	(821.5)	(330)	348.5	76.8
Irrigation/drainage (Historical experiment)			0		4449*	(1260)**				
Steady-state irrigation	3332	11775	(129)				(8484.5)	159	3320.5	71.5
		Tracer input (g)	Tracer removed during sampling (g)	Tracer collected in outflow (g)					Residual (g)	1 – (Residual / Net input) × 100 (%)
$^2\text{H}_2\text{O}$ tracer		11.06	(0.21)	(7.60)					3.25	70.0
Average leak										71.2

\*Estimated value using soil dimensions from Hewlett and Hibbert 1963 and volumetric soil moisture value from Hewlett 1961. \*\*Hewlett and Hibbert 1963.

Notes: Negative values are given in parentheses. Net inflow and net input account for water and tracer, respectively, that were removed during sampling.

## References

- Ambroise, B. 2004. Variable 'active' versus 'contributing' areas or periods: a necessary distinction. *Hydrological Processes*, 18: 1149–1155.
- Ameli, A. A., N. Amvrosiadi, T. Grabs, H. Laudon, I. F. Creed, J. J. McDonnell, and K. Bishop. 2016. Hillslope permeability architecture controls on subsurface transit time distribution and flow paths. *Journal of Hydrology*, 543: 17–30.
- Anderson, M. G., and T. P. Burt. 1977. A laboratory model to investigate the soil moisture conditions on a draining slope. *Journal of Hydrology*, 33: 383–390.
- . 1980. Interpretation of recession flow. *Journal of Hydrology*, 46: 89–101.
- Anderson, S. P., W. E. Dietrich, D. R. Montgomery, R. Torres, M. E. Conrad, and K. Loague. 1997. Subsurface flow paths in a steep, unchanneled catchment. *Water Resources Research*, 33: 2637–2653.
- Ankenbauer, K., and S. P. Loheide. 2016. The effects of soil organic matter on soil water retention and plant water use in a meadow of the Sierra Nevada, CA. *Hydrological Processes*, 31: 891–901.
- Appels, W. M., C. B. Graham, J. E. Freer, and J. J. McDonnell. 2015. Factors affecting the spatial pattern of bedrock groundwater recharge at the hillslope scale. *Hydrological Processes*, 29: 4594–4610.
- Bernier, P. Y. 1985. Variable source areas and storm-flow generation: an update of the concept and a simulation effort. *Journal of Hydrology*, 79: 195–213.
- Beven, K. 1982. On subsurface stormflow: An analysis of response times. *Hydrological sciences journal*, 27: 505–521.
- Beven, K. and P. Germann. 1982. Macropores and water flow in soils. *Water Resources Research*, 18: 1311–1325.
- Beven, K. J. and M. J. Kirkby. 1979. A physically based, variable contributing area model of basin hydrology / Un modèle à base physique de zone d'appel variable de l'hydrologie du bassin versant. *Hydrological Sciences Journal*, 24: 43–69.
- Bonell, M. 1998. Selected challenges in runoff generation research in forests from the hillslope to headwater drainage basin scale. *Journal of the American Water Resources Association*, 34: 765–785.
- Boussinesq, J. 1904. Recherches théoriques sur l'écoulement des nappes d'eau infiltrées dans le sol et sur le débit des sources. *Journal de Mathématiques Pures et Appliquées*, 10: 5–78.

- Brutsaert, W., and Nieber, J.L. 1977. Regionalized drought flow hydrographs from a mature glaciated plateau. *Water Resources Research*, 3: 637–643.
- Campbell Scientific. 1996. Instruction manual. CS615 Water Content Reflectometer. Campbell Scientific, Logan, UT.
- Carey, S. K., D. Tetzlaff, J. Seibert, C. Soulsby, J. Buttle, H. Laudon, J. McDonnell, K. McGuire, D. Caissie, J. Shanley, M. Kennedy, K. Devito, and J. W. Pomeroy. 2010. Inter-comparison of hydro-climatic regimes across northern catchments: synchronicity, resistance and resilience. *Hydrological Processes*, 24: 3591–3602.
- Cheetham, M. D., A. F. Keene, R. T. Bush, L. A. Sullivan, and W. D. Erskine. 2008. A comparison of grain-size analysis methods for sand-dominated fluvial sediments. *Sedimentology*, 55: 1905–1913.
- Clothier, B. E., S. R. Green, and M. Deurer. 2008. Preferential flow and transport in soil: progress and prognosis. *European Journal of Soil Science*, 59: 2–13.
- Dunne, T. 1983. Relation of field studies and modeling in the prediction of storm runoff. *Journal of Hydrology*, 65: 25–48.
- Dunne, T. and R. D. Black. 1970. Partial area contributions to storm runoff in a small New England watershed. *Water Resources Research*, 6: 1296–1311.
- Elder, K., Marshall, H. P., Elder, L., Starr, B., Karlson, A., and J. Robertson. 2014. Design and installation of a tipping bucket snow lysimeter. Proceedings, International Snow Science Workshop. Banff.
- Elsenbeer, H. (2001). Hydrologic flowpaths in tropical rainforest soils— a review. *Hydrological Processes*, 15(10), 1751-1759.
- Frankenberger, J. R., E. S. Brooks, M. T. Walter, M. F. Walter, and T. S. Steenhuis. 1999. A GIS-based variable source area hydrology model. *Hydrological Processes*, 13: 805–822.
- Freer, J., J. J. McDonnell, K. J. Beven, N. E. Peters, D. A. Burns, R. P. Hooper, B. Aulenbach, and C. Kendall. 2002. The role of bedrock topography on subsurface storm flow. *Water Resources Research*, 38: 1269.
- Freeze, A. 1972. Role of subsurface flow in generating surface runoff 2. Upstream source areas. *Water Resources Research*, 8: 1272–1283.
- Gabrielli, C. P., U. Morgenstern, M. K. Stewart, and J. J. McDonnell. 2018. Contrasting groundwater and streamflow ages at the Maimai Watershed. *Water Resources Research*, 54: 3937–3957.

- Genereux, D. P., and H. F. Hemond. 1990. Three-component tracer model for stormflow on a small Appalachian forested catchment—comment. *Journal of Hydrology*, 117: 377–380.
- Golden, H. E., C. R. Lane, D. M. Amaty, K. W. Bandilla, H. R. Kiperwas, C. D. Knightes, and H. Ssegane. 2014. Hydrologic connectivity between geographically isolated wetlands and surface water systems: A review of select modeling methods. *Environmental Modelling and Software*, 53: 190–206.
- Hale, V. C., and J. J. McDonnell. 2016. Effect of bedrock permeability on stream base flow mean transit time scaling relations: 1. A multiscale catchment intercomparison. *Water Resources Research*, 52: 1358–1374.
- Harr, R. D. 1977. Water flux in soil and subsoil on a steep forested slope. *Journal of Hydrology*, 33: 37–58.
- Hendrickx, J. M. H., and M. Flurry. Uniform and preferential flow mechanisms in the vadose zone, in *Conceptual Models of Flow and Transport in the Fractured Vadose Zone*, edited by National Research Council, pp. 163–209, Natl. Acad., Washington, D. C., 2001.
- Hewlett, J. D. 1961a. Soil moisture as a source of base flow from steep mountain watersheds. U.S. Forest Service, Southeastern Forest Experiment Station Paper 132, 11 pp.
- . 1961b. Watershed management. Pp.61 – 66. In: Report for 1961 Southeastern Forest Expt. Sta. Asheville, N.C. USDA Forest Serv., Southeastern Forest Expt. Sta.
- Hewlett, J. D. and A. R. Hibbert. 1963. Moisture and energy conditions within a sloping soil mass during drainage. *Journal of Geophysical Research*, 68: 1081–1087.
- . 1967. Factors affecting the response of small watersheds to precipitation in humid areas. pp. 275–290. In: *Forest Hydrology*. eds. Sopper, W. E. and Lull, H. W., Pergamon Press, New York.
- Hopp, L. and J. J. McDonnell. 2009. Connectivity at the hillslope scale: identifying interactions between storm size, bedrock permeability, slope angle and soil depth. *Journal of Hydrology*, 376: 378–391.
- Jackson, C. R., E. Du, J. Klaus, N. A. Griffiths, M. Bitew, and J. J. McDonnell. 2016. Interactions among hydraulic conductivity distributions, subsurface topography, and transport thresholds revealed by a multitracer hillslope irrigation experiment. *Water Resources Research*, 52: 6186–6206.
- Keim, R. F., H. J. Tromp-van Meerveld, and J. J. McDonnell. 2006. A virtual

- experiment on the effects of evaporation and intensity smoothing by canopy interception on subsurface stormflow generation. *Journal of Hydrology*, 327: 352–364.
- Kirkby, M. 1988. Hillslope runoff processes and models. *Journal of Hydrology*, 100: 315–339.
- Klaus, J. and C. R. Jackson. 2018. Interflow is not binary: A continuous shallow perched layer does not imply continuous connectivity. *Water Resources Research*, 54. <https://doi.org/10.1029/2018WR022920>.
- Laseter, S. H., C. R. Ford, J. M. Vose, and L. W. Swift, Jr. 2012. Long-term temperature and precipitation trends at the Coweeta Hydrologic Laboratory, Otto, North Carolina, USA. *Hydrology Research*, 43.6: 890–901.
- Lehmann, P., C. Hinz, G. McGrath, H. J. Tromp-van Meerveld, and J. J. McDonnell. 2007. Rainfall threshold for hillslope outflow: an emergent property of flow pathway connectivity. *Hydrology and Earth System Sciences*, 11: 1047–1063.
- Lyon, S. W., M. T. Walter, P. Gérard-Marchant, and T. S. Steenhuis. 2004. Using a topographic index to distribute variable source area runoff predicted with the SCS curve-number equation. *Hydrological Processes*, 18: 2757–2771.
- McGlynn, B. L., and J. J. McDonnell. 2003. Quantifying the relative contributions of riparian and hillslope zones to catchment runoff. *Water Resources Research*, 39: 1310.
- McGuire, K. J., and J. J. McDonnell. 2010. Hydrological connectivity of hillslopes and streams: characteristic time scales and nonlinearities. *Water Resources Research*, 46: W10543.
- Miller, B. A., and R. J. Schaetzl. 2012. Precision of soil particle size analysis using laser diffractometry. *Soil Science Society of America Journal*, 76: 1719–1727.
- Moore, R. D. 1997. Storage-outflow modeling of streamflow recessions, with application to a shallow-soil forested catchment. *Journal of Hydrology*, 198: 260–270.
- Mosley, M. P. 1979. Streamflow generation in a forested watershed, New Zealand. *Water Resources Research*, 15: 795–806.
- Mualem, Y. 1976. A new model for predicting the hydraulic conductivity of unsaturated porous media. *Water Resources Research*, 12: 513–522.
- Nash, J. E. and J. V. Sutcliffe. 1970. River flow forecasting through conceptual models, Part 1—A discussion of principles. *Journal of Hydrology*, 10: 282–290.

- Nippgen, F., B. L. McGlynn, and R. E. Emanuel. 2015. The spatial and temporal evolution of contributing areas. *Water Resources Research*, 51: 4550–4573.
- Pangle, L. A., M. Kim, C. Cardoso, M. Lora, A. A. M. Neto, T. H. M. Volkmann, Y. Wang, P. A. Troch, and C. J. Harman. 2017. The mechanistic basis for storage-dependent age distributions of water discharged from an experimental hillslope. *Water Resources Research*, 53: 2733–2754.
- Peters, A., and Durner, W. (2008). Simplified evaporation method for determining soil hydraulic properties. *Journal of Hydrology*, 356(1-2), 147-162.
- Pfister, L., N. Martínez-Carreras, C. Hissler, J. Klaus, G. E. Carrer, M. K. Stewart, and J. J. McDonnell. 2017. Bedrock geology controls on catchment storage, mixing, and release: a comparative analysis of 16 nested catchments. *Hydrological Processes*, 31: 1828–1845.
- Post, D. A., and J. A. Jones. 2001. Hydrologic regimes of forested, mountainous, headwater basins in New Hampshire, North Carolina, Oregon, and Puerto Rico. *Advances in Water Resources*, 24: 1195–1210.
- Pye, K. 1983. Formation of quartz silt during humid tropical weathering of dune sands. *Sedimentary Geology*, 34: 267–282.
- Reynolds, W. D., D. E. Elrick, E. G. Youngs, H. W. G. Booltink, and J. Bouma. 2002. Saturated and field saturated water flow parameters: Laboratory methods. In *Methods of Soil Analysis Part 4, Physical Methods*, SSSA Book Ser., vol. 5, Dane, J. H. and J. W. Hopmans (eds). Soil Science Society of America: Madison, WI; 688–690.
- Rothacher, J. 1965. Streamflow from small watersheds on the western slope of the Cascade Range of Oregon. *Water Resources Research*, 1: 125–134.
- Scholl, D. G., and A. R. Hibbert. 1973. Unsaturated flow properties used to predict outflow and evapotranspiration from a sloping lysimeter. *Water Resources Research*, 9: 1645–1655.
- Šimůnek, J., M. Th. Van Genuchten, and M. Šejna. 2012. The HYDRUS Software Package for Simulating Two- and Three-Dimensional Movement of Water, Heat, and Multiple Solutes in Variably-Saturated Porous Media, Technical Manual, Version 2.0, PC Progress, Prague, Czech Republic, pp. 258.
- Sloan, P. G. and I. D. Moore. 1984. Modeling subsurface stormflow on steeply sloping forested watersheds. *Water Resources Research*, 20(12): 1815–1822.
- Stagnitti, F., M. B. Parlange, T. S. Steenhuis, and J.-Y. Parlange. 1986. Drainage from a uniform soil layer on a hillslope. *Water Resources Research*, 22: 631–634.

- Steenhuis, T. S., J.-Y. Parlange, W. E. Sanford, A. Heilig, F. Stagnitti, and M. F. Walter. 1999. Can we distinguish Richards' and Boussinesq's equations for hillslopes?: the Coweeta experiment revisited. *Water Resources Research*, 35: 589–593.
- Di Stefano, C., V. Ferro, and S. Mirabile. 2010. Comparison between grain-size analyses using laser diffraction and sedimentation methods. *Biosystems Engineering*, 106: 205–215.
- Strzepek, K., G. Yohe, J. Neumann, and B. Boehlert. 2010. Characterizing changes in drought risk for the United States from climate change. *Environmental Research Letters*, 5: 044012. doi: 10.1088/1748-9326/5/4/044012.
- Tani, M. 1997. Runoff generation processes estimated from hydrological observations on a steep forested hillslope with a thin soil layer. *Journal of Hydrology*, 200: 84–109.
- Terajima T., A. Mori, and H. Ishii. 1993. Comparative study of deep percolation amount in two small catchments in granitic mountain. *Japanese Journal of Hydrological Sciences*, 23: 105–118.
- Torres, R., W. E. Dietrich, D. R. Montgomery, S. P. Anderson, and K. Loague. 1998. Unsaturated zone processes and the hydrologic response of a steep, unchanneled catchment. *Water Resources Research*, 34: 1865–1879.
- Tromp-van Meerveld, H. J., and J. J. McDonnell. 2006. Threshold relations in subsurface stormflow: 2. The fill and spill hypothesis. *Water Resources Research*, 42: W02411.
- Tromp-van Meerveld, H. J., N. E. Peters, and J. J. McDonnell. 2007. Effect of bedrock permeability on subsurface stormflow and the water balance of a trenched hillslope at the Panola Mountain Research Watershed, Georgia, USA. *Hydrological Processes*, 21: 750 – 769.
- van Geldern, R. and J. A. C. Barth. 2012. Optimization of instrument setup and post-run corrections for oxygen and hydrogen stable isotope measurements of water by isotope ratio infrared spectroscopy (IRIS). *Limnology and Oceanography: Methods*, 10: 1024–1036.
- van Genuchten, M. T. 1980. A closed-form equation for predicting the hydraulic conductivity of unsaturated soils. *Soil Science Society of America Journal*, 44: 892–898.
- Vicente-Serrano, S. M., J.-I. Lopez-Moreno, S. Beguería, J. Lorenzo-Lacruz, A. Sanchez-Lorenzo, J. M. García-Ruiz, C. Azorin-Molina, E. Morán-Tejeda, J. Revuelto, R. Trigo, F. Coelho, and F. Espejo. 2014. Evidence of increasing drought severity caused by temperature rise in southern Europe. *Environmental Research Letters*, 9: 044001. doi: 10.1088/1748-9326/9/4/044001.

- Ward, R. C. 1984. On the response to precipitation of headwater streams in humid areas. *Journal of Hydrology*, 74: 171–189.
- Weiler, M., J. J. McDonnell, I. Tromp-van Meerveld, and T. Uchida. 2005. Subsurface stormflow runoff generation processes. In *Encyclopedia of Hydrological Sciences*, Anderson M. G. (Ed.), John Wiley & Sons Ltd, pp. 1719–1732.
- Wen, B., A. Aydin, and N. S. Duzgoren-Aydin. 2002. A comparative study of particle size analyses by sieve-hydrometer and laser diffraction methods. *Geotechnical Testing Journal*, 25: 434–442.
- Weyman, D. R. 1973. Measurements of the downslope flow of water in a soil. *Journal of Hydrology*, 20: 267–288.
- Wolock, D. M. and G. J. McCabe, Jr. 1995. Comparison of single and multiple flow direction algorithms for computing topographic parameters in TOPMODEL. *Water Resources Research*, 31: 1315–1324.
- Yu, M., Q. Li, M. J. Hayes, M. D. Svoboda, and R. R. Heim. 2014. Are droughts becoming more frequent or severe in China based on the Standardized Precipitation Evapotranspiration Index: 1951–2010? *International Journal of Climatology*, 34: 545–558.
- Zaslavsky, D. and G. Sinai. 1981. Surface hydrology: IV. Flow in sloping layered soil, *Journal of the Hydraulics Division*, 107: 53–64.
- Zecharias, Y.B., and W. Brutsaert. 1988. Recession characteristics of groundwater outflow and baseflow from mountainous watersheds. *Water Resources Research*: 24: 1651–1658.

### Chapter 3: Transport of a $^{15}\text{NO}_3^-$ tracer along an experimental hillslope and evidence for coupled nitrification-denitrification

**Authors:** Raymond M. Lee<sup>1\*</sup>, Brian D. Strahm<sup>1</sup>, Kevin J. McGuire<sup>1,2</sup>, Jennifer D. Knoepp<sup>3</sup>, Durelle T. Scott<sup>4</sup>

<sup>1</sup>Department of Forest Resources and Environmental Conservation, Virginia Tech, Blacksburg, VA 24061, USA

<sup>2</sup>Virginia Water Resources Research Center, Virginia Tech, Blacksburg, VA 24061, USA

<sup>3</sup>Coweeta Hydrologic Laboratory, USDA Forest Service, Otto, NC 28763, USA

<sup>4</sup>Department of Biological Systems Engineering, Virginia Tech, Blacksburg, VA 24061, USA

**Abstract:** Nitrate ( $\text{NO}_3^-$ ) export can vary widely among watersheds with similar nitrogen loading, geology, and vegetation because of differing internal retention mechanisms. We utilized a constructed experimental hillslope model at Coweeta Hydrologic Laboratory to conduct a coupled stable isotope tracer experiment and show where and when there was retention or removal of  $\text{NO}_3^-$  relative to conservative movement of  $\text{NO}_3^-$ . We used soil lysimeters to track the transport of a  $^{15}\text{NO}_3^-$  tracer relative to a  $^2\text{H}_2\text{O}$  tracer through the soil subsurface and quantify any lags in breakthrough. After application of the tracer, a portion of the  $^{15}\text{NO}_3^-$  tracer passed vertically through the highly retentive and biologically active soil surface layer then began moving laterally after ~16 d. There was a noticeable separation in tracer breakthrough curves, as the peaks in  $\delta^{15}\text{N}$  were delayed relative to the peaks in  $\delta^2\text{H}$  by 1, 6, 9 and 18.5 d for slope distances of 0, 2, 4, and 5 m, respectively, from tracer addition to the outlet. The peak in  $\delta^{15}\text{N}$  breakthrough at the deep (65 cm) lysimeter located where the tracer was added was 86 times larger compared to the peak at the outlet, though the peak in

$\delta^2\text{H}$  breakthrough was nearly an order of magnitude smaller (only 9.5 times difference) when comparing data at the same locations. We estimated nitrification and denitrification fluxes using an isotope mixing model and mass balance approach in the saturated riparian zone. Nitrification and denitrification fluxes were nearly equal and were more than six times larger than lateral input and output fluxes in throughflow. Multiple retention and removal mechanisms can significantly delay export of added  $\text{NO}_3^-$  on a hillslope, with implications of high sink strength at the watershed scale.

**Keywords:** steady state hydrology; tracer experiment; nutrient cycling; nitrate; deuterium

### 3.0. Introduction

Fate and transport of nitrate ( $\text{NO}_3^-$ ) in a forest ecosystem can indicate if there has been a shift in how the forest functions as a net  $\text{NO}_3^-$  sink or source (Aber et al. 2003) and also elucidate biological consequences (e.g., algal production) in receiving lotic and lentic systems (Dodds and Smith 2016). However, mechanisms controlling fate and transport of  $\text{NO}_3^-$  are not well understood because few studies have experimentally tracked them all the way from the hillslope to the stream. Many studies investigate retention processes at the smaller core or plot scale, or measure stream water  $\text{NO}_3^-$  concentrations at the outlet and then infer potential processes at larger scales or for the watershed.

Given that we do not fully understand the combined interactions of  $\text{NO}_3^-$  process mechanisms, export of  $\text{NO}_3^-$  from watersheds is highly unpredictable. The standard conceptual model of N processing suggests that N export should increase as rates of biomass accumulation slow during late stages of succession in mature forests, though there is evidence to the contrary. There are no clear monotonic trends of  $\text{NO}_3^-$  export in reference forests (Argerich et al. 2013). Stream water  $\text{NO}_3^-$  concentrations increased in highly disturbed forests (e.g., forests that receive high inorganic N deposition [Watmough et al. 2005] or experienced destructive insect pest outbreaks [Rhoades et al. 2017]); yet, there are consistent, decadal decreases in stream water  $\text{NO}_3^-$  concentrations in other moderately disturbed forests (Goodale et al. 2005; Lucas et al. 2016). These different observations of timing and mass of N export suggest we must focus on internal N cycling processes in soil, rather than limit our focus to external N additions and stream water export. In homeostatic mature forests, the unexpected decreases in  $\text{NO}_3^-$  export cannot be due only to biologically mediated mechanisms that increase storage of N in biologically active surface soils

(immobilization) and vegetation. A proposed revision to this conceptual model highlights the role of the mineral soil horizons as an important retention sink (Lovett et al. 2018). Additionally, denitrification processes are important because they remove N from soils altogether (Goodale et al. 2005; Lucas et al. 2016).

Ultimately, conversion of a headwater forest from a  $\text{NO}_3^-$  sink to source depends on the net effects of competing and interacting biogeochemical and hydrological processes that either retain or transport the  $\text{NO}_3^-$  in the hillslope (Burt and Pinay 2005). Cumulative export of  $\text{NO}_3^-$  from hillslopes to the stream can then be scaled up to express total export of  $\text{NO}_3^-$  from the landscape. Different locations on the hillslope can play different roles in the formation of hot spots and hot moments (cf. McClain et al. 2003), where and when disproportionately large rates of reactions (e.g., nitrification, denitrification) can rapidly occur. When a hot spot is coupled with a hydrologic transport mechanism so that the hot spot reactions impact the dynamics of the ecosystem, then the hot spot is considered an ecosystem control point (Bernhardt et al. 2017). A potential hot spot alone may not largely impact ecosystem functioning because hydrologic transport rates control mobilization of N, translocating N from upslope to initiate the abovementioned reactions or translocating N downslope to cease these reactions and then potentially impact other regions of the landscape.

The coupling of biogeochemical processing and hydrologic transport rates is spatially and temporally variable. Nitrification hot spots, attributed to heterotrophic fungi, autotrophs, or acid-tolerant chemolithotrophs, are scattered across the forest landscape (Peterjohn et al. 1996; Burt and Pinay 2005; Morse et al. 2015). Nitrate can be processed in hot spots in uplands, where there

is large variability in processing rates (e.g., uptake, mineralization, and nitrification), vegetation type and density, moisture availability, and soil properties (Burt and Pinay 2005). Understanding  $\text{NO}_3^-$  dynamics at the hillslope to stream interface is critical because there is generally a transition to higher soil moisture and increased transport of nutrients from upslope, the combination of which can rapidly initiate microbial reactions. Flowpaths in uplands transport  $\text{NO}_3^-$  to the riparian zone, where  $\text{NO}_3^-$  can be exported (Hill et al. 2000; Ross et al. 2012) or denitrified rapidly if suitable redox conditions are met in anaerobic microzones (Ocampo et al. 2006). Other topographic features of watersheds, such as convergent hillslopes, can also experience transient saturation and become anoxic (Duncan et al. 2013), triggering denitrification and converting it from a source to sink.

We conducted a controlled experiment in which the journey of a  $\text{NO}_3^-$  hot spot was directly monitored from hillslope to stream. We added an isotopically labeled  $\text{NO}_3^-$  tracer ( $^{15}\text{NO}_3^-$ ) on an experimental hillslope and used a series of lysimeters to track its course relative to a conservative water tracer ( $^2\text{H}_2\text{O}$ , later recovered as  $^2\text{H}-^{16}\text{O}-^2\text{H}$  and hereafter referred to as  $^2\text{H}$ ) along a 5 m stretch of hillslope down through a riparian zone with a permanent water table exiting into a stream. The dual tracer allowed us to make inferences about retention processes as the  $^2\text{H}$  was the control for conservative transport of a solute (Becker and Coplen 2001) and also elucidated water transport dynamics along the hillslope. Through this experiment we answered the following research questions: What is the timing of a conservative tracer moving through the hillslope? Is there a delay in movement of the  $^{15}\text{NO}_3^-$  tracer compared to the conservative tracer? Where and why does it occur? What roles do nitrification and denitrification play?

### 3.1. Methods

#### 3.1.1. Study site

The Coweeta Hydrologic Laboratory of the USDA Forest Service Southern Research Station (hereafter Coweeta) is a forested watershed in the southern Appalachian Mountain Range of southwestern North Carolina. The 55-year-old experimental hillslope model at Coweeta is a concrete-lined planar trough ( $0.91 \times 0.91 \times 15.0$  m) that was packed with sieved C horizon soil, which was homogenous, well-mixed, and packed to a bulk density of  $1.3 \text{ g cm}^{-3}$  (Hewlett and Hibbert 1963). Soil in the model was the C horizon of a Saunook soil series (previously known as Halewood), which is a sandy loam that averages 60% sand, 18% silt, and 22% clay. There are two segments: a hillslope segment built at a 40% ( $21.8^\circ$ ) slope and a toeslope segment that is flat, extending 0.3 m and representing a constructed riparian zone (Fig. 3.1). The riparian zone was filled with a mixture of sand and gravel to simulate stream bank conditions and to allow drainage. Water exited through an outflow pipe 0.46 m above the ground and represented the input to a stream. Following the hydrologic experiments for which it was originally constructed (Hewlett and Hibbert 1963), the model sat undisturbed for nearly 50 years.

Before starting the experiment, we modified state conditions at the model in order to control all aspects of the hydrological cycle, including inputs (irrigation; exclusion of rain) and outputs (transpiration). In 2012, four trees (up to 40 cm ground line diameter) that had grown in the model were cut at the base and tops removed. The model was devegetated throughout the experiment by applying herbicide before, but not during, the experiment to control for variability in soil-plant interactions (e.g., transpiration and uptake of tracers and N). During autumn leaf fall before the start of the experiment, leaf litter was collected over an adjacent surface area equal to

the model and added evenly across the model surface. The model was also covered by a curved plastic (laminated reinforced polyethylene) shelter ~2 m high and open at the top and bottom ends of the model to allow airflow across the surface of the model. This shelter prevented meteoric water input while allowing gaseous exchange between the soil and atmosphere, and also allowing transmission of 83% of incoming diffuse light.

The model was irrigated to maintain hydrologic steady state and constant soil moisture content for the entire experiment. The irrigation sprinkler system was designed with 10 spray nozzles mounted on 30 cm risers that were oriented vertically to the water supply line, which ran parallel to the model down both sides. The risers were pulled over and tied down across the model so that spray nozzles sprayed at the soil from ~20 cm above the soil surface and water loss due to overspray was minimized. Spray nozzles were calibrated to deliver water to the model surface at a consistent rate across the entire model. Irrigation water was sourced from a local chlorinated groundwater well and was treated by dual activated carbon and reverse osmosis filters prior to irrigation. Filters were changed before but not during the experiment. The goal of treatment was to remove a majority of ions and return the water to conditions similar to local throughfall. We measured pH and major ion concentrations of the irrigation water before and during the experiment. Mean values were: pH = 6.5; electrical conductivity = 5.65  $\mu\text{S}$ ;  $\text{NO}_3^- = 0.02 \text{ mg L}^{-1}$ ; chloride = 0.07  $\text{mg L}^{-1}$ ; sulfate = 0.25  $\text{mg L}^{-1}$ ; calcium = 0.36  $\text{mg L}^{-1}$ .

The soil model was considered to be at hydrologic steady state when inflow and outflow were stable on a daily timestep and there was no change in storage. The daily irrigation rate (6.1 mm  $\text{d}^{-1}$ ; 86  $\text{L d}^{-1}$ ) was high, as it was similar to the mean daily average gross precipitation rate (6.5

mm d<sup>-1</sup>; 89 L d<sup>-1</sup>) in the wettest year on record at low elevation in the Coweeta basin, and also equal to the mean daily average precipitation rate at high elevation (Laseter et al. 2012). Input was monitored with an in-line flow meter (25 mL resolution) installed in the irrigation line, and was also occasionally verified with tipping bucket rain gauges (Model ECRN-100, Meter, Pullman, WA; 4 mL resolution). Outflow was measured by a tipping bucket (Snowmetrics, Fort Collins, CO; Elder et al. 2014; 500 mL resolution) at the outlet. Potential evapotranspiration was calculated using data from a meteorological station (Models VP-3, PYR, and Davis Cup Anemometer; Meter, Pullman, WA) at the hillslope and a simplified Penman equation (Valiantzas 2006). Potential evapotranspiration was low (14 % of inflow) and actual evapotranspiration was assumed to be negligible for several reasons: irrigating only once at a cooler time of the day (08:00) minimized exposure of wet soil to the warm atmosphere; the shelter minimized interaction with wind; and there was no live vegetation to transpire water. There was a steady rate of leakage (~30 % of inflow; see Chapter 2) approximated to occur at the bottom of the lower hillslope position of the model.

### **3.1.2. Tracer application**

The goal of the dual tracer addition was to add a mass of NO<sub>3</sub><sup>-</sup> tracer to the mineral soil without inducing large flow at the moment of tracer addition but with the potential for subsequent transport through the hillslope via irrigation. As such, we added a small volume of highly concentrated and enriched tracer solution to the mineral soil surface. Specifically, tracers were added at 07:50 on 13 Jun 2017, just prior to an irrigation event at 08:00. Leaf litter was pulled back and tracers were poured by hand onto the mineral soil surface within a 33 cm × 33 cm area (0.1 m<sup>2</sup>; Fig. 3.1), in the center (transverse axis) of the model, 5 m upslope of the outlet. The leaf

litter was placed back over the mineral soil after the irrigation event that followed the tracer addition.

Our tracer solution consisted of 577.6 mg of  $\text{K}^{15}\text{NO}_3^-$  (80.02 mg of  $\text{NO}_3^-$ -N; 6 atom %  $^{15}\text{N}$ ) mixed with 10.0 mL of  $^2\text{H}_2\text{O}$  (99.9 atom %  $^2\text{H}$ ) and 90.0 mL of deionized water. Isotopic abundances of  $\delta^{15}\text{N}$  and  $\delta^2\text{H}$  are reported in per mil (‰) relative to a natural abundance standard (AIR or VSMOW) as  $\delta^{15}\text{N}$  or  $\delta^2\text{H} = (R_x/R_s - 1) \times 1000$ , where  $R_x$  and  $R_s$  are the  $^{15}\text{N}/^{14}\text{N}$  or  $^2\text{H}/^1\text{H}$  ratios for the sample and standard, respectively. Expressed on an areal basis, the relative mass of N added to the 0.1 m<sup>2</sup> addition site (8 kg N ha<sup>-1</sup>) was roughly equal to 140% of that which is loaded over one year at the current rate of atmospheric deposition (5.7 kg N ha<sup>-1</sup> yr<sup>-1</sup>; Adams et al. 2014) or 133% of the mass of  $\text{NO}_3^-$ -N which would be added to the soil where the highest rates of N fixation were observed at Coweeta ( $\text{NO}_3^-$ -N concentrations of 10 mg kg<sup>-1</sup> were observed in upper 10 cm of soil [Knoepp et al. 2014]). Further, the mass of the  $\text{NO}_3^-$ -N tracer was roughly equal to 4 times the estimated mass of  $\text{NO}_3^-$ -N in soil solution in the hillslope below the addition site, based on estimates using pre-addition volumetric soil water content and outflow  $\text{NO}_3^-$ -N concentration data.

The experiment was performed during the growing season, when N mineralization rates are highest (Knoepp and Swank 1998), beginning at tracer addition (13 Jun 2017) and ending when tracers in the outflow returned to background levels (1 Nov 2017). Labeled water samples were considered to contain recovered tracer if the isotopic signature exceeded background levels. We defined background levels as the mean of samples collected both 1) before the tracer was added and 2) after the tracer addition but in locations upslope of the addition, which were monitored to

ensure that there was no evidence of upslope migration of the tracers.

### **3.1.3. Water chemistry and analysis**

Soil solutions were collected at the outlet, and also along the hillslope from eight Teflon-silica porous cup lysimeters with tension maintained at  $-30$  kPa by a continuous vacuum pump (Prenart, Frederiksberg, Denmark). Pairs of lysimeters captured soil solution at two depths (25 cm, hereafter “shallow”, and 65 cm, hereafter “deep”) in the B horizon at four locations along the slope. Shallow lysimeters were 45 cm from the left side-wall (looking upslope; 1.6, 3.5, 5.4, and 7.3 m upslope) and deep lysimeters were 30 cm from the left side-wall (1.1, 3.0, 4.9, and 6.8 m upslope; Fig. 3.1). One pair of lysimeters was at the tracer addition, and one pair was upslope and two pairs were downslope of the tracer addition (Fig. 3.1). A slurry of silica flour and deionized water was used to seat the lysimeters in the mineral soil during installation to ensure good contact.

Irrigation events occurred once per day from 08:00 to 08:10. Samples were collected from lysimeters once per day at 09:00 (1 h after irrigation), and at the outlet throughout the day at varying flow conditions: 07:50, 08:10 (peak flow), 09:00, and 20:00 to capture variations in soil water flow. Results are presented as daily volumetric flow-weighted averages. Sampling intervals ranged from daily to weekly and were adjusted throughout the experiment to capture rising peaks in the breakthrough curves of the tracers.

Samples were filtered through  $0.7 \mu\text{m}$  pore glass microfiber filters, except for samples for  $^{15}\text{NO}_3^-$  analysis, which were filtered through  $0.2 \mu\text{m}$  pore polyethersulfone filters to remove naturally

present bacteria that could consume  $\text{NO}_3^-$  in samples. Samples were collected in HDPE containers that were acid-washed and rinsed with sample water. A set of subsamples were analyzed for pH (Appendix A.1) immediately and another set of subsamples were frozen and analyzed later for  $^{15}\text{NO}_3^-$ ,  $\text{NO}_3^-$ ,  $\text{NH}_4^+$ , TN, DOC (Appendix A.2), and major anions (Appendix A.3) and cations (Appendix A.4). Samples analyzed for  $^2\text{H}$  were collected in 8 mL glass vials sealed with cone top caps to eliminate headspace and avoid isotopic fractionation.

Isotopic analysis of  $^{15}\text{NO}_3^-$  was done by bacterial denitrification method at the UC Davis Stable Isotope Laboratory in Davis, CA (precision  $< 0.2 \text{ ‰}$ ; Sigman et al. 2001). Isotopic analysis of  $^2\text{H}$  was done on an isotopic liquid water and water vapor analyzer (precision  $\leq 0.5 \text{ ‰}$ ; Model L1102-i, Picarro, Santa Clara, CA), which measured absorption by molecules only (i.e.,  $^1\text{H}-^{16}\text{O}-^1\text{H}$  and  $^1\text{H}-^{16}\text{O}-^2\text{H}$ ), from which the  $^2\text{H}/^1\text{H}$  ratio was determined. Analysis was done at the Water Quality Lab at Virginia Tech using a sampling protocol, post-processing correction, and normalization procedures, all of which were modified to maximize precision, accuracy, and efficiency (van Geldern and Barth 2012).

Analyses for  $\text{NO}_3^-$  (precision  $< 0.007 \text{ mg L}^{-1}$ ) and  $\text{NH}_4^+$  (precision  $< 0.03 \text{ mg L}^{-1}$ ) concentrations were done using a colorimetric nutrient analyzer (Model AutoAnalyzer 3, Seal Analytical, Mequon, WI) and analyses for total nitrogen (TN; precision  $< 0.02 \text{ mg L}^{-1}$ ) and dissolved organic carbon (DOC; precision  $< 0.05 \text{ mg L}^{-1}$ ) were done using a TN/DOC analyzer (Model TOC-L, Shimadzu, Kyoto, Japan). Concentrations of dissolved organic nitrogen (DON) were calculated by subtracting  $\text{NO}_3^-$  and  $\text{NH}_4^+$  concentrations from TN concentrations (negative values were assumed to be equal to zero).

### 3.1.4. Estimating nitrification and denitrification using mass balance calculations

In order to better understand the probable N cycling drivers behind retention, we hypothesized that any dampening of the  $\delta^{15}\text{N}$  signal as the tracer traveled downslope would have to be from either the addition of locally produced, ambient unlabeled  $\text{NO}_3^-$  (i.e., nitrification); the removal of labeled  $\text{NO}_3^-$  (i.e., microbial immobilization, denitrification, adsorption) thereby exacerbating apparent dilution of the remaining tracer with downslope unlabeled  $\text{NO}_3^-$ ; or some combination thereof (Burt and Pinay 2005; Curtis et al. 2011). We used a multiple end-member mixing model populated with data from multiple lysimeters and the outflow to estimate the masses of  $\text{NO}_3^-$ -N and  $^{15}\text{NO}_3^-$ -N (Eq. 1 and 2, respectively, below) passing through the saturated zone. All values for the following terms were experiment-long (141 d) flow-weighted averages and linearly interpolated observations, estimations, and values taken from the literature. Terms are illustrated conceptually in Figure 3.2.

Mass balances were calculated using the following equations:

$$M_{\text{throughflow}} + M_{\text{nit}} = M_{\text{outflow}} + M_{\text{Dnit}} + M_{\text{leak}} + M_{\Delta\text{S}} \quad (1)$$

$$\begin{aligned} & (F_{\text{throughflow}} \times M_{\text{throughflow}}) + (F_{\text{nit}} \times M_{\text{nit}}) = \\ & (F_{\text{outflow}} \times M_{\text{outflow}}) + (F_{\text{Dnit}} \times M_{\text{Dnit}}) + (F_{\text{leak}} \times M_{\text{leak}}) + (F_{\Delta\text{S}} \times M_{\Delta\text{S}}) \end{aligned} \quad (2)$$

where  $M_i = \text{NO}_3^- - \text{N}_i \times Q_i$ ;  $\text{NO}_3^- - \text{N}_i$  is the  $\text{NO}_3^-$ -N concentration ( $\text{mg L}^{-1}$ );  $Q_i$  is either the cumulative flow (L) that passed at  $i$  location (set equal to a fraction of inflow estimated by the areal proportion of that location relative to that entire hillslope) or, when calculating change in storage, the volume of water in the riparian zone; and  $F_i$  is the mole fractional abundance of  $\text{NO}_3^-$ -N (e.g.,  $^{15}\text{N}/[^{14}\text{N} + ^{15}\text{N}]$ ). Subscripts refer to: input that was hydrologically and laterally

transported into the saturated zone from upslope (subscript “throughflow”;  $\delta^{15}\text{N}$  and  $\text{NO}_3^-$  were set equal to observations from the deep lysimeter upslope of the saturated zone at 4 m); input from nitrification (subscript “nit”;  $\delta^{15}\text{N}$  was set equal to the background level (2 ‰), which is a common assumption [Burns and Kendall 2002]); loss to outflow (subscript “outflow”;  $\delta^{15}\text{N}$  and  $\text{NO}_3^-$  were set equal to observations from outflow); loss to denitrification (subscript “Dnit”;  $\delta^{15}\text{N}$  was set equal to observations from the lysimeter in the saturated zone minus 20 ‰ as an approximation of denitrification [Barford et al. 1999]); loss to leakage (subscript “leak”;  $\delta^{15}\text{N}$  and  $\text{NO}_3^-$  were set equal to observations from the lysimeter in the saturated zone); and change in storage (subscript “ $\Delta\text{S}$ ”;  $\delta^{15}\text{N}$  and  $\text{NO}_3^-$  were set to the means of the initial ( $n = 5$ ) and final ( $n = 5$ )  $\delta^{15}\text{N}$  and  $\text{NO}_3^-$  concentrations collected when we drained the riparian zone; the volume of water drained from the riparian zone was assumed to be the volume of storage).

We rearranged the terms in Eq. 1 and 2 to solve for mass of  $\text{NO}_3^-$ -N for one of the two unknown terms, namely, the nitrification term ( $M_{\text{nit}}$ ), using the following equation:

$$M_{\text{nit}} = \frac{([F_{\text{Q}} \times M_{\text{Q}}] + [F_{\text{Dnit}} \times M_{\text{up}}] + [F_{\text{leak}} \times M_{\text{leak}}] - [F_{\text{Dnit}} \times M_{\text{Q}}] - [F_{\text{Dnit}} \times M_{\text{leak}}] - [F_{\text{up}} \times M_{\text{up}}] - [F_{\Delta\text{S}} \times M_{\Delta\text{S}}])}{F_{\text{nit}} - F_{\text{Dnit}}} \quad (3)$$

Then we solved for the denitrification term ( $M_{\text{Dnit}}$ ):

$$M_{\text{Dnit}} = M_{\text{up}} + M_{\text{nit}} - M_{\text{Q}} - M_{\text{Leak}} \quad (4)$$

We calculated change in storage for aqueous-phase  $\text{NO}_3^-$ -N and assumed there was little change

in solid-phase  $\text{NO}_3^-$ -N given that there was little difference in  $\delta^{15}\text{N}$  and  $\text{NO}_3^-$ -N mass in a soil core excavated in the riparian zone compared to background (data not shown).

## 3.2. Results

### 3.2.1. Transport of tracers along the hillslope

Most of the  $^{15}\text{NO}_3^-$  tracer was retained in the solid-phase in the top 0–10 cm of soil immediately after addition and throughout the experiment, according to unpublished soil data. A portion of the  $^{15}\text{NO}_3^-$  tracer in aqueous-phase in soil solution passed through the soil surface, given that  $\delta^{15}\text{N}$  was elevated where  $\delta^2\text{H}$  was also elevated at the shallow (Fig. 3.3) and deep lysimeters (Fig. 3.4). Elevated tracer levels were observed at the outlet and in the deep lysimeters at or downslope of the tracer addition, but not in the shallow lysimeters downslope of the tracer addition (Fig. 3.3) nor in the lysimeters upslope of the tracer addition.

There appeared to be both preferential flow and bulk flow transport mechanisms. Vertical movement of both tracers was evident one day (25 h) of addition, after which isotopic signatures of both tracers were elevated at the tracer addition area at shallow ( $\delta^2\text{H} = -23.0\text{‰}$ ;  $\delta^{15}\text{N} = 57.4\text{‰}$ ; Fig. 3.3) and deep lysimeters ( $\delta^2\text{H} = 424.0\text{‰}$ ;  $\delta^{15}\text{N} = 9867.5\text{‰}$ ; Fig 3.4). Shortly thereafter,  $^{15}\text{NO}_3^-$  tracer breakthrough appeared to precede the  $^2\text{H}$  tracer breakthrough at the tracer addition shallow lysimeter because there was a peak in  $\delta^{15}\text{N}$  ( $150.6\text{‰}$ )  $3 \pm 1$  d after addition, followed by the peak in  $\delta^2\text{H}$  ( $-18.7\text{‰}$ )  $4 \pm 1$  d after addition (Fig. 3.3). At the deep lysimeter at 0 m, there was a peak in  $\delta^{15}\text{N}$  ( $2968.8\text{‰}$ )  $4 \pm 1$  d after addition, followed by an initial peak in  $\delta^2\text{H}$  ( $118.5\text{‰}$ )  $5 \pm 1$  d after addition (Fig. 3.4). This initial  $\delta^{15}\text{N}$  and  $\delta^2\text{H}$  movement was presumed to be driven by preferential flow because second peaks occurred 11–14 d later when the bulk of the

dual tracer plume began to migrate downslope. Specifically, there was a second peak in  $\delta^2\text{H}$  (117.1 ‰; Fig. 3.4) 16 d after addition, followed by a second peak in  $\delta^{15}\text{N}$  (2990.9 ‰; Fig. 3.4) 18 d after addition.

Following the vertical movement of the dual tracer bulk plume, breakthrough peaks of the tracers were observed successively in all deep lysimeters laterally downslope (Fig. 3.4). Further, lag time increased between the peaks in  $\delta^{15}\text{N}$  and  $\delta^2\text{H}$  as the plume moved downslope. The peaks in  $\delta^{15}\text{N}$  were delayed relative to the peaks in  $\delta^2\text{H}$  by 1, 6, and 9 d, respectively, at the downslope lysimeters, and by 18.5 d at the outlet (Fig. 3.4). The  $\delta^2\text{H}$  returned to within the range of background levels 35, 50, 46 d, and 49 d after tracer addition in increasingly downslope lysimeters and in outflow, respectively. The  $\delta^{15}\text{N}$  returned to within the range of background levels much later than did  $\delta^2\text{H}$ , 78 d (all of the deep lysimeters) and 119 d (in outflow) after tracer addition.

There were considerable and consistent decreases in the magnitudes of the peaks in both tracers as they moved down the hillslope. The decreases were larger with  $\delta^{15}\text{N}$  than  $\delta^2\text{H}$ . The breakthrough of  $\delta^{15}\text{N}$  was considerably dampened over a longer time period at the outlet (4–5 m) compared to along the hillslope (0–4 m). The second peak in  $\delta^{15}\text{N}$  breakthrough at the deep lysimeter at the tracer addition at 0 m (when the bulk of the tracer plume began to move downslope) was 86 times (on an atom % basis) larger compared to the peak at the outlet, though the peak in  $\delta^2\text{H}$  breakthrough was nearly an order of magnitude smaller (only 10 times difference) when comparing data also at the deep lysimeter at the tracer addition and the outlet.

### 3.2.2. Transport of nitrogen species and carbon

Nitrate was the dominant form of N in soil solution and outflow during the experiment (Fig. 3.5, 3.6), as there was a negligible presence of  $\text{NH}_4^+$  in soil solution (mean =  $0.01 \pm 0.001$  and range =  $0.00\text{--}0.18 \text{ mg L}^{-1}$ ) and outflow (mean =  $0.02 \pm 0.002$  and range =  $0.00\text{--}0.23 \text{ mg L}^{-1}$ ). It was unlikely that the  $^{15}\text{NO}_3^-$  tracer was in another form of aqueous-phase inorganic N. Nitrate concentrations were higher at the shallow lysimeters (mean =  $2.14 \pm 0.07$  and range =  $0.60\text{--}7.16 \text{ mg L}^{-1}$ ) than at the deep lysimeters (mean =  $0.38 \pm 0.03$  and range =  $0.01\text{--}2.03 \text{ mg L}^{-1}$ ) and outlet (mean =  $0.22 \pm 0.02$  and range =  $0.02\text{--}2.18 \text{ mg L}^{-1}$ ). There was a noticeably earlier increase in  $\text{NO}_3^-$  concentrations at the deep lysimeter at 0 m, followed by increases in deep lysimeters downslope afterward (Fig 3.6). Nitrate concentrations increased in deep lysimeters coincident with the beginning of autumn, which was much later than when concentrations had increased in shallower lysimeters. Nitrate concentrations in outflow increased after they had increased along the hillslope.

The pH was relatively unchanged across the hillslope across time, with higher values at the deep lysimeters (mean =  $7.31 \pm 0.07$ ), lower values at the shallow lysimeters (mean =  $6.28 \pm 0.05$ ), and values in between them at the outlet (Appendix A1). Dissolved organic carbon concentrations were low, unvarying, and similar between shallow (mean =  $0.66 \pm 0.04$  and range =  $0.40\text{--}1.32 \text{ mg L}^{-1}$ ) and deep (mean =  $0.53 \pm 0.02$  and range =  $0.29\text{--}0.95 \text{ mg L}^{-1}$ ) lysimeters, with higher concentrations at the outflow (mean =  $1.02 \pm 0.06$  and range =  $0.42\text{--}2.30 \text{ mg L}^{-1}$ ; Appendix A2). Anion and cation concentrations are shown in Appendices A3 and A4. There was no correlation between N concentrations and soil temperature over the study period.

### 3.2.3. Coupled nitrification and denitrification rates

We calculated a gross nitrification addition of 32.4 g  $\text{NO}_3^-$ -N ( $0.24 \text{ mg N kg}^{-1} \text{ d}^{-1}$ ;  $108.9 \text{ mg N m}^{-2} \text{ d}^{-1}$ ) explains the shift in  $\delta^{15}\text{N}$  breakthrough between the lysimeter in the saturated zone and outflow over the duration of the experiment (Table 3.1). We also calculated that a nearly equal mass of  $\text{NO}_3^-$ -N (32.1 g;  $0.24 \text{ mg N kg}^{-1} \text{ d}^{-1}$ ;  $108.6 \text{ mg N m}^{-2} \text{ d}^{-1}$ ) was removed by denitrification, resulting in no net change in  $\text{NO}_3^-$ -N mass in the saturated zone. The mass of  $\text{NO}_3^-$  inputs and outputs due to microbial cycling were large relative to the mass laterally transported into (5.0 g) and then out of (3.6 g) the saturated zone. The leak removed a smaller mass (1.4 g) and storage water was a negligible sink (0.3 g). The proportion of mass loss through the leak at the bottom of the hillslope ( $M_{\text{leak}}$ ) relative to export ( $M_{\text{up}}$ ) was slightly higher for  $\text{NO}_3^-$ -N mass (39.9 %) than for water (38.8 %).

### 3.3. Discussion

We carried out a controlled experiment to track the transport of a reactive  $^{15}\text{NO}_3^-$  tracer relative to a conservative  $^2\text{H}$  tracer applied on an experimental hillslope. Our major findings were 1) stark differences in the breakthrough curves between the two tracers and with each tracer along the hillslope, and 2) high, but counterbalancing, rates of coupled nitrification and denitrification. There was an increasing lag in transport of the  $^{15}\text{NO}_3^-$  tracer relative to the conservative  $^2\text{H}$  tracer as they traveled down the hillslope (Fig. 3.3, 3.4). There were also large reductions in the magnitude of peaks in both  $\delta^2\text{H}$  and  $\delta^{15}\text{N}$  in soil solution as the dual tracer plume moved downslope (Fig. 3.4). Decreases in the peaks of  $\delta^2\text{H}$  were likely due primarily to dilution with unlabeled irrigation water and secondarily to hydromechanical dispersion with increased transport distance. However, decreases in the peaks of  $\delta^{15}\text{N}$  were due to N retention or removal

in the mineral soil.

### **3.3.1. $\text{NO}_3^-$ transport on the hillslope versus riparian zone**

Characteristics of the  $\delta^{15}\text{N}$  tracer breakthrough curves showed distinct lateral transport processes in the unsaturated hillslope at different times, which suggested preferential and bulk flow processes, and in the saturated riparian zone. The shorter spread of the bulk flow breakthrough curve on the hillslope (0–4 m) suggested a faster transport time and that  $\delta^{15}\text{N}$  was reaction limited, whereas the longer spread of the breakthrough curve in the riparian zone (4–5 m) suggested that  $\delta^{15}\text{N}$  was transport limited. Dilution of  $\delta^{15}\text{N}$  may explain processes on the hillslope, but not in the riparian zone. This suggests that characteristics of bedrock and the location of a leak in the hillslope boundary conditions, which is a surrogate for a crack in natural bedrock, can impact the export of  $\text{NO}_3^-$  loss through leakage depending on the concentration of  $\text{NO}_3^-$  at the location of the leak.

We assumed the potential for microbial activity was high in the saturated riparian zone for the following reasons. Aqueous-phase  $\delta^{15}\text{N}$  signatures in soil solution decreased with depth and along the hillslope (Fig. 3.4), yet there was little concomitant evidence of a net increase in solid-phase N mass with depth or along the hillslope. Furthermore, a constantly maintained water table could lead to low dissolved oxygen conditions necessary for denitrification. Moreover, the high irrigation regime was designed to maximize potential for hydrological transport of both tracers. The bottom of the depth profile was wet enough to create a nearly continuous lateral flow zone in a thin (i.e., a few cm estimated by soil moisture measurements) saturated wedge that formed up to and past the tracer addition. A conduit via subsurface water flow between the hillslope and

the saturated riparian zone maximized the potential for rapid delivery of water and nutrients after an irrigation event, reducing the storage time of that water and potential for  $\text{NO}_3^-$  in it to interact biogeochemically in the soil (Welsch et al. 2001; Stieglitz et al. 2003; Ocampo et al. 2006).

However, after each irrigation event, there was a time when the hillslope soils drained during the day, and hydraulic conductivity and gradient dropped, allowing time for  $\text{NO}_3^-$  interaction with soil. In denitrifying soils, most N is lost from soils during brief periods beginning a few hours after irrigation (Smith and Tiedje 1979), which, in this study, coincided with warmer temperatures in the day.

### **3.3.2. Coupled nitrification-denitrification in the riparian zone**

The peak of  $\delta^{15}\text{N}$  decreased one order of magnitude, from 348.5 to 34.7 ‰, and  $\text{NO}_3^-$  concentrations (corresponding with the peaks in  $\delta^{15}\text{N}$ ) changed from 0.06 to 0.08  $\text{mg L}^{-1}$ , respectively, between the lysimeter situated in the saturated riparian zone, and the outlet.

The nitrification term dominated the inputs at the riparian zone. Our estimated gross nitrification rates ( $0.24 \text{ mg N kg}^{-1} \text{ d}^{-1}$ ;  $108.9 \text{ mg N m}^{-2} \text{ d}^{-1}$ ) were similar to those observed in a forest soil ( $0.02\text{--}2.8 \text{ mg N kg}^{-1} \text{ d}^{-1}$ ; Owen et al. 2010), spruce monoculture soil ( $0.68 \text{ mg N kg}^{-1} \text{ d}^{-1}$ ; Kelly et al. 2011), ponderosa pine during summer ( $25 \text{ mg N m}^{-2} \text{ d}^{-1}$ ; Stark and Hart 1997), and temperate forest sites ( $24.1\text{--}32.6 \text{ mg N m}^{-2} \text{ d}^{-1}$ ; Fang et al. 2015), but below those in Douglas-fir during spring ( $304 \text{ mg N m}^{-2} \text{ d}^{-1}$ ; Stark and Hart 1997), when nitrification rates were highest. Rates of net N mineralization, making a large pool of N available for nitrification, could have been high in the hillslope due to decaying tree root masses in the soil model. Decomposing woody roots have been shown to increase rates of net N mineralization and release (Hart 1999; Chen et al. 2001).

Nitrate concentrations in our hillslope soils were likely much higher than they would be if live vegetation were there to take up the  $\text{NO}_3^-$  made available by both nitrification and the tracer application (Bonito et al. 2003). Mineral soils at depths of 10–20 cm and deeper have been shown to be an important source of  $\text{NO}_3^-$  in the absence of plant roots, and potential nitrification can be larger in deeper mineral soil than in the organic horizons (Persson and Wirén 1995). This is unsurprising because in a study of mid-Appalachian forested streams, > 70 % of  $\text{NO}_3^-$  was cycled through microbes and nitrified before being exported from the hillslope (Williard et al. 2001). It is common for the majority of  $\text{NO}_3^-$  in stream water export to be microbial in origin (Burns and Kendall 2002; Pardo et al. 2004; Rose et al. 2015). Thus, we assumed that a general pattern of summer nitrification (Sahrawat 2008) explains the apparent pattern of  $\delta^{15}\text{N}$  dilution. Nitrification rates in soils near the stream have been shown to be a predictor of  $\text{NO}_3^-$  export (Ross et al. 2012).

Similar to nitrification, the denitrification term dominated the total loss (denitrification + leaching). Denitrification was 86.4 % of total loss, which was similar to other forest systems, where denitrification accounts for the majority (48–86 %; Fang et al. 2015) of loss. Our denitrification rates ( $0.24 \text{ mg N kg}^{-1} \text{ d}^{-1}$ ;  $107.8 \text{ mg N m}^{-2} \text{ d}^{-1}$ ) were higher than most rates observed in riparian soils, including the surface (0–10 cm depth) soil of riparian forest sites ( $16.2 \text{ mg N m}^{-2} \text{ d}^{-1}$  N-enriched; Ullah and Zinati 2006), a regularly inundated riparian zone of a tidal freshwater zone ( $44.7\text{--}48.4 \text{ mg N m}^{-2} \text{ d}^{-1}$ ; Ensign et al. 2008), hardwood wetland plots ( $55.4 \text{ mg N m}^{-2} \text{ d}^{-1}$ ; Morse et al. 2015), and riparian forest soils ( $78 \text{ mg N m}^{-2} \text{ d}^{-1}$ ; Pinay et al. 1993). Our rates were similar to a disturbed forested wetland receiving treated sewage effluent ( $100 \text{ mg N}$

$\text{m}^{-2} \text{d}^{-1}$ ; Boustany et al. 1997) and were lower than in an N-enriched soil in a northern hardwood forest ( $290 \text{ mg N m}^{-2} \text{d}^{-1}$ ; Kulkarni et al. 2014). Although there was a large estimate of denitrification at our site, there was no net increase in  $\text{NH}_4^+$  concentrations between the hillslope and the outlet (Figure 3.5). We hypothesize that the production of  $\text{NH}_4^+$  was the rate limiting step in microbial cycling. Once  $\text{NH}_4^+$  was produced, nitrifiers and denitrifiers were ready to process their respective substrates.

Denitrification is typically limited by the availability of  $\text{NO}_3^-$  and the presence of an anoxic environment (Groffman and Tiedje 1989; Boustany et al. 1997; Stark and Hart 1997; Barton et al. 1999). After anoxic conditions were met, the absence of vegetation likely led to the accumulation of a large pool of available  $\text{NO}_3^-$  and, in turn, an increase in denitrification rates, which have been observed to increase also after  $\text{NO}_3^-$  fertilization (Barton et al. 1999). Our denitrification rate was much larger than the maximum observation among disturbed forest soils ( $10.96 \text{ mg N m}^{-2} \text{d}^{-1}$ ; Barton et al. 1999). Therefore, we hypothesized that high rates of nitrification fueled denitrification by providing an additional source of  $\text{NO}_3^-$ .

The estimate that the denitrification flux was nearly 1:1 with the nitrification flux indicated that the riparian zone was an area of high microbial activity. A study in a largely disturbed wetland forest receiving treated sewage effluent showed that average N removal efficiency ranged from 95–100 % when  $\text{NH}_4^+/\text{NO}_3^- \leq 1$ , but average N removal efficiencies were as low as 57 % when  $\text{NH}_4^+/\text{NO}_3^- > 1$ , indicating that denitrification was limited by the availability of  $\text{NO}_3^-$  produced by nitrification (Boustany et al. 1997). High nitrification and denitrification rates that we observed were the same magnitude in subtidal sediment cores taken from the German Bight (Marchant et

al. 2016) and denitrification rates were higher than the daily input of river-sourced  $\text{NO}_3^-$  in an intertidal riparian habitat in low discharge periods (Ensign et al. 2008). Denitrification can be dominant over nitrification in an N-saturated forest (Zhu et al. 2013). Denitrification is often underestimated, and has been observed to be up to six times higher than  $\text{NO}_3^-$  leaching and export in some studies (Fang et al. 2015).

### **3.4. Conclusion**

Nitrate is commonly considered to be a highly mobile anion in soil water. However, in this study, a pulse of isotopically labeled  $^{15}\text{NO}_3^-$  and water ( $^2\text{H}$ ) was added to a hillslope and the portion of  $^{15}\text{NO}_3^-$  that passed through a highly retentive, biologically active soil surface layer showed evidence of retention and removal in deeper mineral layers and at the saturated riparian zone. There was an increasing lag in the breakthrough of  $^{15}\text{NO}_3^-$  relative to  $^2\text{H}$  as dual tracers traveled down a hillslope irrigated at hydrologic steady state. We estimated a mass balance of  $\text{NO}_3^-$ -N over the study period (141 d) and found that a significant pool of  $\text{NO}_3^-$  was generated by nitrification processes, while a pool nearly the same size was removed through denitrification processes. This suggested high flux rates and rapid microbial cycling of  $\text{NO}_3^-$ , which had a short residence time. A conceptual model of  $\text{NO}_3^-$  retention and transport must account for the potential of such rapid cycling along the hillslope, especially if there is a large and persistent saturated zone that provides an environment suitable for microbial activity.

### **3.5. Acknowledgements**

This research was supported, in part, by the Virginia Agricultural Experiment Station and the McIntire-Stennis Program of the U.S. Department of Agriculture (USDA) National Institute of

Food and Agriculture (NIFA). Additionally, this work was supported by grants from the Virginia Water Resources Research Center, the Edna Bailey Sussman Foundation, and the Institute for Critical Technology and Applied Science at Virginia Tech. The authors are grateful to the staff at Coweeta Hydrologic Laboratory for assistance and hospitality while in the field. The authors also thank Dave Mitchem and Kelly Peeler for technical assistance in the lab.

## Figures and Tables

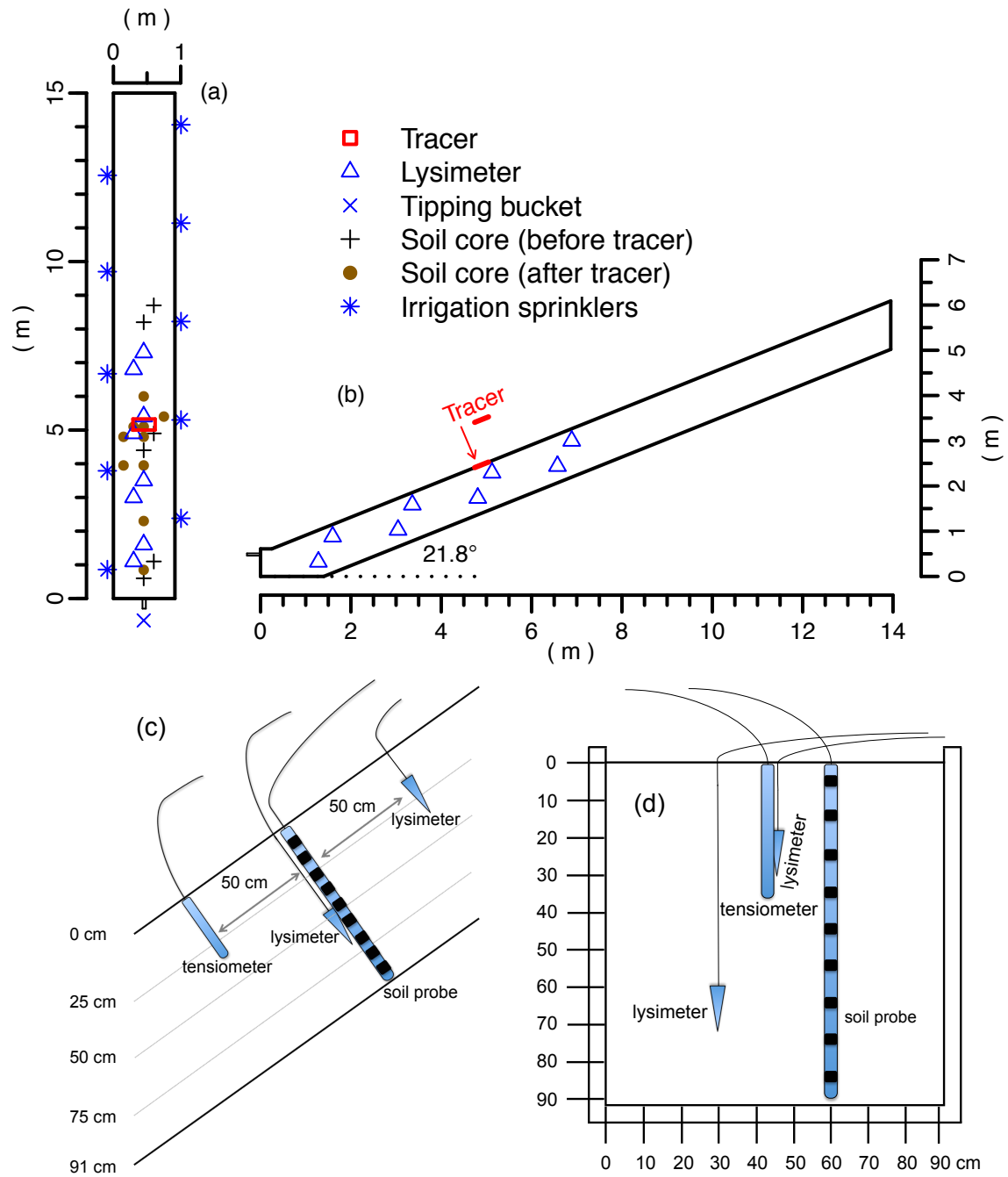


Figure 3.1. (a) Top view of the soil model with locations of instruments, soil core sampling sites, and tracer addition. The aspect ratio is 2:1. (b) Side view of the soil model with locations of lysimeters and tracer addition. The aspect ratio is 1:1. (c) Zoomed-in side view of lysimeter pair

and other instrumentation (field tensiometer and capacitance-based soil moisture sensor) in the soil from a concurrent experiment. Figure is not to scale. (d) Zoomed-in front view of lysimeter pair and other instrumentation. Figure is not to scale.

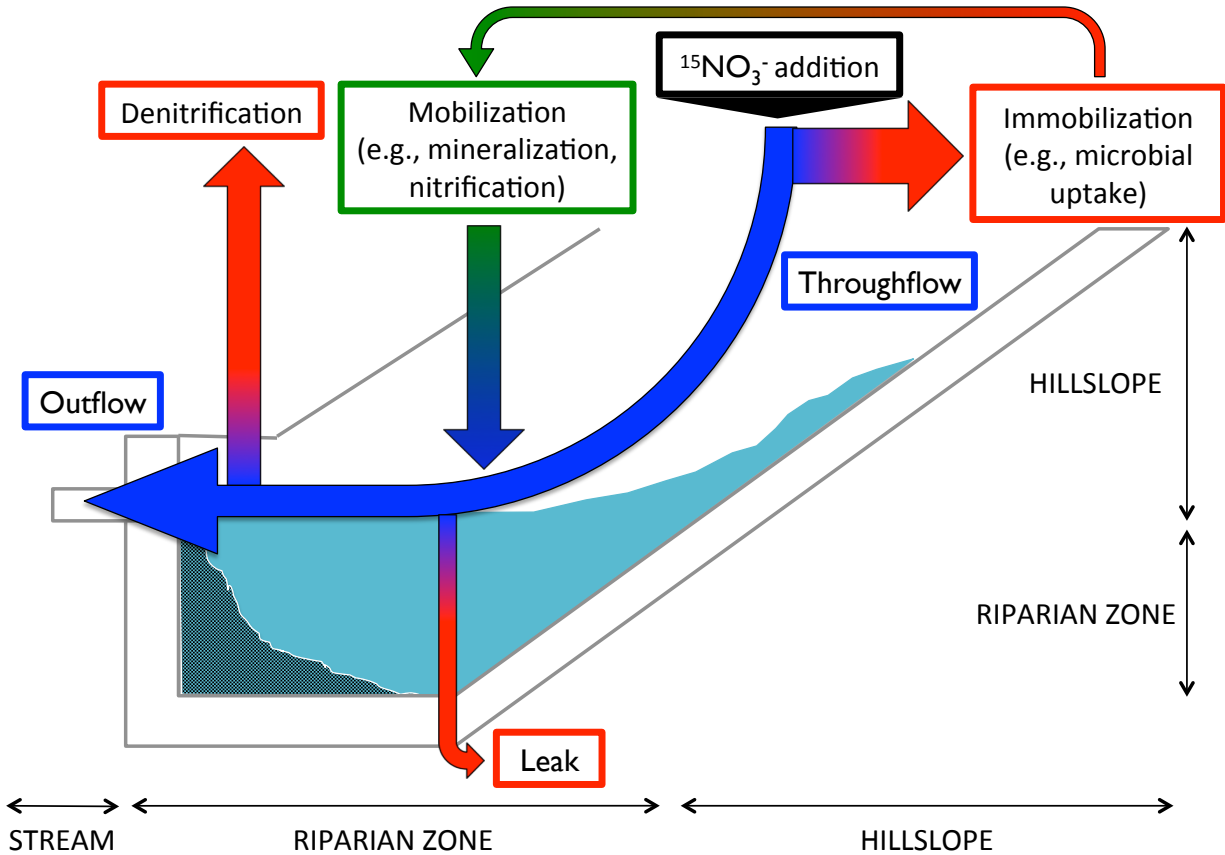


Figure 3.2. Conceptual model of fate and transport of  $\text{NO}_3^-$  through the study hillslope, from  $\text{NO}_3^-$  addition at the hillslope surface to  $\text{NO}_3^-$  export at the outlet. An idealized water table and saturated zone are shown in blue; an idealized configuration of a separate sand fill is shown near the outlet. Mechanisms that make  $\text{NO}_3^-$  available are shown in black or green and include addition (black) and mobilization (green); the mechanism that transports  $\text{NO}_3^-$  is shown in blue and is subsurface lateral throughflow or outflow at the outlet; mechanisms that retain or remove  $\text{NO}_3^-$  are shown in red and include immobilization, denitrification, and loss to leakage. The width of arrows (not to scale) show relative significance of the respective mechanism.

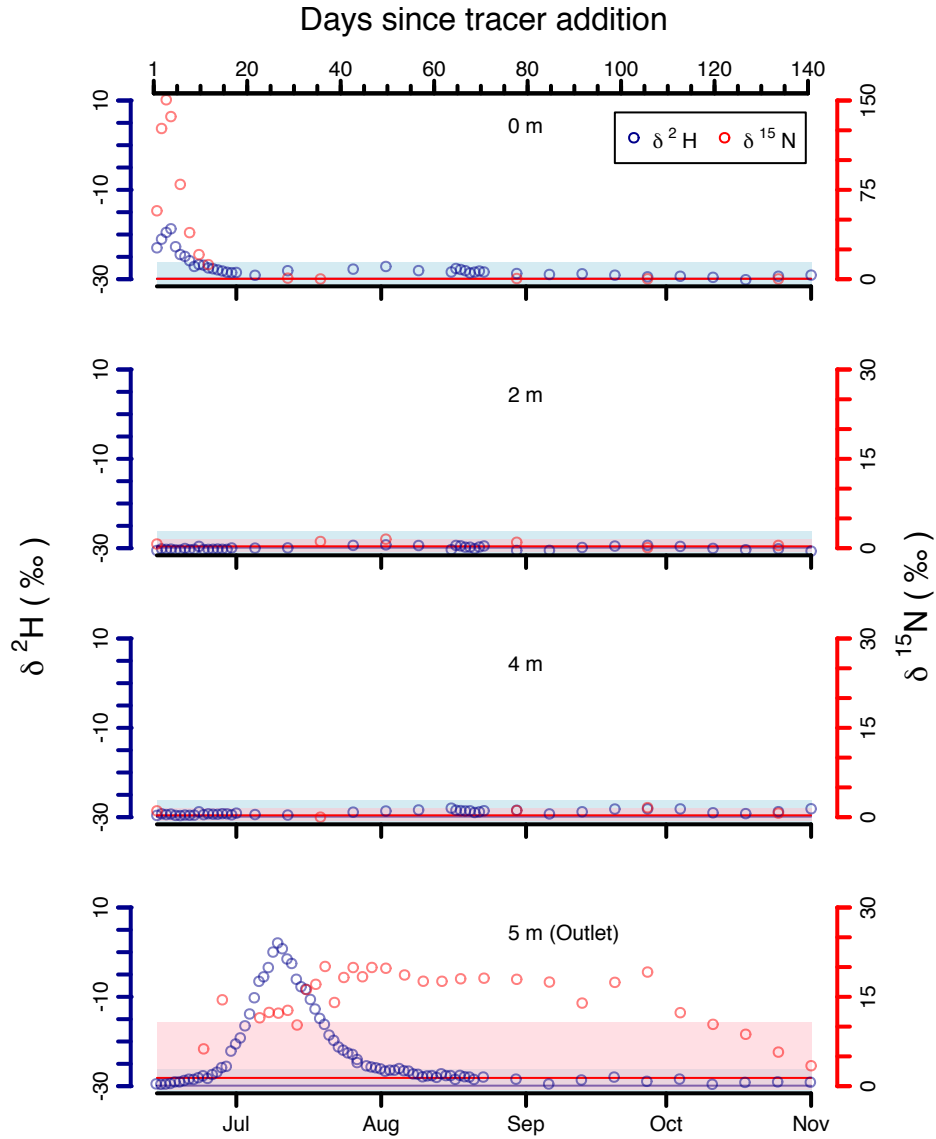


Figure 3.3. Time series of  $\delta^2\text{H}$  and  $\delta^{15}\text{N}$  at shallow lysimeters (25 cm depth) and outlet. A colored band shows the range of background composition taken before the addition of the tracer; the colored line inside the band indicates the median background value. Downslope distance away from the tracer addition is given in the middle of each panel.

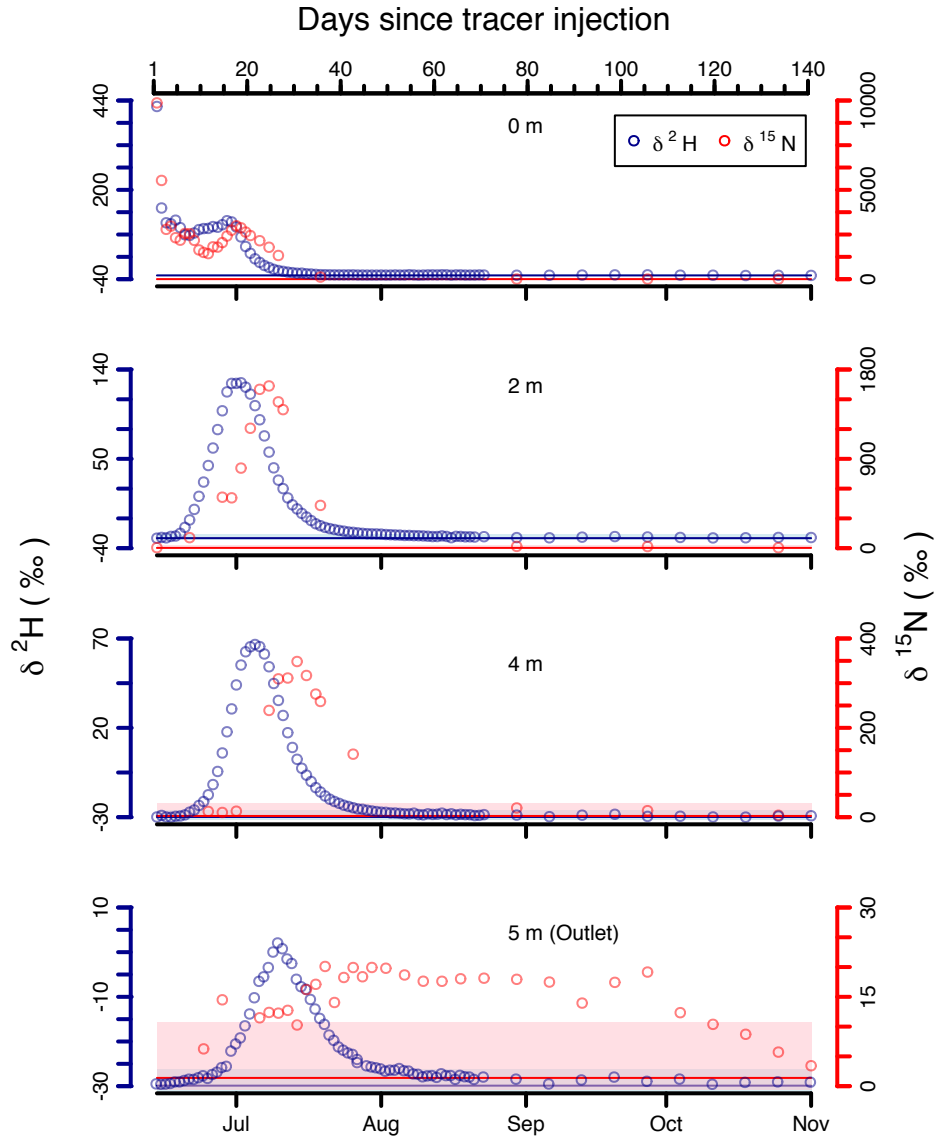


Figure 3.4. Time series of  $\delta^2\text{H}$  and  $\delta^{15}\text{N}$  at deep lysimeters (65 cm depth) and outlet. A colored band shows the range of background composition taken before the addition of the tracer; the colored line inside the band indicates the median background value. Downslope distance away from the tracer addition is given in the middle of each panel.

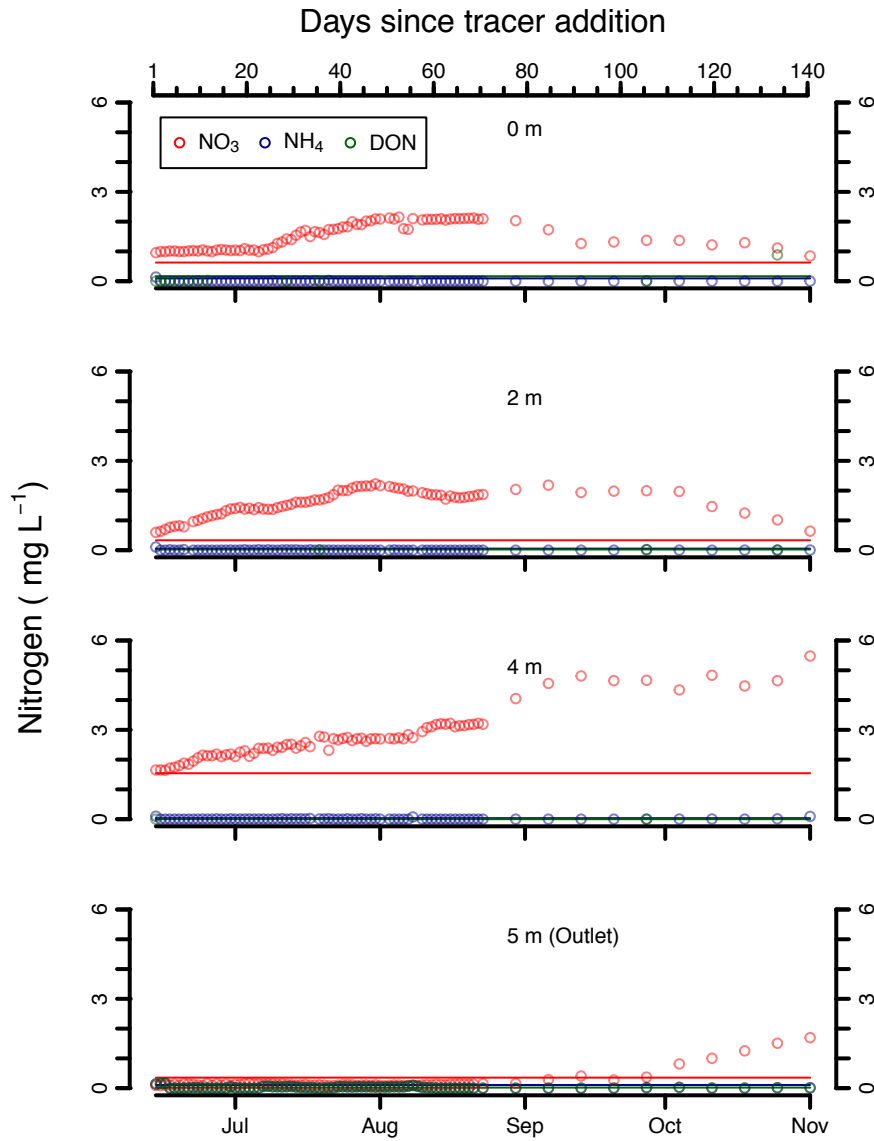


Figure 3.5. Time series of  $\text{NO}_3^-$ ,  $\text{NH}_4^+$ , and DON concentrations at shallow lysimeters (25 cm depth) and outlet. The colored line indicates the median background value. Downslope distance away from the tracer addition is given in the middle of each panel.

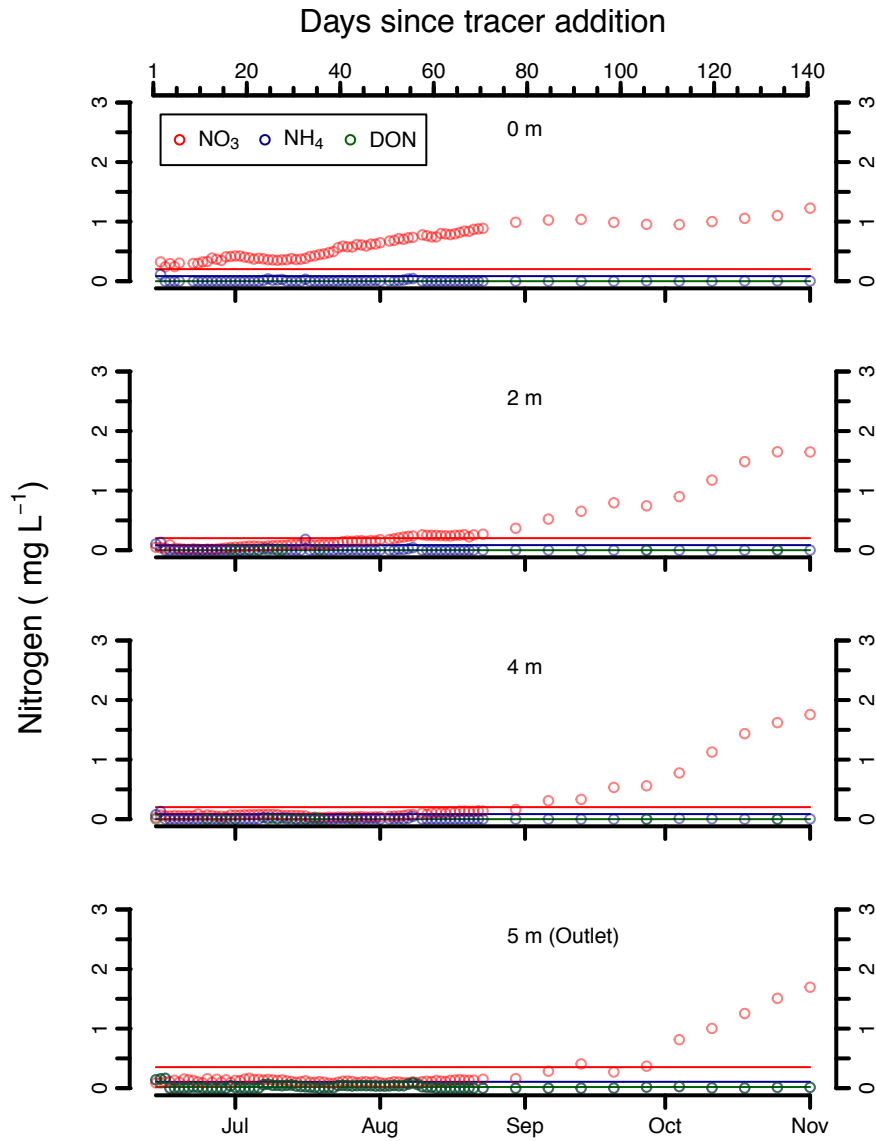


Figure 3.6. Time series of  $\text{NO}_3^-$ ,  $\text{NH}_4^+$ , and DON at deep lysimeters (65 cm depth) and outlet. The colored line indicates the median background value. Downslope distance away from the tracer addition is given in the middle of each panel.

Table 3.1. Mass balance of  $\text{NO}_3^-$ -N in the saturated riparian zone. Change in storage refers to aqueous-phase  $\text{NO}_3^-$ -N in soil solution in the riparian zone.

Pool	Mass (g)	Percent of total input (%)	Flux ( $\text{mg N kg}^{-1} \text{ d}^{-1}$ )	Flux ( $\text{mg N m}^{-2} \text{ d}^{-1}$ )
Lateral transport ( $M_{\text{up}}$ )	5.0	13.3		
Nitrification ( $M_{\text{nit}}$ )	32.4	86.7	0.24	108.9
		Percent of total output (%)		
Export ( $M_{\text{O}}$ )	3.6	9.7		
Denitrification ( $M_{\text{Dnit}}$ )	32.1	86.4	0.24	107.8
Leak ( $M_{\text{leak}}$ )	1.4	3.9		
Storage ( $M_{\Delta S}$ )	0.3	0.8		

## References

- Aber et al. 2003 Aber, J. D., C. L. Goodale, S. V. Ollinger, M.-L. Smith, A. H. Magill, M. E. Martin, R. A. Hallett, and J. L. Stoddard. 2003. Is nitrogen deposition altering the nitrogen status of northeastern forests? *BioScience*, 53: 375–389.
- Adams, M. B., J. D. Knoepp, and J. R. Webster. 2014. Inorganic nitrogen retention by watersheds at Fernow Experimental Forest and Coweeta Hydrologic Laboratory. *Soil Science Society of America Journal*, 78: S95–S104.
- Argerich, A., S. L. Johnson, S. D. Sebestyen, C. C. Rhoades, E. Greathouse, J. D. Knoepp, M. B. Adams, G. E. Likens, J. L. Campbell, W. H. McDowell, F. N. Scatena, and G. G. Ice. 2013. Trends in stream nitrogen concentrations for forested reference catchments across the USA. *Environmental Research Letters*, 8: 1–8.
- Barford, C. C., J. P. Montoya, M. A. Altabet, and R. Mitchell. 1999. Steady-state nitrogen isotope effects of N<sub>2</sub> and N<sub>2</sub>O production in *Paracoccus denitrificans*. *Applied and Environmental Microbiology*, 65: 989–994.
- Barton, L., C. D. A. McLay, L. A. Schipper, and C. T. Smith. 1999. Annual denitrification rates in agricultural and forest soils: a review. *Australian Journal of Soil Research*, 37: 1073–1093.
- Becker, M. W., and T. B. Coplen. 2001. Use of deuterated water as a conservative artificial groundwater tracer. *Hydrogeology Journal*, 9: 512–516.
- Bernhardt, E. S., J. R. Blaszczak, C. D. Ficken, M. L. Fork, K. E. Kaiser, and E. C. Seybold. 2017. Control points in ecosystems: Moving beyond the hot spot hot moment concept. *Ecosystems*, 20: 665–682.
- Bonito, G. M., D. C. Coleman, B. L. Haines, and M. L. Cabrera. 2003. Can nitrogen budgets explain differences in soil nitrogen mineralization rates of forest stands along an elevation gradient? *Forest Ecology and Management*, 176: 563–574.
- Boustany, R. G., C. R. Crozier, J. M. Rybezyk, and R. R. Twilley. 1997. Denitrification in a South Louisiana wetland forest receiving treated sewage effluent. *Wetlands Ecology and Management*, 4: 273–283.
- Burns, D. A. and C. Kendall. 2002. Analysis of  $\delta^{15}\text{N}$  and  $\delta^{18}\text{O}$  to differentiate NO<sub>3</sub><sup>-</sup> sources in runoff at two watersheds in the Catskill Mountains of New York. *Water Resources Research*, 38: 1–11.
- Burt, T. P. and G. Pinay. 2005. Linking hydrology and biogeochemistry in complex landscapes. *Progress in Physical Geography*, 29: 297–316.

- Chen, H., M. E. Harmon, and R. P. Griffiths. 2001. Decomposition and nitrogen release from decomposing woody roots in coniferous forests of the Pacific Northwest: a chronosequence approach. *Canadian Journal of Forest Research*, 31: 246–260.
- Curtis, C. J., C. D. Evans, C. L. Goodale, and T. H. E. Heaton. 2011. What have stable isotope studies revealed about the nature and mechanisms of N saturation and nitrate leaching from semi-natural catchments? *Ecosystems*, 14: 1021–1037.
- Dodds, W. K. and V. H. Smith. 2016. Nitrogen, phosphorus, and eutrophication in streams. *Inland Waters*, 6: 155–164.
- Duncan, J. M., P. M. Groffman, and L. E. Band. 2013. Towards closing the watershed nitrogen budget: Spatial and temporal scaling of denitrification. *Journal of Geophysical Research: Biogeosciences*, 118: 1105–1119.
- Elder, K., H. P. Marshall, L. Elder, B. Starr, A. Karlson, and J. Robertson. 2014. Design and installation of a tipping bucket snow lysimeter. *Proceedings, International Snow Science Workshop, 816–824, Banff, California, USA*.
- Ensign, S. H., M. F. Piehler, and M. W. Doyle. 2008. Riparian zone denitrification affects nitrogen flux through a tidal freshwater river. *Biogeochemistry*, 91: 133–150.
- Fang, Y., K. Koba, A. Makabe, C. Takahashi, W. Zhu, T. Hayashi, A. A. Hokari, R. Urakawa, E. Bai, B. Z. Houlton, D. Xi, S. Zhang, K. Matsushita, Y. Tu, D. Liu, F. Zhu, Z. Wang, G. Zhou, D. Chen, T. Makita, H. Toda, X. Liu, Q. Chen, D. Zhang, Y. Li, and M. Yoh. 2015. Microbial denitrification dominates nitrate losses from forest ecosystems. *Proceedings of the National Academy of Sciences*, 112: 1470–1474.
- Goodale, C. L., J. D. Aber, P. M. Vitousek, and W. H. McDowell. 2005. Long-term decreases in stream nitrate: Successional causes unlikely; Possible links to DOC? *Ecosystems*, 8: 334–337.
- Groffman, P. M. and J. M. Tiedje. 1989. Denitrification in north temperate forest soils: spatial and temporal patterns at the landscape and seasonal scales. *Soil Biology and Biochemistry*, 21: 613–620.
- Hart, S. C. 1999. Nitrogen transformations in fallen tree boles and mineral soil of an old-growth forest. *Ecology*, 80: 1385–1394.
- Hewlett, J. D. and A. R. Hibbert. 1963. Moisture and energy conditions within a sloping soil mass during drainage. *Journal of Geophysical Research*, 68: 1081–1087.
- Hill, A. R., K. J. DeVito, S. Campagnolo, and K. Sanmugadas. 2000. Subsurface denitrification in a forest riparian zone: interactions between hydrology and supplies of nitrate and organic carbon. *Biogeochemistry*, 51: 193 – 223.

- Kelly, C. N., S. H. Schoenholtz, and M. B. Adams. 2011. Soil properties associated with net nitrification following watershed conversion from Appalachian hardwoods to Norway spruce. *Plant Soil*, 344: 361–376.
- Knoepp, J. D. and W. T. Swank. 1998. Rates of nitrogen mineralization across an elevation and vegetation gradient in the southern Appalachians. *Plant and Soil*, 204: 235–241.
- Knoepp, J. D., W. T. Swank, and B. L. Haines. 2014. Long- and short-term changes in nutrient availability following commercial sawlog harvest via cable logging. Pages 57–84 in W. T. Swank and J. R. Webster, editors. *Long-term response of a forest watershed ecosystem: Clearcutting in the southern Appalachians*. Oxford University Press, London.
- Kulkarni, M. V., A. J. Burgin, P. M. Groffman, and J. B. Yavitt. 2014. Direct flux and <sup>15</sup>N tracer methods for measuring denitrification in forest soils. *Biogeochemistry*, 117: 359–373.
- Laseter, S. H., C. R. Ford, J. M. Vose, and L. W. Swift. 2012. Long-term temperature and precipitation trends at the Coweeta Hydrologic Laboratory, Otto, North Carolina, USA. *Hydrology Research*, 43(6): 890–901.
- Lovett, G. M., C. L. Goodale, S. V. Ollinger, C. B. Fuss, A. P. Ouimette, and G. E. Likens. 2018. Nutrient retention during ecosystem succession: a revised conceptual model. *Frontiers in Ecology and the Environment*, 16: 1–7.
- Lucas, R. W., R. A. Sponseller, M. J. Gundale, J. Stendahl, J. Fridman, P. Högberg, and H. Laudon. 2016. Long-term declines in stream and river inorganic nitrogen (N) export correspond to forest change. *Ecological Applications*, 26: 545–556.
- Marchant, H. K., M. Holtappels, G. Lavik, S. Ahmerkamp, C. Winter, and M. M. M. Kuypers. 2016. Coupled nitrification-denitrification leads to extensive N loss in subtidal permeable sediments. *Limnology and Oceanography*, 61: 1033–1048.
- McClain, M., E. W. Boyer, C. L. Dent, S. E. Gergel, N. B. Grimm, P. M. Groffman, S. C. Hart, J. W. Harvey, C. A. Johnston, E. Mayorga, W. H. McDowell, and G. Pinay. 2003. Biogeochemical hot spots and hot moments at the interface of terrestrial and aquatic ecosystems. *Ecosystems*, 6: 301–312.
- Morse, J. L., J. Durán, F. Beall, E. M. Enanga, I. F. Creed, I. Fernandez, P. M. Groffman. 2015. Soil denitrification fluxes from three northeastern North American forests across a range of nitrogen deposition. *Oecologia*, 177: 17–27.
- Ocampo, C. J., M. Sivapalan, and C. E. Oldham. 2006. Field exploration of coupled hydrological and biogeochemical catchment responses and a unifying perceptual

- model. *Advances in Water Resources*, 29: 161–180.
- Owen, J. S., H. B. King, M. K. Wang, and H. L. Sun. 2010. Net nitrogen mineralization and nitrification rates in forest soil in northeastern Taiwan. *Soil Science and Plant Nutrition*, 56: 177–185.
- Pardo, L. H., C. Kendall, J. Pett-Ridge, and C. C. Y. Chang. 2004. Evaluating the source of streamwater nitrate using  $\delta^{15}\text{N}$  and  $\delta^{18}\text{O}$  in nitrate in two watersheds in New Hampshire, USA. *Hydrological Processes*, 18: 2609–2712.
- Persson, T. and A. Wirén. 1995. Nitrogen mineralization and potential nitrification at different depths in acid forest soils. *Plant and Soil*, 168–169: 55–65.
- Peterjohn, W. T., M. B. Adams, and F. S. Gilliam. 1996. Symptoms of nitrogen saturation in two central Appalachian hardwood forest ecosystems. *Biogeochemistry*, 35: 507–522.
- Pinay, G., L. Roques, and A. Fabre. 1993. Spatial and temporal patterns of denitrification in a riparian forest. *Journal of Applied Ecology*, 30: 581–591.
- Rhoades, C. C., R. M. Hubbard, and K. Elder. 2017. A decade of streamwater nitrogen and forest dynamics after a mountain pine beetle outbreak at the Fraser Experimental Forest, Colorado. *Ecosystems*, 20: 380–392.
- Rose, L. A., S. D. Sebestyen, E. M. Elliott, and K. Koba. 2015. Drivers of atmospheric nitrate processing and export in forested catchments. *Water Resources Research*, 51: 1333–1352.
- Ross, D. S., J. B. Shanley, J. L. Campbell, G. B. Lawrence, S. W. Bailey, G. E. Likens, B. C. Wemple, G. Fredriksen, and A. E. Jamison. 2012. Spatial patterns of soil nitrification and nitrate export from forested headwaters in the northeastern United States. *Journal of Geophysical Research*, 117: G01009.
- Sahrawat, K. L. 2008. Factors affecting nitrification in soils. *Communications in Soil Science and Plant Analysis*, 39: 1436–1446.
- Smith, M. S. and J. M. Tiedje. 1979. Phases of denitrification following oxygen depletion in soil. *Soil Biology and Biochemistry*, 11: 261–267.
- Stark, J. M. and S. C. Hart. 1997. High rates of nitrification and nitrate turnover in undisturbed coniferous forests. *Nature*, 385: 61–64.
- Stieglitz, M., J. Shaman, J. McNamara, V. Engel, J. Shanley, and G. W. Kling. 2003. An approach to understanding hydrologic connectivity on the hillslope and the implications for nutrient transport. *Global Biogeochemical Cycles*, 17: 1105.

- Ullah, S. and G. M. Zinati. 2006. Denitrification and nitrous oxide emissions from riparian forests soils exposed to prolonged nitrogen runoff. *Biogeochemistry*, 81: 253–267.
- Valiantzas, J. D. 2006. Simplified versions for the Penman evaporation equation using routine weather data. *Journal of Hydrology*, 331: 690–702.
- van Geldern, R. and J. A. C. Barth. 2012. Optimization of instrument setup and post-run corrections for oxygen and hydrogen stable isotope measurements of water by isotope ratio infrared spectroscopy (IRIS). *Limnology and Oceanography: Methods*, 10: 1024–1036.
- Watmough, S. A., J. Aherne, C. Alewell, P. Arp, S. Bailey, T. Clair, P. Dillon, L. Duchesne, C. Eimers, I. Fernandez, N. Foster, T. Larssen, E. Miller, M. Mitchell, and S. Page. 2005. Sulphate, nitrogen and base cation budgets at 21 forested catchments in Canada, the United States and Europe. *Environmental Monitoring and Assessment*, 109: 1–36.
- Welsch, D. L., C. N. Kroll, J. J. McDonnell, and D. A. Burns. 2001. Topographic controls on the chemistry of subsurface stormflow. *Hydrological Processes*, 15: 1925–1938.
- Williard, K. W. J., D. R. DeWalle, P. J. Edwards, and W. E. Sharpe. 2001.  $^{18}\text{O}$  isotopic separation of stream nitrate sources in mid-Appalachian forested watersheds. *Journal of Hydrology*, 252: 174–188.
- Zhu, J., J. Mulder, L. Bakken, and P. Dörsch. 2013. The importance of denitrification for  $\text{N}_2\text{O}$  emissions from an N-saturated forest in SW China: results from in situ  $^{15}\text{N}$  labeling experiments. *Biogeochemistry*, 116: 103–117.

## Chapter 4: Lagged export of a $^{15}\text{NO}_3^-$ tracer relative to a conservative tracer on an experimental hillslope

**Authors:** Raymond M. Lee<sup>1\*</sup>, Brian D. Strahm<sup>1</sup>, Kevin J. McGuire<sup>1,2</sup>, Jennifer D. Knoepp<sup>3</sup>, Durelle T. Scott<sup>4</sup>

<sup>1</sup>Department of Forest Resources and Environmental Conservation, Virginia Tech, Blacksburg, VA 24061, USA

<sup>2</sup>Virginia Water Resources Research Center, Virginia Tech, Blacksburg, VA 24061, USA

<sup>3</sup>Coweeta Hydrologic Laboratory, USDA Forest Service, Otto, NC 28763, USA

<sup>4</sup>Department of Biological Systems Engineering, Virginia Tech, Blacksburg, VA 24061, USA

**Abstract:** After nitrate ( $\text{NO}_3^-$ ) is made available in a forest soil, whether from addition (e.g., atmospheric deposition or fixation) or internal transformation (e.g., mineralization and nitrification), the  $\text{NO}_3^-$  is then subjected to competing biogeochemical and hydrological processes that either retain or transport  $\text{NO}_3^-$ . We conducted a coupled, labeled stable isotope tracer experiment to elucidate the net effects of these processes on a pulse addition of  $\text{NO}_3^-$  (as  $^{15}\text{NO}_3^-$ ) relative to a conservative tracer ( $^2\text{H}_2\text{O}$ ) on a devegetated experimental hillslope that was irrigated at hydrologic steady state. Retention of the  $^{15}\text{NO}_3^-$  tracer was high (63.1 %) in the surface soil (0–10 cm) in the tracer addition area, with little movement in the surrounding soil, despite high rates of water input immediately after tracer addition and throughout the experiment. The excess mass of  $^{15}\text{NO}_3^-$  recovered at the outlet (5 m below the tracer addition) was less than 3% of the original mass injected. Breakthrough of  $^{15}\text{NO}_3^-$  was delayed relative to the  $^2\text{H}$ . The  $\delta^2\text{H}$  in outflow returned to background concentrations after 48 d, whereas for  $\delta^{15}\text{N}$  it

took 120 d. Retention of  $\text{NO}_3^-$  and lag in  $\text{NO}_3^-$  transport of have important implications for the quantity and timing of  $\text{NO}_3^-$  export at the watershed scale.

**Keywords:** hydrology; biogeochemistry; nutrient cycling; nitrogen; tracer experiment

#### 4.0. Introduction

In forested watersheds, transport dynamics of  $\text{NO}_3^-$  are important because  $\text{NO}_3^-$  is the primary form of atmospherically deposited N (Aber et al. 2003) and is the dominant form of dissolved inorganic N in streamwater export in most forest watersheds (Campbell et al. 2004), especially those that have experienced disturbance (e.g., increased atmospheric deposition of reactive N; Perakis et al. 2002). Nitrate becomes available in soil all along hillslopes, due either to addition from the atmosphere (e.g., deposition or fixation) or internal soil transformation processes (e.g., mineralization and nitrification). Then this available  $\text{NO}_3^-$  moves laterally when and where the rate of  $\text{NO}_3^-$  transport exceeds the rates of retention (e.g., immobilization) and removal (e.g., denitrification). It is important to determine if soils act as a  $\text{NO}_3^-$  sink or source controlling how much  $\text{NO}_3^-$  is available to leach downslope and eventually into another system (e.g., groundwater or downstream). In N-limited forest ecosystems, much of the available  $\text{NO}_3^-$  is retained by microbes in the biologically active soil surface (Aber et al. 1998; Qualls et al. 2000) or taken up by vegetation (Adams et al. 2014). Nitrate that passes through areas with strong retention sink potential is hydrologically transported to the subsurface environment. Mobile  $\text{NO}_3^-$  can then adsorb onto colloidal surfaces of soil particles through abiotic geochemical interactions in soil (Kahl et al. 1999; Strahm and Harrison 2006; Strahm and Harrison 2007). Nitrate that was not biologically or geochemically retained and reaches the bottom of the hillslope can be denitrified in the riparian zone (Davidson and Swank 1986). Any  $\text{NO}_3^-$  that is not retained or denitrified is exported into the stream.

Transport of  $\text{NO}_3^-$  can also vary due to soil physical properties and hydrologic dynamics that control water movement. Variable lengths and hydraulic conductivities of flow paths can

attenuate, delay, or accelerate flow, causing variations of water travel times associated with different flow paths in a hillslope (Kirkby 1988). As water moves into and out of neighboring soil layers or slope positions, the amount of time spent in any section of these is an important consideration for the quantity and timing of  $\text{NO}_3^-$  transport (Cirimo and McDonnell 1997; van der Velde et al. 2010). Antecedent moisture conditions on the hillslope affect processing rates and the transport efficiency that control the timing of peaks in stream  $\text{NO}_3^-$  concentrations, which can occur before peak discharge in wet conditions and later in dry conditions (Christopher et al. 2008). When water moves quickly through hillslope soils with high nitrification rates to the stream, there is often higher  $\text{NO}_3^-$  export because the  $\text{NO}_3^-$  bypasses biogeochemical retention processes (Welsch et al. 2001; Ross et al. 2012; Zhang et al. 2016). During storm periods of high discharge, a large proportion (e.g., 33% [Sebestyen et al. 2014]) of this stormflow  $\text{NO}_3^-$  can be unprocessed and atmospherically derived (Rose et al. 2015).

Excess reactive N has been a concern for decades because the input is larger than the output so there is considerable accumulation (Aber et al. 1989; Aber et al. 2003; Galloway et al. 2003). It is difficult to determine the residence time of N at the watershed scale, but some have estimated it to be on the scale of years to centuries (Schlesinger 2008; Sebiló et al. 2013) and it is still unclear how N is removed from a system. Soil N retention and transport processes differ depending on the status of the soil system, which affects interpretations of the relative importance of N retention and transport. Some forests receive relatively large N loads or have high microbial reaction rates, but have low N export, and it is not clear why (Yanai et al. 2013; Adams et al. 2014). This suggests the need to better understand internal cycling and transport of  $\text{NO}_3^-$ , in and through the hillslope and riparian area, the smallest unit with spatial and temporal

resolution to reflect many relevant  $\text{NO}_3^-$  retention (e.g., reaction) and transport (e.g., flow-generation) processes, and both of which control  $\text{NO}_3^-$  loading to streams.

Our aim was to elucidate the spatial and temporal dynamics of  $\text{NO}_3^-$  retention and transport along a hillslope down to the hillslope/stream boundary. Controlled N tracer studies are a common method of investigating the interplay between retention and transport processes (Bedard-Haughn et al. 2003). Therefore, we added a pulse of isotopically enriched  $^{15}\text{NO}_3^-$  tracer, which simulated a biologically active “hot spot” and “hot moment” (McClain et al. 2003), and a complementary conservative water stable isotope tracer ( $^2\text{H}_2\text{O}$ ) on an experimental hillslope. Timing of transport of  $^{15}\text{NO}_3^-$  and  $^2\text{H}$  tracers were calculated for two aqueous-phase pools (outflow, and soil solution that remained in the riparian zone); a mass balance was calculated for the aqueous-phase pools and two solid-phase pools (O and 0–10 cm horizons at the tracer addition area). Our research questions included: Where (e.g., litter, soil, outflow) is the added  $^{15}\text{NO}_3^-$  recovered? What is the timing and quantity of export of a pulse of  $^{15}\text{NO}_3^-$  added on a hillslope?

## **4.1. Methods**

### **4.1.1. Study site**

The USDA Forest Service Coweeta Hydrologic Laboratory (hereafter Coweeta) is a forested drainage basin in the southern Appalachian Mountain Range of southwestern North Carolina.

The hillslope model at Coweeta was designed to represent hillslopes of the basin. It is a concrete-lined planar trough ( $0.91 \times 0.91 \times 15.0$  m) that was packed with sieved C horizon soil (Saunook series, previously known as Halewood) that was thoroughly sieved and packed to a bulk density

of  $1.3 \text{ g cm}^{-3}$  (Hewlett and Hibbert 1963; Fig. 4.1). The soil, a sandy loam averaging 60% sand, 18% silt, and 22% clay, was obtained from an area adjacent to the model. The hillslope segment was built at a 40% ( $21.8^\circ$ ) slope with a flat toeslope segment, extending 0.3 m, representing a constructed riparian zone. The riparian zone was filled with a mixture of sand and gravel to simulate stream bank conditions and to allow drainage. Water exiting an outflow pipe at a height of 0.46 m above the ground was assumed to flow into a hypothetical stream.

Trees growing in the model (up to 40 cm ground line diameter) were cut at the base and removed from the model in 2012, and root systems were left in place. In 2015, a raised curved shelter was constructed over the model. The shelter was open at the top and bottom ends of the model, allowing airflow across the surface of the model. The shelter was made of a laminated reinforced polyethylene film, which prevented meteoric water input while allowing gaseous exchange between the soil and atmosphere and allowing transmission of 83% of incoming diffuse light. Fallen leaf litter was collected in autumn over a surface area equal and nearby to the model, and added back evenly onto the model. The model was maintained in a devegetated state using herbicide applied before, but not during, the experiment.

#### **4.1.2. Irrigation and water balance**

The soil model surface was irrigated evenly with a sprinkler system (Fig. 4.1) to maintain hydrologic steady state from 10 d before the tracer addition to the end of the experiment. Hydrologic steady state was defined as when input and output flow rates were no longer changing and the water balance was closed (see Chapter 2). The daily irrigation rate ( $6.1 \text{ mm d}^{-1}$ ;  $86 \text{ L d}^{-1}$ ) after the tracer addition was similar to the mean daily gross precipitation rate ( $6.5 \text{ mm}$

$\text{d}^{-1}$ ;  $89 \text{ L d}^{-1}$ ) in the wettest year on record at low elevation in the Coweeta basin, which is equal to the mean daily precipitation rate at high elevation (Laseter et al. 2012). Water input was measured with an in-line flow meter installed in the irrigation line and with a resolution of  $\pm 25$  mL to ensure that water application rates onto the model were accurate. Inflow was verified on several occasions using rain gauges (Model ECRN-100, Meter, Pullman, WA; 4 mL resolution). The irrigation input was constant except for 5 d 91–96 d after tracer addition, when the irrigation equipment malfunctioned. Outflow was measured by a tipping bucket (Snowmetrics, Fort Collins, CO; Elder et al. 2014; 500 mL resolution) placed at the outlet. We calculated potential evapotranspiration (PET) using a simplified Penman equation (Valiantzas 2006) and data from a meteorological station (Models VP-3, PYR, and Davis Cup Anemometer; Meter, Pullman, WA) installed inside the shelter, and found that PET equaled 14 % of inflow. We assumed actual evapotranspiration was negligible because we irrigated one time per day (08:00), reducing the exposure of wet soil to the warm atmosphere; the shelter protected the soil, minimizing exposure to wind; and there was no live vegetation to transpire water out of the model. There was a steady rate of leakage ( $\sim 30$  % of inflow; Chapter 2; see results below).

The irrigation system applied groundwater-sourced chlorinated drinking water that we first processed through carbon and reverse osmosis filters to remove ions and return the water to conditions similar to local throughfall. Filters were not changed for the duration of the experiment. We measured pH and major ion concentrations of the irrigation water before and during the experiment. Mean values were: pH = 6.5; electrical conductivity =  $5.65 \mu\text{S}$ ;  $\text{NO}_3^- = 0.02 \text{ mg L}^{-1}$ ; chloride =  $0.07 \text{ mg L}^{-1}$ ; sulfate =  $0.25 \text{ mg L}^{-1}$ ; calcium =  $0.36 \text{ mg L}^{-1}$ .

### 4.1.3. Tracer application

We aimed to add a mass of  $\text{NO}_3^-$ - $^{15}\text{N}$  in excess of local soil that would become mobile and detectable in soil solution and outflow (Curtis et al. 2011). Our tracer solution was 577.6 mg of  $\text{K}^{15}\text{NO}_3^-$  (80 mg of  $\text{NO}_3^-$ -N; 6.0 atom %  $^{15}\text{N}$ ; 4.8 mg of  $^{15}\text{NO}_3^-$ -N) mixed with 10 mL of  $^2\text{H}_2\text{O}$  (99.9 atom %  $^2\text{H}$ ; 11.06 mg  $^2\text{H}$ ) and 90 mL of deionized water added to a 0.1 m<sup>2</sup> addition area (Fig. 4.1). The scaled mass of  $\text{NO}_3^-$ -N (8 kg N ha<sup>-1</sup>) was roughly equal to 140% of that which is loaded over one year at the current rate of atmospheric deposition (5.7 kg N ha<sup>-1</sup> yr<sup>-1</sup>; Adams et al. 2014), and also equal to 133% of the mass which would be added to the soil at the highest observed rates of nitrification (10 mg kg<sup>-1</sup> in the upper 10 cm of soil) at Coweeta (Knoepp et al. 2014). The mass of the  $\text{NO}_3^-$ -N tracer was roughly equal to 4 times the estimated mass of  $\text{NO}_3^-$ -N in soil solution in the hillslope below the addition site, based on estimates using pre-addition volumetric soil water content and  $\text{NO}_3^-$ -N concentration data.

The tracer solution was poured on the soil surface at 07:50, just prior to an irrigation event at 08:00. Leaf litter was pulled back prior to addition and tracers were poured onto the soil surface inside an area not more than 33 cm long and 33 cm wide (0.1 m<sup>2</sup>; Fig.3.1), in the center (transverse axis) of the model and directly beneath a sprinkler head to ensure the tracers interacted with the irrigation water. The leaf litter was placed back over the soil after the irrigation event that followed the tracer addition. The addition area was 5 m upslope of the outlet and 10 m downslope from the top of the hillslope, providing a large volume of irrigation water from upslope of the addition area to induce transport of the tracers.

### 4.1.4. Water chemistry and analysis

Water samples were collected at varying frequency from the outlet beginning one week (7 Jun 2017) before the tracer addition, continuing until  $^{15}\text{NO}_3^-$  and  $^2\text{H}$  signatures returned approximately to the background level (1 Nov 2017). Irrigation occurred each day from 08:00 to 08:10. Samples were collected at the outlet at varying flow conditions: 07:50, 08:10 (peak flow), 09:00, and 20:00 to account for dilution and flushing behavior in the outflow. Initial sampling intervals were daily, then extended longer to weekly, adjusted to capture rising peaks in the breakthrough curves of the tracers. One month (1 Dec 2017) after the end of the experiment, water was sampled at an auxiliary outlet pipe (5 cm above the ground) below the primary outlet at the bottom of the model to determine aqueous-phase mass of tracer stored in the riparian zone and assess mixing.

Water samples were filtered through 0.7  $\mu\text{m}$  pore glass microfiber filters, except for samples for  $^{15}\text{NO}_3^-$  analysis, which were filtered through 0.2  $\mu\text{m}$  pore polyethersulfone filters to remove naturally present bacteria that could consume  $\text{NO}_3^-$  in samples. Samples analyzed for  $\text{NO}_3^-$  and  $^{15}\text{NO}_3^-$  were collected in HDPE containers that were first acid-washed and rinsed with sample water, then frozen and analyzed. Analyses for  $\text{NO}_3^-$  were done using a colorimetric nutrient analyzer (precision  $< 0.007 \text{ mg L}^{-1}$ ; Model AutoAnalyzer 3, Seal Analytical, Mequon, WI). Isotopic analysis of  $^{15}\text{NO}_3^-$  was done by a bacterial denitrification method (precision  $< 0.2 \text{ ‰}$ ; Sigman et al. 2001) at the UC Davis Stable Isotope Laboratory in Davis, CA. Samples analyzed for  $^2\text{H}$  were collected in 8 mL glass jars sealed with poly-seal cone caps to eliminate headspace and avoid isotopic fractionation. Isotopic analysis of  $^2\text{H}$  was done on an isotopic liquid water analyzer (precision  $\leq 0.5 \text{ ‰}$ ; Model L1102-i, Picarro, Santa Clara, CA) at the Water Quality Lab at Virginia Tech using a modified sampling protocol and post-processing correction and

normalization procedures, all of which maximized precision and accuracy (van Geldern and Barth 2012).

#### **4.1.5. Soil sampling and analysis**

Soil sampling was conducted to characterize the downslope (longitudinal) component of the  $^{15}\text{NO}_3^-$  tracer plume, as opposed to the cross-slope or transverse movement of the tracer. Soil cores were collected along the hillslope also before the addition of the tracers (Fig. 4.1) using a 2 cm soil probe during instrument installation, including soil moisture probes and tensiometers, for a concurrent hillslope drainage experiment (Chapter 2). Additional soil cores (2.2 cm diameter) were collected after the experiment; PVC pipes were placed in all holes to minimize disturbance to the drainage pattern. Each soil core collected after the experiment included a final 2 cm long segment, which was the bottommost increment of soil and which characterized the most hydrologically saturated zone through which the tracers could travel. All soil cores were segmented into 10 cm depth increments. We accounted for soil compaction during extraction by assuming that compaction was uniform throughout the core and then scaled the recovered core evenly, relative to its corresponding hole.

We also characterized the amount of  $^{15}\text{NO}_3^-$  tracer retained in litter and mineral soil at the tracer addition area (Fig. 4.1) by sampling this area intensively after all water collection ceased.

Twenty-five litter and soil (0–10 cm depth) samples were collected across a  $5 \times 5$  square grid with evenly spaced points overlaying the tracer addition area, additional litter samples were collected outside the tracer addition area. Soil samples (0.5 cm diameter) were collected with a stainless steel tube.

All litter and soil samples were air dried, then oven dried at 65 °C. Litter was weighed to determine dry mass; soils were weighed to calculate bulk density and dry mass. Homogenous subsamples of all samples were ground and ball-milled, then analyzed for solid-phase chemistry. The  $^{15}\text{N}$  signatures were analyzed using an IsoPrime 100 EA-IRMS (precision  $\leq 0.01$  ‰; Elementar, Ronkonkoma, NY) and the masses of total N were analyzed using a Vario MAX CNS (precision  $\leq 0.002\%$ ; Elementar, Ronkonkoma, NY).

#### 4.1.6. Data analysis

Isotopic abundance signatures of  $^{15}\text{NO}_3^-$  and  $^2\text{H}$  are described using  $\delta$  notation, which is defined as the relative difference between the heavy/light isotope ratio ( $[\text{atom } \% ^{15}\text{N}]/[\text{atom } \% ^{14}\text{N}]$  or  $[\text{atom } \% ^2\text{H}]/[\text{atom } \% ^1\text{H}]$ ) of a sample ( $R_{\text{sample}}$ ) and the natural abundance of an international standard ( $R_{\text{standard}}$ ) in parts per thousand (i.e., ‰ or per mil):

$$\delta^{15}\text{N} \text{ or } \delta ^2\text{H} = \left( \frac{R_{\text{sample}} - R_{\text{standard}}}{R_{\text{standard}}} \right) \times 1000 \quad (1)$$

where  $R_{\text{standard}}$  is the isotope ratio of atmospheric nitrogen (0.0036765;  $^{15}\text{N}/^{14}\text{N}$ ) or of Vienna Standard Mean Ocean Water (0.00015576;  $^2\text{H}/^1\text{H}$ ), respectively.

Labeled water samples were considered to contain recovered tracer if the isotopic signature exceeded the mean of background signatures, whereas label solid samples were considered to contain recovered tracer if the isotopic signature exceeded the range of background signatures (justification discussed below). Isotopic signatures of solid-phase  $\delta^{15}\text{N}$  in litter and soil samples

that were collected at the tracer addition area were linearly interpolated across the collection area. Background samples for aqueous-phase tracers were collected before the experiment. They include outflow and soil solution collected from constant-tension lysimeters that were installed throughout the hillslope at 25 and 65 cm depths. Background samples for the O horizon were collected after the experiment from along the hillslope, excluding the tracer addition area and including upslope of the tracer. Background samples for the 0–10 cm horizon were collected before the experiment when installing soil instruments (Fig. 4.1; Chapter 2).

Mass recovery of our tracers was calculated for all labeled samples considered to contain tracer. The mass of the labeled sample was calculated, then corrected by subtracting corresponding background reference values and the balance was assumed to be the proportion of excess (i.e., tracer input)  $^{15}\text{N}$  or  $^2\text{H}$  mass. The recovered masses of  $^{15}\text{NO}_3^- - \text{N}_{\text{rec-aqueous}}$  (mg) within aqueous-phase pools (outflow, and soil solution in the riparian zone) were calculated by the following equation for each pool:

$$^{15}\text{NO}_3^- - \text{N}_{\text{rec-aqueous}} = (F_{\text{label}} - F_{\text{background}}) \times \text{NO}_3^- - \text{N}_{\text{label}} \times Q_{\text{label}} \quad (2)$$

where  $F_i$  is the mole fractional abundance (e.g.,  $^{15}\text{N}/[^{14}\text{N} + ^{15}\text{N}]$ ) in the label sample (denoted by the subscript “label”) and non-label background reference sample (denoted by the subscript “background”);  $\text{NO}_3^- - \text{N}_{\text{label}}$  is the concentration ( $\text{mg L}^{-1}$ ) of  $\text{NO}_3^- - \text{N}$  in the label sample; and  $Q_{\text{label}}$  is the integrated volume (L) of the pool for which the label sample represents.

The recovered masses of  $^2\text{H}_{\text{rec}}$  (mg) in the aqueous-phase pools were calculated by the following equation for each pool:

$$^2\text{H}_{\text{rec}} = (F_{\text{label}} - F_{\text{background}}) \times \rho_{^2\text{H}} \times Q_{\text{label}} \quad (3)$$

where  $F_i$  is the mole fractional abundance (e.g.,  $^2\text{H}/[^1\text{H} + ^2\text{H}]$ ) in the labeled sample (denoted by the subscript “label”) and non-label background reference sample (denoted by the subscript “background”);  $\rho_{2\text{H}}$  is the density of deuterium (1,107 g L<sup>-1</sup>); and  $Q_{\text{label}}$  is the integrated volume (L) of the pool for which the label sample represents.

The recovered masses of  $^{15}\text{NO}_3^- \text{-N}_{\text{rec-solid}}$  (mg) in solid-phase pools (O and 0–10 cm soil horizons at the tracer addition area) were calculated by the following equation for each pool:

$$^{15}\text{NO}_3^- \text{-N}_{\text{rec-solid}} = (F_{\text{label}} - F_{\text{background}}) \times (N_{\text{label}} - N_{\text{background}}) \times m_{\text{label-}i} \quad (4)$$

where  $F_i$  is the mole fractional abundance (e.g.,  $^{15}\text{N}/[^{14}\text{N} + ^{15}\text{N}]$ ) in the label sample (denoted by the subscript “label”) and non-label background reference sample (denoted by the subscript “background”);  $N$  is the N mass (%) in the pool; and  $m_{\text{label-}i}$  is the total dry mass (mg) of the pool (either  $m_{\text{label-litter}}$  for the O horizon or  $m_{\text{label-soil}}$  for the 0–10 cm horizon). The label mass of soil,  $m_{\text{label-soil}}$ , was both measured and calculated using the following equation:

$$m_{\text{label-soil}} = (A_{\text{elevated}} \times 10) \times \rho_d \quad (5)$$

where  $A_{\text{elevated}}$  (cm<sup>2</sup>) is the area of labeled samples that had  $\delta^{15}\text{N}$  signatures above the background level; 10 (cm) is the depth over which we sampled; and  $\rho_d$  ( $0.92 \pm 0.04$  g cm<sup>-3</sup>; range of 0.68–1.10 g cm<sup>-3</sup>) is the mean of bulk density sampled in the 0–10 cm horizon in the tracer addition area.

## 4.2. Results

### 4.2.1. Tracers recovered in outflow

The total mass of  $^{15}\text{NO}_3^-$  tracer ( $^{15}\text{NO}_3^- - \text{N}_{\text{rec-aqueous}}$ ) recovered in outflow by the end of the experiment (141 days after the tracer was injected) was 2.8% of the original mass injected (Fig. 4.2; Table 4.1), indicating a large proportion of  $^{15}\text{NO}_3^-$  tracer was retained in the experimental hillslope. Total mass of  $^2\text{H}$  tracer ( $^2\text{H}_{\text{rec}}$ ) recovered in outflow was 67.4 % of the original mass injected (Fig. 4.2; Table 4.1).  $^2\text{H}_{\text{rec}}$  was similar to the cumulative volume of water (72.1 % of inflow) that exited at the outlet over the same period (Chapter 2). This suggested there was negligible evaporation during the experiment, and, from subtraction, we concluded that 27.9–32.6 % of water and both tracers were lost from the hillslope due to a leak in the concrete structure at the bottom of the hillslope (Chapter 2).

Breakthrough of the  $^{15}\text{NO}_3^-$  tracer was considerably delayed relative to the  $^2\text{H}$  tracer at the outlet (Fig. 4.2). Fifty percent of  $^2\text{H}_{\text{rec}}$  was recovered 30 d after the addition, whereas 50% of  $^{15}\text{NO}_3^- - \text{N}_{\text{rec-aqueous}}$  in outflow was recovered 108 d after the addition. Peaks in  $\delta^2\text{H}$  (27 d after tracer addition) and  $\delta^{15}\text{N}$  (46 d after addition) occurred earlier. The  $\delta^2\text{H}$  returned to within the range of background 48 d after the addition, although  $\delta^2\text{H}$  became only slightly more negative and slowly returned to the median of background concentrations much later (120 d after the addition). The  $\delta^{15}\text{N}$  returned to within the range of background 119 d after the addition, but did not return to the median (1.39 ‰) of background concentrations, as the sampled outflow had a  $\delta^{15}\text{N}$  of 3.43 ‰ at the end of the experiment.

#### **4.2.2. Solid-phase $^{15}\text{NO}_3^- - \text{N}$ tracer recovered in hillslope soil**

Here we present results for solid-phase  $^{15}\text{NO}_3^-$  tracer from soil cores taken to depth along the hillslope, followed by results from intensive sampling of the tracer addition area, although there

was some spatial overlap in both sampling schemes. Firstly, solid-phase  $\delta^{15}\text{N}$  or N did not differ from background values throughout the depth profile (Fig. 4.3) across the hillslope (Fig. 4.4) outside of the tracer addition area. The  $\delta^{15}\text{N}$  (8.0 ‰) in the tracer addition area was elevated relative to the four nearest samples (mean =  $2.77 \pm 0.25$  ‰; range = 2.24–3.43 ‰) in the same horizon, and relative to six more samples (mean =  $2.94 \pm 0.21$  ‰; range = 2.24–3.50 ‰) collected (also in the same horizon) from soil cores downslope of the tracer addition along the hillslope (Fig 4.4). Total nitrogen was similarly elevated (0.15%; given above) in the tracer addition area relative to the four nearest samples (mean =  $0.09 \pm 0.003$  %; range = 0.08–0.10 %) in the same horizon, and relative to six more samples (mean =  $0.09 \pm 0.007$  %; range = 0.06–0.11 %) collected (also in the same horizon) downslope of the tracer addition (Fig 4.4).

Furthermore,  $\delta^{15}\text{N}$  was relatively unchanged with depth in the four nearest cores to the tracer addition area, which ranged from 2.24–8.35 ‰ throughout the depth profiles and from –2.95––2.67 ‰ in the O horizon. Similarly, total N was relatively unchanged in these cores throughout the depth profiles (0.02–0.10 %) and in the O horizon (0.80–1.00 %). There was one elevated value of  $\delta^{15}\text{N}$  (10.24 ‰) at the bottom of the depth profile, 1 m downslope of the tracer addition area (in the center along the transverse axis), but the corresponding value of N (0.03 %) was within the range (0.02–0.04 %) of other samples at that depth (Fig. 4.3, 4.4).

The distribution of label  $\delta^{15}\text{N}$  in the 0–10 cm horizon at the tracer addition area was visually inspected using box, density, and Q-Q (quantile-quantile) plots, and tested statistically (Shapiro-Wilk Normality Test;  $W = 0.77$ ;  $P < 0.001$ ;  $n = 25$ ). This distribution of  $\delta^{15}\text{N}$  was determined to have departed from normality and was likely bimodal in two distinct clusters. One cluster (1.35–

4.36 ‰;  $n = 21$ ) was generally within a range similar to the background values (2.16–4.46 ‰) and another cluster (6.97–9.76 ‰;  $n = 4$ ) was markedly higher (Fig. 4.5c). Therefore, after linearly interpolating our data ( $n = 25$ ) spatially across a high-resolution grid ( $500 \times 500$ ), we considered an interpolated value of  $\delta^{15}\text{N}$  to be elevated above background if it was within the range of the elevated cluster (i.e.,  $\delta^{15}\text{N} \geq 6.97$  ‰).

The area of soil containing tracer was calculated to be a closed contour that was smaller (128.0  $\text{cm}^2$ ) than the area earlier referred to as the tracer addition area (1,089  $\text{cm}^2$ ; Fig. 4.3b), due to uneven application of the tracer at the beginning of the experiment. The  $\delta^{15}\text{N}$  was 8.0 ( $\pm 0.005$ ; range = 6.97–9.76) ‰ and N content was 0.15 ( $\pm 0.001$ ; range = 0.11–0.182) % when averaged over this area of enriched soil and both variables were considerably elevated above the background ( $\delta^{15}\text{N}$  mean =  $3.25 \pm 0.38$  and range = 2.16–4.46 ‰; N mean =  $0.09 \pm 0.009$  and range = 0.07–0.12 %). Therefore, the total mass of  $^{15}\text{NO}_3^- - \text{N}_{\text{rec-solid}}$  recovered in the 0–10 cm horizon within this closed contour at the tracer addition area (hereafter “highly enriched soil”) was the largest recovery pool (63.1 % of the original mass injected; Table 4.1).

Although all label  $\delta^{15}\text{N}$  (–2.04–3.98 ‰) and label N (0.59–1.26 %) in leaf litter in the O horizon at the tracer addition area were elevated above background values ( $\delta^{15}\text{N}$ , –3.76––2.52 ‰; N, 0.34–1.08 %; Fig. 4.3a), there was only a negligible mass of  $^{15}\text{NO}_3^- - \text{N}_{\text{rec-solid}}$  (0% of the original mass injected; Table 4.1) recovered in these samples. This small proportion of  $^{15}\text{NO}_3^- - \text{N}_{\text{rec-solid}}$  to the original mass injected was due to the small total dry mass (58 mg) of litter in the O horizon. Samples (–2.74––1.77 ‰) collected in the O horizon surrounding the tracer addition area were

generally within the range of the background values and were considered not to contain a significant mass of tracer (Fig. 4.3c).

#### **4.2.3. Tracers recovered in the riparian zone**

After the experiment, we drained the soil water (170 L) from the riparian zone, collecting samples during the process. The initial  $\delta^2\text{H}$  ( $-21.86\text{‰}$ ) was above the background and greater than subsequent samples ( $-29.06$ – $-27.96\text{‰}$ ). The  $\delta^{15}\text{N}$  followed a similar pattern. The first two samples ( $12.09$  and  $30.33\text{‰}$ ) greater than background and samples ( $3.36$  and  $8.04\text{‰}$ ) collected at the end of the drainage. Nitrate concentration varied throughout the drainage, with a mean of  $1.99 (\pm 0.06) \text{ mg}^{-\text{L}}$  and range from  $1.37$ – $2.32 \text{ mg}^{-\text{L}}$ . The  $^{15}\text{NO}_3^-$ - $\text{N}_{\text{rec-aqueous}}$  and  $^2\text{H}_{\text{rec}}$  in the riparian zone were small (both  $0.3\%$  of the original mass injected; Table 4.1).

#### **4.3. Discussion**

We added a solution with both  $^{15}\text{NO}_3^-$  and  $^2\text{H}$  tracer to a hillslope to assess the fate and transport of a  $\text{NO}_3^-$  hot spot relative to conservative flow of water. Retention of  $^{15}\text{NO}_3^-$  was high in the soil, particularly in the 0–10 cm horizon, where  $63.1\%$  of the original tracer mass was retained. This suggested that microbial processes were dominant in controlling  $\text{NO}_3^-$  retention in surface soil, and that microbial uptake rates and efficiency exceeded  $\text{NO}_3^-$  transport rates. Our major finding was that the export of the mobilized portion of  $^{15}\text{NO}_3^-$  tracer then lagged considerably behind the conservative  $^2\text{H}$  tracer, despite traveling a relatively small hillslope distance of 5 m in consistently wet soil conditions. A small amount of  $^{15}\text{NO}_3^-$  tracer was exported from the hillslope; however, the breakthrough curve was highly damped and showed a lag compared to the conservative  $^2\text{H}$  tracer, which nearly exited from the hillslope by the time the  $^{15}\text{NO}_3^-$  tracer

began to respond. There were 78 d between export of 50 % of the cumulative mass of the  $^2\text{H}$  and  $^{15}\text{NO}_3^-$  tracers. Below we discuss the significance of the  $^{15}\text{NO}_3^-$  tracer recoveries in solid-phase and aqueous-phase, then we discuss the significance of the delayed export of the  $^{15}\text{NO}_3^-$  tracer and implications at the watershed scale.

#### **4.3.1. Biological soil retention of $\text{NO}_3^-$**

Solid-phase  $^{15}\text{NO}_3^-$  tracer was recovered primarily at the soil surface (0–10 cm depth) at the tracer addition area, suggesting important processes of microbial uptake and retention and/or sorption. The soil retained most of the  $^{15}\text{NO}_3^-$  tracer quickly, given that the soil was irrigated soon (<5 min) after the application of the tracer. At the end of the experiment (141 d after tracer addition) there was a distinctly bimodal distribution of  $\delta^{15}\text{N}$  in the highly enriched soil (Fig. 4.3), despite a sampling scheme with high spatial resolution, suggesting that there was little lateral dispersion of the  $^{15}\text{NO}_3^-$  tracer in soil over the course of the experiment. The inference of a lack of lateral movement of the  $^{15}\text{NO}_3^-$  tracer was supported by observations of  $\delta^{15}\text{N}$ , which remained at background levels in other soil samples. These other samples were collected around the highly enriched soil, across the hillslope, and with depth (Fig. 4.3, 4.4). However, all litter samples in the O horizon had  $\delta^{15}\text{N}$  elevated above background (Fig. 4.5a), which suggests there was uptake of the  $^{15}\text{NO}_3^-$  tracer by an overlaying litter microbial community. Uptake by saprotrophic microbes in the litter layer can be an important aspect in the N cycle (Hobbie et al. 2013; Lladó et al. 2017), though the mass of  $^{15}\text{NO}_3^-$  that was recovered in litter was negligible (Table 4.1).

High soil retention of the  $^{15}\text{NO}_3^-$  tracer resulted in a small proportion of the original  $^{15}\text{NO}_3^-$  mass being exported through outflow (Fig. 4.2), which is a common finding in other N addition studies

at plot and watershed scales in which surface soil (0–5 or 0–10 cm), vegetation, and litter dominate the fate of added  $^{15}\text{N}$ . Most (~70%) added N in stable isotope N tracer studies is retained in soils and vegetation over study periods from 1 to 3 years, regardless of whether the tracer is added as  $^{15}\text{NH}_4$  or  $^{15}\text{NO}_3$  (Aber et al. 1998; Tietema et al. 1998; Curtis et al. 2011; Goodale et al. 2015). Some forests have even higher potential for retention of added N. Approximately 80% of added  $^{15}\text{N}$  was recovered in litter and soils (0–5 cm mineral horizon) 410 d after dual labeled,  $^{15}\text{NH}_4\text{NO}_3$  and  $\text{NH}_4^{15}\text{NO}_3$ , additions in a temperate forest in China (Liu et al. 2017). Tracer additions in outflow were <10% of additions at temperate forests across the northeastern US (Nadelhoffer et al. 1999) and <1% in an N-saturated old-growth tropical forest (Gurmesa et al. 2016). In a northern hardwood forest, N addition failed to increase N leaching at all through the deepest soils (Christ et al. 1995). The retention of added N can be persistent at the hillslope scale, because the added N can be redistributed among microbial and vegetation pools. In a long-term study, tracer  $^{15}\text{N}$  was redistributed between trees and surface soils without any losses so that recovery remained constant at 70% of the  $^{15}\text{N}$  addition between 1 and 5–6 years after the addition (Goodale 2017). There, tracer accumulated in both shallow and deep soil, perhaps through mixing by earthworms.

This is unsurprising because similar results have been observed in many natural systems, where the O horizon is also commonly a primary sink for the removal of inorganic N (Qualls et al. 2000; Blanes et al. 2012). Microbially nitrified  $\text{NO}_3^-$  is the larger fraction of the  $\text{NO}_3^-$  compared to the unprocessed fraction in both soil solution (Costa et al. 2011) and in stream outflow (Williard et al. 2001; Pardo et al. 2004; Burns et al. 2009; Wexler et al. 2014).

However, an important difference between our study and the aforementioned N addition studies is that our study site was devegetated before the experiment, which prevented uptake of  $\text{NO}_3^-$  by roots and suggests that the strength of N retention by the soil microbial community at our study site was comparatively large. This was plausible because at the study site, there was a litter layer and elevated carbon content at the soil surface, due to previous biological production and decomposition activity. In 50 years, the soil (which was originally added as unconsolidated C horizon fill material) on the study hillslope had developed a thin A horizon. Mean organic C content was higher in the 0–10 cm depth layer ( $1.9 \pm 0.1\%$ ) and 10–20 cm depth layer ( $0.9 \pm 0.04\%$ ) than in the rest of the soil profile (20–85 cm depth;  $0.7 \pm 0.01\%$ ; (Chapter 2). Similar to our results, the forest floor at Coweeta (Qualls et al. 1991) and elsewhere (Davidson et al. 1992) is also considered a large sink for  $\text{NO}_3^-$  loading in throughfall and microbial immobilization is a commonly accepted explanation for the removal. Furthermore, undisturbed watersheds have been observed to have a significant capacity to remove  $\text{NO}_3^-$  after it passes below the rooting zone (Sudduth et al. 2013).

#### **4.3.2. Hydrological controls on transport time of $\text{NO}_3^-$**

Our study site was relatively steep and wet, given that it was subjected to regular irrigation events at a relatively high input rate, causing the bottom of the hillslope profile to be wetter and thus creating a nearly continuous lateral flow zone in a saturated wedge that formed up to and past the tracer addition (data not shown). Comparisons between  $^2\text{H}$  and volumetric water recovery suggested evaporation was minimal, and there were no plants to transpire water out of the soil. These conditions would typically lead to rapid transport of water and  $\text{NO}_3^-$  after an irrigation event. Nitrate export could have been hydrologically (transport, mixing, and dilution)

controlled (Ocampo et al. 2006) and  $\text{NO}_3^-$  could have been transported out of the hillslope before there was sufficient time for biogeochemical processing to occur and for it to be processed. However, our results demonstrate that  $\text{NO}_3^-$  lagged behind water from the hillslope to the stream. Nitrate molecules retained in microbial biomass at the soil surface would be delayed considerably longer.

There was a significant lag in breakthrough of the  $^{15}\text{NO}_3^-$  tracer relative to the  $^2\text{H}$  tracer (Fig. 4.2) across a relatively short hillslope distance. This lag would be longer on a more typical hillslope length. For example, the median length of a hillslope in the Coweeta basin was estimated to be about 120 m by calculating flow routes from hilltop to channel (Grieve et al. 2016). In our study, the  $\delta^{15}\text{N}$  peaked in outflow 46 d after moving only 5 m from the tracer addition. We estimated it would require roughly 1,130 d to travel the 120 m of a typical hillslope in the basin, assuming roughly 1-D slope transport and similar retention rates observed in this study. Although, considering that half of the tracer mass exited much later (after 108 d) than when  $\delta^{15}\text{N}$  peaked, the travel time of  $\text{NO}_3^-$  may be over 2,600 d (7 y).

This time period would likely be further extended for various reasons, including the smaller doses of  $\text{NO}_3^-$  being transported, N uptake by plants and cycling along its path, and drier soil conditions that reduce advective transport in upslope positions. It has been observed that most of a watershed is not permanently connected to the stream, and some of a watershed is never connected (e.g., Nippgen et al. 2015). Mid-slope regions may have disconnections between the upper hillslope and saturated zone, and are only rarely connected during large storm and snowmelt events (Stieglitz et al. 2003). Water, alone, estimated from our  $^2\text{H}$  tracer, would

require 664–738 d to travel down a typical hillslope at Coweeta. This estimation for water is similar to the mean transit time (657 d) estimated for baseflow from a steep montane hillslope of similar length (125 m; McGuire and McDonnell 2010). There are about 73.4 km of streams within the Coweeta basin and about 57% of this distance is comprised of first-order streams (Swank and Vose 1997) that would receive such delayed export of  $\text{NO}_3^-$  (relative to water) before  $\text{NO}_3^-$  is further processed or transported downstream. As such, the delay in movement of  $\text{NO}_3^-$  from hillslope to stream can help explain temporal variability in N concentrations in outflow at forest sites that receive relatively large N loads or have high microbial reaction rates (Yanai et al. 2013; Adams et al. 2014).

Additional processes in climate and soil development can have competing effects on timing of water and, therefore,  $\text{NO}_3^-$  export. Forecast increased air temperature and increased severity and frequency of flood and drought periods (Laseter et al. 2012; Burt et al. 2018) can reduce soil moisture and delay transport of  $\text{NO}_3^-$ . This may be more impactful in N-saturated sites, where N export is directly related to abiotic properties, such as precipitation volume and hydrologic processes (Adams et al. 2014). In these sites, precipitation can switch control on N export from biogeochemical to hydrological when precipitation rates are high and there is a large availability of N relative to ambient levels (Creed et al. 1996; Adams et al. 2014). Furthermore, soil development processes can augment preferential flow networks and increase speed of transport of water and  $\text{NO}_3^-$  (Providoli et al. 2005). Moreover, loss of water to bedrock leakage in hillslopes (which is generally small at Coweeta [Velbel 1988]) can either delay or accelerate transport rates, depending on the route water takes. The leak in the study hillslope did not significantly affect sub-daily dimensions of the saturated wedge (data not shown), but in an

earlier drainage experiment from saturated initial conditions, the leak significantly reduced recession flow volume after ~15 d, when the dimensions of the saturated wedge became significantly smaller (Chapter 2). Without bedrock leakage the soil stays wetter and water tables remain higher in between storms (Tromp-van Meerveld and Weiler 2008), thereby increasing potential for transport of  $\text{NO}_3^-$ . There was a loss of 56 to 71% of applied irrigation water that flowed through fractured bedrock (Anderson et al. 1997). Delayed hydrologic responses over many months or even years at low-elevation catchments at Coweeta were suspected to be due to long flowpaths through fractured bedrock (Post and Jones 2001).

#### **4.4. Conclusion**

Our combined tracer ( $^{15}\text{NO}_3^-$  and  $^2\text{H}$ ) addition experiment is an illustration of how the soil microbial community at the surface soil and litter horizons in a devegetated hillslope, without influence from roots, could retain  $\text{NO}_3^-$  inputs with rates similar to other systems that contain plants because of a highly active soil microbial community. A small amount of  $^{15}\text{NO}_3^-$  tracer was exported from the hillslope; however, the breakthrough curve was highly damped and lagged behind a conservative  $^2\text{H}$  tracer. This study suggests that retention processes significantly delay  $\text{NO}_3^-$ , which is commonly thought of as a very mobile anion. The results from this hillslope scale tracer study have implications for lags in  $\text{NO}_3^-$  export in watersheds with high microbial activity and long hillslope lengths. Such a temporal offset between N addition and eventual N export is important in the southern Appalachian Mountains, where sequestration of N, and also carbon and phosphorus, in trees and soil is nearly the highest compared to other ecoregions in the US (Hill et al. 2014), and where the status of high N retention may be changing, given that they

are showing characteristics of being in an early stage of N saturation (Swank and Waide 1988; Swank and Vose 1997; Bonito et al. 2003).

#### **4.5. Acknowledgements**

This research was supported, in part, by the Virginia Agricultural Experiment Station and the McIntire-Stennis Program of the U.S. Department of Agriculture (USDA) National Institute of Food and Agriculture (NIFA). Additionally, this work was supported by grants from the Virginia Water Resources Research Center, the Edna Bailey Sussman Foundation, and the Institute for Critical Technology and Applied Science at Virginia Tech. The authors are grateful to the staff at Coweeta Hydrologic Laboratory for assistance and hospitality while in the field. The authors also thank Dave Mitchem and Kelly Peeler for technical assistance in the lab.

## Figures and Tables

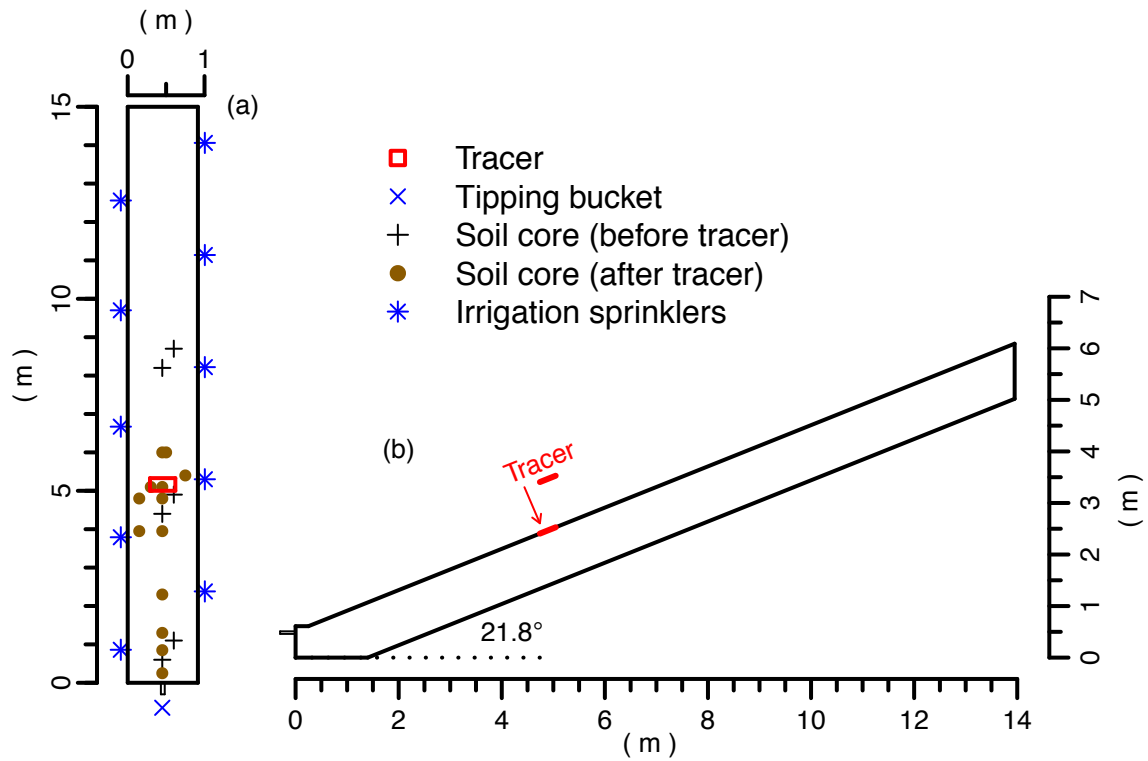


Figure 4.1. (a) Top view of the hillslope model with locations of instruments, soil core sampling sites, and tracer addition. The aspect ratio is 2:1. (b) Side view of the hillslope model with location of tracer addition. The aspect ratio is 1:1.

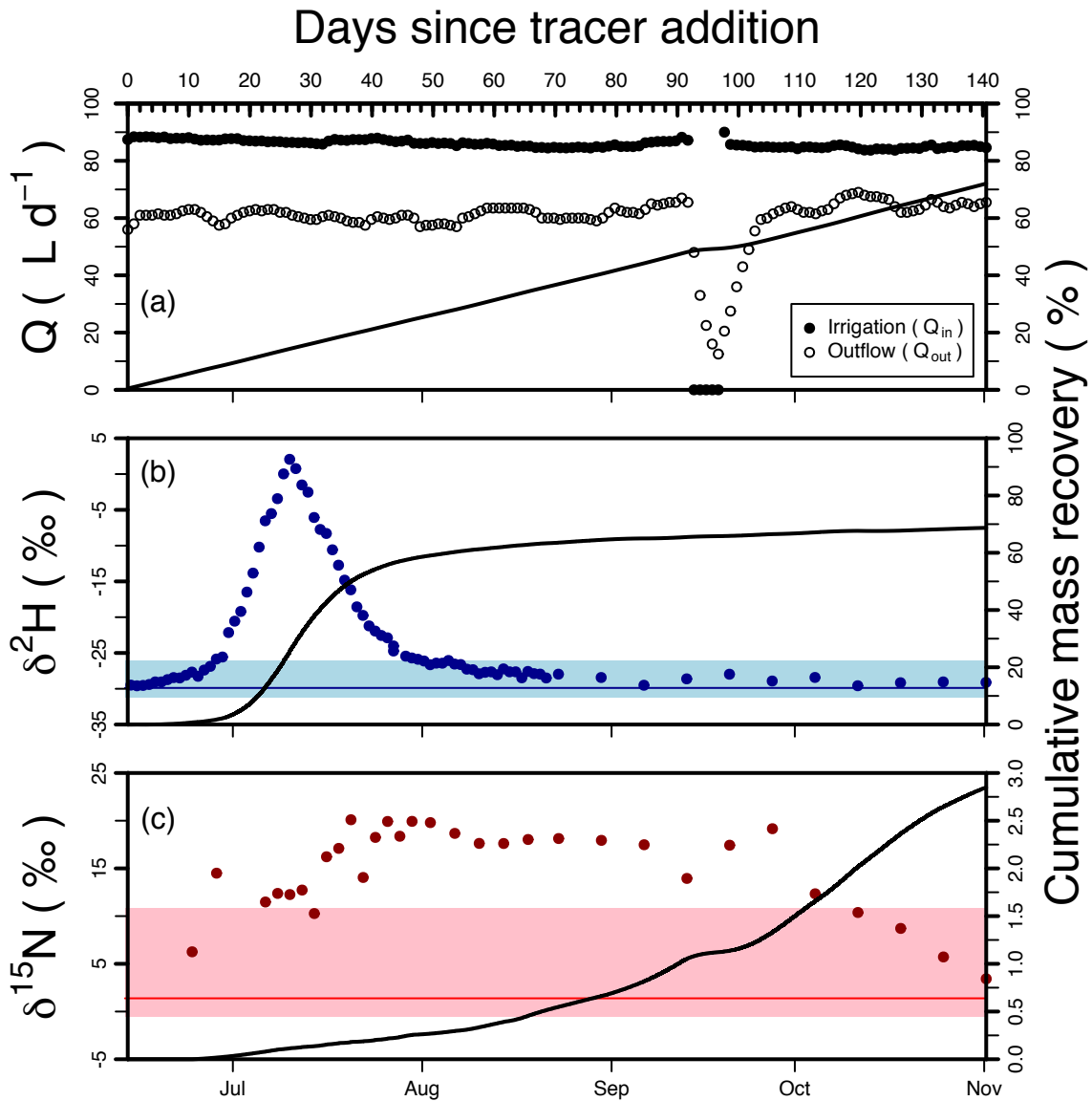


Figure 4.2. (a) Time series of the water balance (points;  $Q_{in}$  and  $Q_{out}$ ) and cumulative volumetric recovery (black line) at the outlet. (b) Time series of isotopic signature of  $\delta^2H$  (points) and cumulative mass recovery (black line) at the outlet. Data are presented as the daily average isotopic composition weighted by volumetric flow at the time each sample was collected. The blue band indicates the range of background concentrations and the line inside the band indicates the median value. (c) Time series of isotopic signature of  $\delta^{15}N$  (points) and cumulative mass recovery (black line) at the outlet. The red band indicates the range of background concentrations

and the line inside the band indicates the median value. Monthly labels at the bottom indicate the first day of the month.

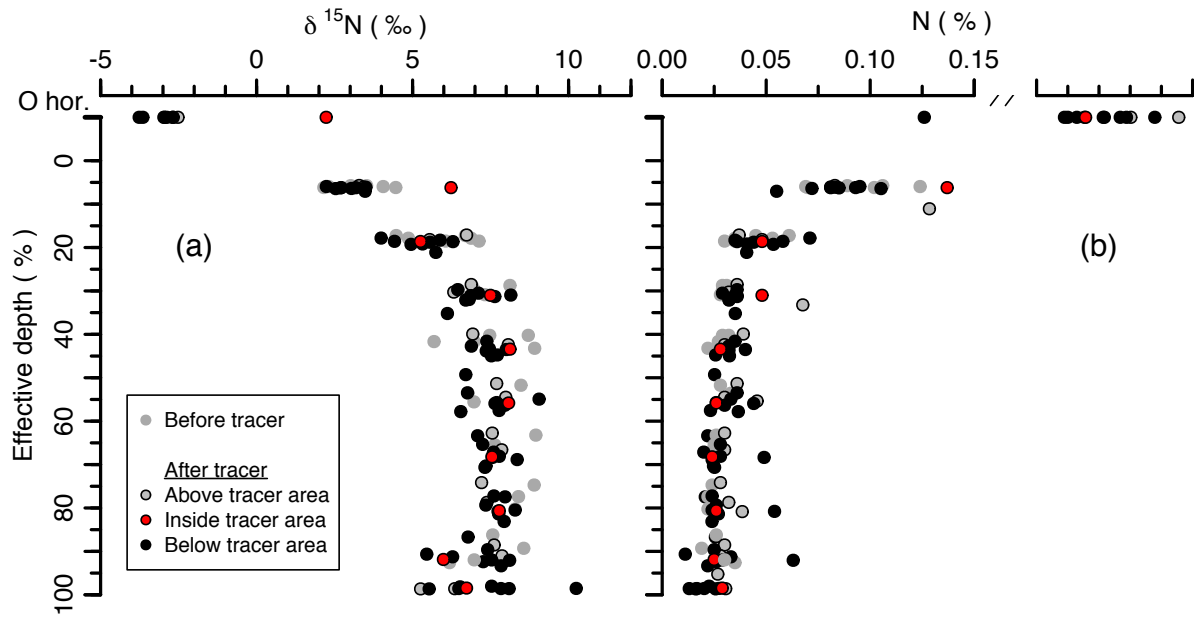


Figure 4.3. (a) Soil profiles of  $\delta^{15}\text{N}$  (‰) and (b) N (%) collected before and after the experiment. Data points for the samples collected inside the tracer addition area (Fig. 4.1a) are highlighted in red.

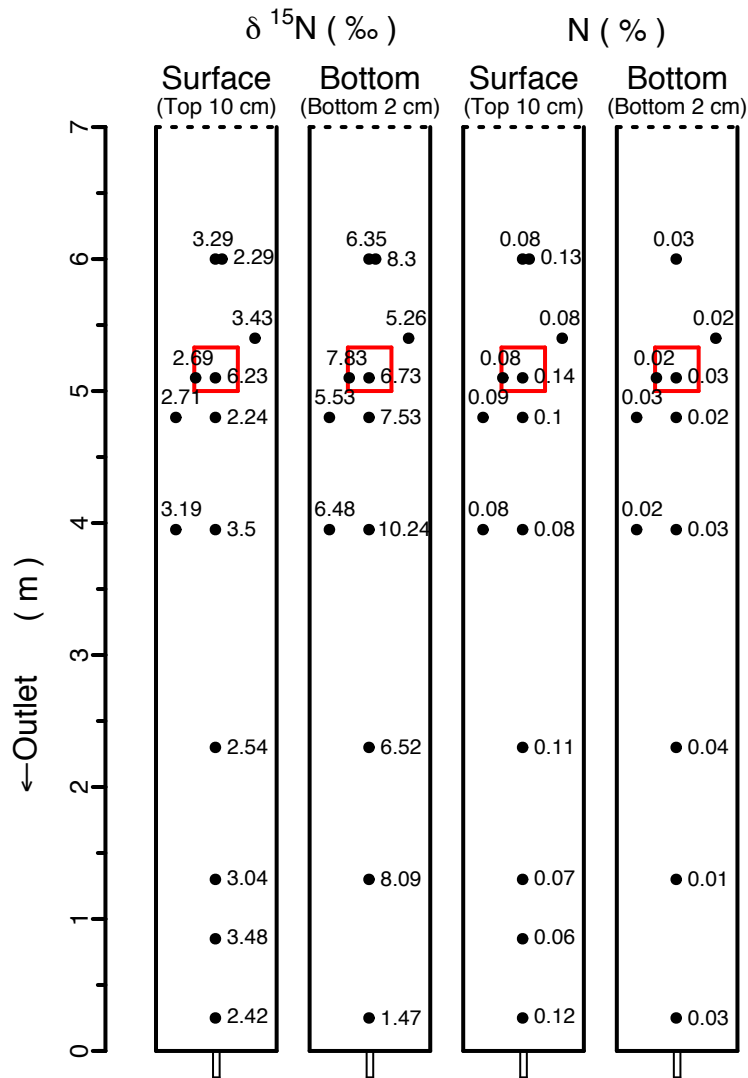


Figure 4.4. Topview of  $\delta^{15}\text{N}$  (‰) and N (%) at the surface (0–10 cm) and bottom (bottom 2 cm) of the soil model at the end of the experiment. The tracer addition area is highlighted in red. The aspect ratio is 1:1.

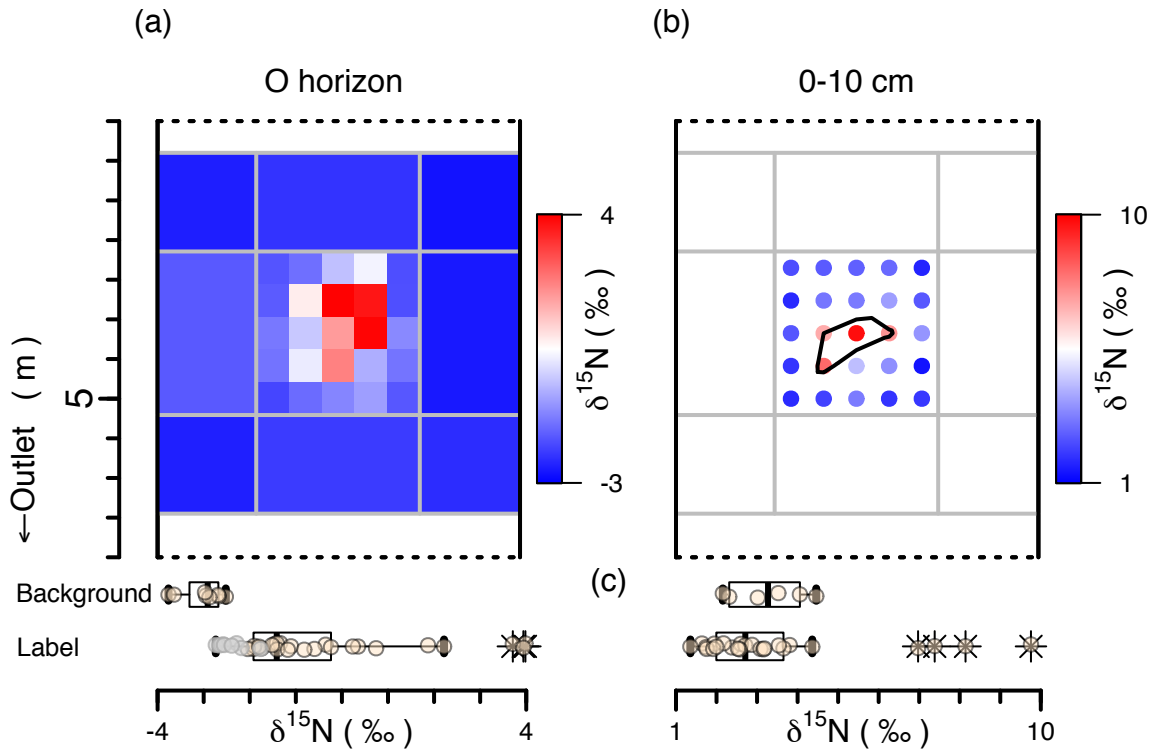


Figure 4.5. Heat maps of  $\delta^{15}\text{N}$  (‰) from the top view of the (a) O horizon and (b) 0–10 cm layer of the soil profile. The tracer addition area is overlaid by a  $5 \times 5$  grid in the center of each plot. A black contour line in (b) shows the highly enriched area inside which  $\delta^{15}\text{N}$  values were above background. This contour was determined by spatial linear interpolation of the data points. (c) Boxplots of  $\delta^{15}\text{N}$  (‰) for the background and label samples. Whiskers extend a distance equal to up to 1.5 times the inter-quartile range, and data beyond that distance are represented individually by asterisks. Points in the background boxplots correspond to data taken along the hillslope (O horizon samples were taken after tracer addition only outside of the tracer addition area; 0–10 cm layer samples were taken before tracer addition; see Fig. 4.1). Points in the label boxplot for the O horizon correspond to samples collected from two areas: yellow points correspond to the tracer addition area, and grey points correspond to the area (rectangles with grey borders in panel [a]) outside of the tracer addition area.

Table 4.1. Mass balance calculations of pools and fluxes of the  $^2\text{H}$  and  $^{15}\text{NO}_3^-$ -N tracers.

Pools	$^2\text{H}$		$^{15}\text{NO}_3^-$ -N	
	(g)	(%)	(mg)	(%)
Addition	11.0 6	100	4.8	100
<u>Recovery</u>				
Outflow	7.46	67.4	0.14	2.9
O horizon*	—	—	1.2e-4	0.0
0–10 cm horizon*	—	—	3.03	63.1
Riparian zone	0.03	0.3	0.02	0.3
Total	7.49	67.7	4.00	66.3

\*Within and/or around the tracer addition area (Fig. 4.5).

## References

- Aber, J. D., K. J. Nadelhoffer, P. Steudler, and J. M. Melillo. 1989. Nitrogen saturation in northern forest ecosystems. *BioScience*, 39: 378–386.
- Aber, J., W. McDowell, K. Nadelhoffer, A. Magill, G. Berntson, M. Kamakea, S. McNulty, W. Currie, L. Rustad, and I. Fernandez. 1998. Nitrogen saturation in temperate forest ecosystems. *BioScience*, 48: 921–934.
- Aber, J. D., C. L. Goodale, S. V. Ollinger, M.-L. Smith, A. H. Magill, M. E. Martin, R. A. Hallett, and J. L. Stoddard. 2003. Is nitrogen deposition altering the nitrogen status of northeastern forests? *BioScience*, 53: 375–389.
- Adams, M. B., J. D. Knoepp, and J. R. Webster. 2014. Inorganic nitrogen retention by watersheds at Fernow Experimental Forest and Coweeta Hydrologic Laboratory. *Soil Science Society of America Journal*, 78: S95–S104.
- Anderson, S. P., W. E. Dietrich, D. R. Montgomery, R. Torres, M. E. Conrad, and K. Loague. 1997. Subsurface flow paths in a steep, unchanneled catchment. *Water Resources Research*, 33: 2637–2653.
- Bedard-Haughn, A., J. W. van Groenigen, and C. van Kessel. 2003. Tracing <sup>15</sup>N through landscapes: potential uses and precautions. *Journal of Hydrology*, 272: 175–190.
- Blanes, M. C., B. A. Emmett, B. Viñepla, and J. A. Carreira. 2012. Alleviation of P limitation makes tree roots competitive for N against microbes in a N-saturated conifer forest: A test through P fertilization and <sup>15</sup>N labelling. *Soil Biology & Biochemistry*, 48: 51–59.
- Bonito, G. M., D. C. Coleman, B. L. Haines, and M. L. Cabrera. 2003. Can nitrogen budgets explain differences in soil nitrogen mineralization rates of forest stands along an elevation gradient? *Forest Ecology and Management*, 176: 563–574.
- Burns, D. A., E. W. Boyer, E. M. Elliott, and C. Kendall. 2009. Sources and transformations of nitrate from streams draining varying land uses: evidence from dual isotope analysis. *Journal of Environmental Quality*, 38: 1149–1159.
- Burt, T. P., C. F. Miniati, S. H. Laseter, and W. T. Swank. 2018. Changing patterns of daily precipitation totals at the Coweeta Hydrologic Laboratory, North Carolina, USA. *International Journal of Climatology*, 38: 94–104.
- Campbell, J. L., J. W. Hornbeck, M. J. Mitchell, M. B. Adams, M. S. Castro, C. T. Driscoll, J. S. Kahl, J. N. Kochenderfer, G. E. Likens, J. A. Lynch, P. S. Murdoch, S. J. Nelson, and J. B. Shanley. 2004. Input-output budgets of inorganic nitrogen for 24 forest watersheds in the northeastern United States: a review. *Water, Air, and Soil Pollution*, 151: 373–396.

- Christ, M., Y. Zhang, G. E. Likens, and C. T. Driscoll. 1995. Nitrogen retention capacity of a northern hardwood forest soil under ammonium sulfate additions. *Ecological Applications*, 5: 802–812.
- Christopher, S. F., M. J. Mitchell, M. R. McHale, E. W. Boyer, D. A. Burns, and C. Kendall. 2008. Factors controlling nitrogen release from two forested catchments with contrasting hydrochemical responses. *Hydrological Processes*, 22: 46–62.
- Cirino, C. P. and J. J. McDonnell. 1997. Linking the hydrologic and biogeochemical controls of nitrogen transport in near-stream zones of temperate-forested catchments: a review. *Journal of Hydrology*, 199: 88–120.
- Costa, A. W., G. Michalski, A. J. Schauer, B. Alexander, E. J. Steig, and P. B. Shepson. 2011. Analysis of atmospheric inputs of nitrate to a temperate forest ecosystem from  $\Delta^{17}\text{O}$  isotope ratio measurements. *Geophysical Research Letters*, 38 (L15805): 1–6.
- Creed, I. F., L. E. Band, N. W. Foster, I. K. Morrison, J. A. Nicolson, R. S. Semkin, and D. S. Jeffries. 1996. Regulation of nitrate-N release from temperate forests: a test of the N flushing hypothesis. *Water Resources Research*, 32: 3337–3354.
- Curtis, C. J., C. D. Evans, C. L. Goodale, and T. H. E. Heaton. 2011. What have stable isotope studies revealed about the nature and mechanisms of N saturation and nitrate leaching from semi-natural catchments? *Ecosystems*, 14: 1021–1037.
- Davidson, E. A. and W. T. Swank. 1986. Environmental parameters regulating gaseous nitrogen losses from two forested ecosystems via nitrification and denitrification. *Applied and Environmental Microbiology*, 52: 1287–1292.
- Davidson, E. A., S. C. Hart, and M. K. Firestone. 1992. Internal cycling of nitrate in soils of a mature coniferous forest. *Ecology*, 73: 1148–1156.
- Elder, K., H. P. Marshall, L. Elder, B. Starr, A. Karlson, and J. Robertson. 2014. Design and installation of a tipping bucket snow lysimeter. *Proceedings, International Snow Science Workshop*, 816–824, Banff, California, USA.
- Galloway, J. N., J. D. Aber, J. W. Erisman, S. P. Seitzinger, R. W. Howarth, E. B. Cowling, and B. J. Cosby. 2003. The nitrogen cascade. *BioScience*, 53: 341–356.
- Goodale, C. L., G. Fredriksen, M. S. Weiss, C. K. McCalley, J. P. Sparks, and S. A. Thomas. 2015. Soil processes drive seasonal variation in retention of  $^{15}\text{N}$  tracers in a deciduous forest catchment. *Ecology*, 96: 2653–2668.
- Goodale, C. L. 2017. Multiyear fate of a  $^{15}\text{N}$  tracer in a mixed deciduous forest: retention, redistribution, and differences by mycorrhizal association. *Global Change Biology*, 23: 867–880.

- Grieve, S. W. D., S. M. Mudd, and M. D. Hurst. 2016. How long is a hillslope? *Earth Surface Processes and Landforms*, 41: 1039–1054.
- Gurmesa, G. A., X. Lu, P. Gundersen, Q. Mao, K. Zhou, Y. Fang, and J. Mo. 2016. High retention of  $^{15}\text{N}$ -labeled nitrogen deposition in a nitrogen saturated old-growth tropical forest. *Global Change Biology*, 22: 3608–3620.
- Hewlett, J. D. and A. R. Hibbert. 1963. Moisture and energy conditions within a sloping soil mass during drainage. *Journal of Geophysical Research*, 68: 1081–1087.
- Hill, B. H., R. K. Kolka, F. H. McCormick, and M. A. Starry. 2014. A synoptic survey of ecosystem services from headwater catchments in the United States. *Ecosystem Services*, 7: 106–115.
- Hobbie, E. A., L. T. A. van Diepen, E. A. Lilleskov, A. P. Ouimette, A. C. Finzi, and K. S. Hofmockel. 2013. Fungal functioning in a pine forest: evidence from a  $^{15}\text{N}$ -labeled global change experiment. *New Phytologist*, 210: 1431–1439.
- Kahl, J., S. Norton, I. Fernandez, L. Rustad, and M. Handley. 1999. Nitrogen and sulfur input-output budgets in the experimental and reference watersheds, Bear Brook watershed in Maine (BBWM). *Environmental Monitoring and Assessment*, 55: 113–131.
- Kirkby, M. 1988. Hillslope runoff processes and models. *Journal of Hydrology*, 100: 315–339.
- Knoepp, J. D., W. T. Swank, and B. L. Haines. 2014. Long- and short-term changes in nutrient availability following commercial sawlog harvest via cable logging. Pages 57–84 *in* W. T. Swank and J. R. Webster, editors. *Long-term response of a forest watershed ecosystem: Clearcutting in the southern Appalachians*. Oxford University Press, London.
- Laseter, S. H., C. R. Ford, J. M. Vose, and L. W. Swift. 2012. Long-term temperature and precipitation trends at the Coweeta Hydrologic Laboratory, Otto, North Carolina, USA. *Hydrology Research*, 43(6): 890–901.
- Liu, J., B. Peng, Z. Xia, J. Sun, D. Gao, W. Dai, P. Jiang, and E. Bai. 2017. Different fates of deposited  $\text{NH}_4^+$  and  $\text{NO}_3^-$  in a temperate forest in northeast China: a  $^{15}\text{N}$  tracer study. *Global Change Biology*, 23: 2441–2449.
- Lladó, S., R. López-Mondéjar, and P. Baldrian. 2017. Forest soil bacteria: Diversity, involvement in ecosystem processes, and response to global change. *Microbiology and Molecular Biology Reviews*, 81: 1–27.
- McClain, M, E. W. Boyer, C. L. Dent, S. E. Gergel, N. B. Grimm, P. M. Groffman, S. C.

- Hart, J. W. Harvey, C. A. Johnston, E. Mayorga, W. H. McDowell, and G. Pinay. 2003. Biogeochemical hot spots and hot moments at the interface of terrestrial and aquatic ecosystems. *Ecosystems*, 6: 301–312.
- McGuire, K. J. and J. J. McDonnell. 2010. Hydrological connectivity of hillslopes and streams: Characteristic time scales and nonlinearities. *Water Resources Research*, 46, W10543.
- Nadelhoffer, K. J., B. A. Emmett, P. Gundersen, O. J. Kjønaas, C. J. Koopmans, P. Schleppi, A. Tietema, and R. F. Wright. 1999. Nitrogen deposition makes a minor contribution to carbon sequestration in temperate forests. *Nature*, 398: 145–148.
- Nippgen, F., B. L. McGlynn, and R. E. Emanuel. 2015. The spatial and temporal evolution of contributing areas. *Water Resources Research*, 51: 4550–4573.
- Ocampo, C. J., C. E. Oldham, and M. Sivapalan. 2006a. Nitrate attenuation in agricultural catchments: Shifting balances between transport and reaction. *Water Resources Research*, 42(W01408): 1–16.
- Pardo, L. H., C. Kendall, J. Pett-Ridge, and C. C. Y. Chang. 2004. Evaluating the source of streamwater nitrate using  $\delta^{15}\text{N}$  and  $\delta^{18}\text{O}$  in nitrate in two watersheds in New Hampshire, USA. *Hydrological Processes*, 18: 2609–2712.
- Perakis, S. S. and L. O. Hedin. 2002. Nitrogen loss from unpolluted South American forests mainly via dissolved organic compounds. *Nature*, 415: 416–420.
- Post, D. A. and J. A. Jones. 2001. Hydrologic regimes of forested, mountainous, headwater basins in New Hampshire, North Carolina, Oregon, and Puerto Rico. *Advances in Water Resources*, 24: 1195–1210.
- Providoli, I., H. Bugmann, R. Siegwolf, N. Buchmann, and P. Schleppi. 2005. Flow of deposited inorganic N in two Gleysol-dominated mountain catchments traced with  $^{15}\text{NO}_3^-$  and  $^{15}\text{NH}_4^+$ . *Biogeochemistry*, 76: 453–475.
- Qualls, R. G., B. L. Haines, and W. T. Swank. 1991. Fluxes of dissolved organic nutrients and humic substances in a deciduous forest. *Ecology*, 72: 254–266.
- Qualls, R. G., B. L. Haines, W. T. Swank, and S. W. Tyler. 2000. Soluble organic and inorganic nutrient fluxes in clearcut and mature deciduous forests. *Soil Science Society of America Journal*, 64: 1068–1077.
- Rose, L. A., S. D. Sebestyen, E. M. Elliott, and K. Koba. 2015. Drivers of atmospheric nitrate processing and export in forested catchments. *Water Resources Research*, 51: 1333–1352.
- Ross, D. S., J. B. Shanley, J. L. Campbell, G. B. Lawrence, S. W. Bailey, G. E. Likens,

- B. C. Wemple, G. Fredriksen, and A. E. Jamison. 2012. Spatial patterns of soil nitrification and nitrate export from forested headwaters in the northeastern United States. *Journal of Geophysical Research*, 117: G01009.
- Schlesinger, W. H. 2008. On the fate of anthropogenic nitrogen. *Proceedings of the National Academy of Sciences*, 106: 203–208.
- Sebestyen, S. D., J. B. Shanley, E. W. Boyer, C. Kendall, and D. H. Doctor. 2014. Coupled hydrological and biogeochemical processes controlling variability of nitrogen species in streamflow during autumn in an upland forest. *Water Resources Research*, 50, doi: 10.1002/2013WR013670.
- Sebilo, M., B. Mayer, B. Nicolardot, G. Pinay, and A. Mariotti. 2013. Long-term fate of nitrate fertilizer in agricultural soils. *Proceedings of the National Academy of Sciences*, 110: 18185–18189.
- Stieglitz, M., J. Shaman, J. McNamara, V. Engel, J. Shanley, and G. W. Kling. 2003. An approach to understanding hydrologic connectivity on the hillslope and the implications for nutrient transport. *Global Biogeochemical Cycles*, 17: 1105.
- Strahm, B. D. and R. B. Harrison. 2006. Nitrate sorption in a variable-charge forest soil of the Pacific Northwest. *Soil Science*, 171: 313–321.
- Strahm, B. D., and R. B. Harrison. 2007. Mineral and organic matter controls on the sorption of macronutrient anions in variable-charge soils. *Soil Science Society of America Journal*, 71: 1–8.
- Swank, W. T., and J. M. Vose. 1997. Long-term nitrogen dynamics of Coweeta forested watersheds in the southeastern United States of America. *Global Biogeochemical Cycles*, 11: 657–671.
- Swank, W. T. and J. B. Waide. 1988. Characterization of baseline precipitation and stream chemistry and nutrient budgets for control watersheds. pp. 57–79. In: *Forest Hydrology and Ecology at Coweeta*. eds. Swank, W. T., and D. A. Crossley, Jr. Springer-Verlag, New York. 469 p.
- Tietema, A., B. A. Emmett, P. Gundersen, O. J. Kjønaas, and C. J. Koopmans. The fate of <sup>15</sup>N-labelled nitrogen deposition in coniferous forest ecosystems. *Forest Ecology and Management*, 101: 19–27.
- Tromp-van Meerveld, I. and M. Weiler. 2008. Hillslope dynamics modeled with increasing complexity. *Journal of Hydrology*, 361: 24–40.
- Valiantzas, J. D. 2006. Simplified versions for the Penman evaporation equation using routine weather data. *Journal of Hydrology*, 331: 690–702.

- van der Velde, Y., G. H. de Rooij, J. C. Rozemeijer, F. C. van Greer, and H. P. Broers. 2010. Nitrate response of a lowland catchment: On the relation between stream concentration and travel time distribution dynamics. *Water Resources Research*, 46: W11534. doi: 10.1029/2010WR009105.
- van Geldern, R. and J. A. C. Barth. 2012. Optimization of instrument setup and post-run corrections for oxygen and hydrogen stable isotope measurements of water by isotope ratio infrared spectroscopy (IRIS). *Limnology and Oceanography: Methods*, 10: 1024–1036.
- Velbel, M. A. 1988. Weathering and soil-forming processes. pp. 93–102. In: *Forest Hydrology and Ecology at Coweeta*. eds. Swank, W. T., and D. A. Crossley, Jr. Springer-Verlag, New York. 469 p.
- Welsch, D. L., C. N. Kroll, J. J. McDonnell, and D. A. Burns. 2001. Topographic controls on the chemistry of subsurface stormflow. *Hydrological Processes*, 15: 1925–1938.
- Wexler, S. K., C. L. Goodale, K. J. McGuire, S. W. Bailey, and P. M. Groffman. 2014. Isotopic signals of summer denitrification in a northern hardwood forested catchment. *Proceedings of the National Academy of Sciences*, 111: 16413–16418.
- Williard, K. W. J., D. R. DeWalle, P. J. Edwards, and W. E. Sharpe. 2001.  $^{18}\text{O}$  isotopic separation of stream nitrate sources in mid-Appalachian forested watersheds. *Journal of Hydrology*, 252: 174–188.
- Yanai, R. D., M. A. Vadeboncoeur, S. P. Hamburg, M. A. Arthur, C. B. Fuss, P. M. Groffman, T. G. Siccama, and C. T. Driscoll. 2013. From missing source to missing sink: Long-term changes in the nitrogen budget of a northern hardwood forest. *Environmental Science and Technology*, 47: 11440–11448.
- Zhang, J., P. Tian, J. Tang, L. Yuan, Y. Ke, Z. Cai, B. Zhu, and C. Müller. 2016. The characteristics of soil N transformations regulate the composition of hydrologic N export from terrestrial ecosystem. *Journal of Geophysical Research Biogeosciences*, 121: 1409–1419.

## Chapter 5: Conclusions

Fate and transport of  $\text{NO}_3^-$  in the environment is a major component of global change. Global-scale environmental conditions (e.g., atmospheric deposition of  $\text{NO}_3^-$ , climate, pest outbreak) are forecast to change significantly and that may impact how a forest ecosystem functions as a  $\text{NO}_3^-$  sink or source. Decades-long collection of stream water quality, soils, and biometric data has yielded a suitable record for many researchers to begin updating standard conceptual models of  $\text{NO}_3^-$  cycling in forest ecosystems. However, the relative importance and timing of  $\text{NO}_3^-$  cycling processes are not well understood because few studies have experimentally tracked them all the way from the uplands to the stream. This dissertation is a novel investigation of such  $\text{NO}_3^-$  transport and reaction processes at the hillslope scale. Studying  $\text{NO}_3^-$  processing along a hillslope is necessary because the hillslope, unlike the plot or core scale, reflects net effects of spatial and temporal variability in  $\text{NO}_3^-$  transport (flow-generation) and reaction processes, and headwater forested watersheds are generally comprised of hillslopes. The overarching aim of this dissertation was to answer the question: *What is the fate of a pulse of  $\text{NO}_3^-$  introduced on a hillslope?* In order to answer this question, I conducted two field experiments on an experimental hillslope soil model to elucidate processes that move water and process  $\text{NO}_3^-$ .

In Chapter 2, I repeated the soil drainage experiment that was first done by Hewlett and Hibbert (1963). I expected that 53 years of tree growth, litterfall inputs and processing, invertebrate burrowing, and associated pedogenic processes would substantially alter drainage from Hewlett and Hibbert's 1963 inclined soil model. I found significant changes to soil properties, including horizonation, development of an organic layer, and conversion from mostly sand to mostly silt, though two repetitions of the Hewlett and Hibbert drainage experiment revealed no significant

changes in the recession curve for the first 10 days. However, the long, slow drainage after that could not be reproduced. My data suggested a leak was created in the boundary conditions of the soil model. This leak was analogous to soil leakage into bedrock fractures and had the largest impact on the duration of drainage, reducing it by nearly an order of magnitude in our experiments compared to the original. This suggests that leakage to bedrock, which is common in many natural hillslopes, could have larger impacts on drainage in between precipitation events, rather than immediately after an event. My results further support the Variable Source Area paradigm because late recession flow still reaches the stream, but at different timescales depending on the route taken by water. Flow through bedrock may be a more important term in a water balance if drought frequency and duration increase.

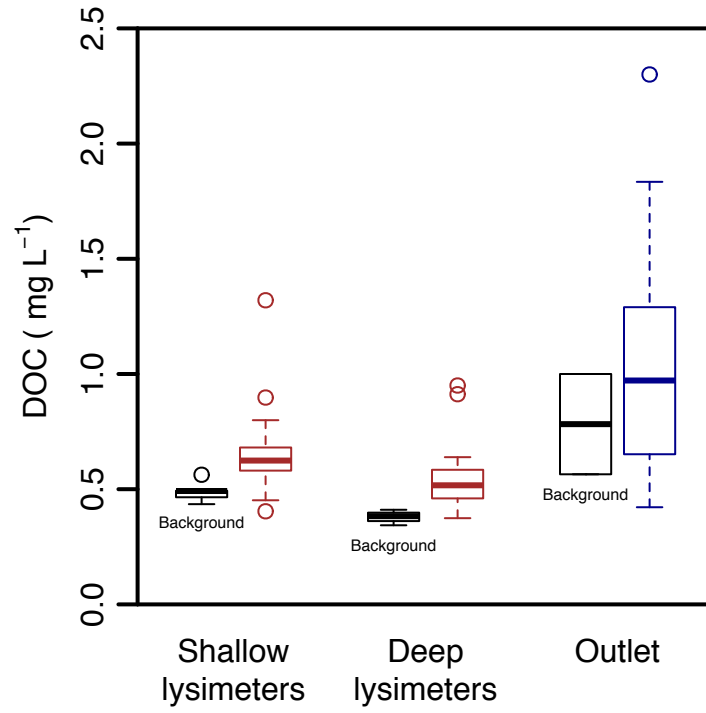
In Chapter 3, I aimed to answer several questions about competing processes that impact fate and transport of  $\text{NO}_3^-$ . What is the timing of a conservative tracer moving through the hillslope? Is there a delay in movement of a  $\text{NO}_3^-$  tracer compared to the conservative tracer? Where and why does it occur? What roles do nitrification and denitrification play? I added a pulse of isotopically labeled  $^{15}\text{NO}_3^-$  and water ( $^2\text{H}$ ) to a hillslope and the portion of  $^{15}\text{NO}_3^-$  that passed through a highly retentive, biologically active soil surface layer was still subjected to retention/removal mechanisms in mineral soil. There was an increasing lag in breakthrough of  $^{15}\text{NO}_3^-$  relative to  $^2\text{H}$  as the  $^{15}\text{NO}_3^-$  traveled down a hillslope irrigated at hydrologic steady state. I estimated mass balances of  $\text{NO}_3^-$ -N over the study period (141 d) in the saturated riparian zone and found that a significant flux of  $\text{NO}_3^-$  was generated by nitrification processes, while a flux nearly the same size was removed through denitrification processes. This suggested high flux rates (more than 5 times larger than lateral transport into or out of the riparian zone) and rapid microbial cycling of  $\text{NO}_3^-$ , resulting in a short residence time. I concluded that a conceptual model of  $\text{NO}_3^-$  retention

and transport must account for the potential of such rapid cycling along the hillslope, especially if there is a large and persistent saturated zone that creates conditions suitable for high microbial activity.

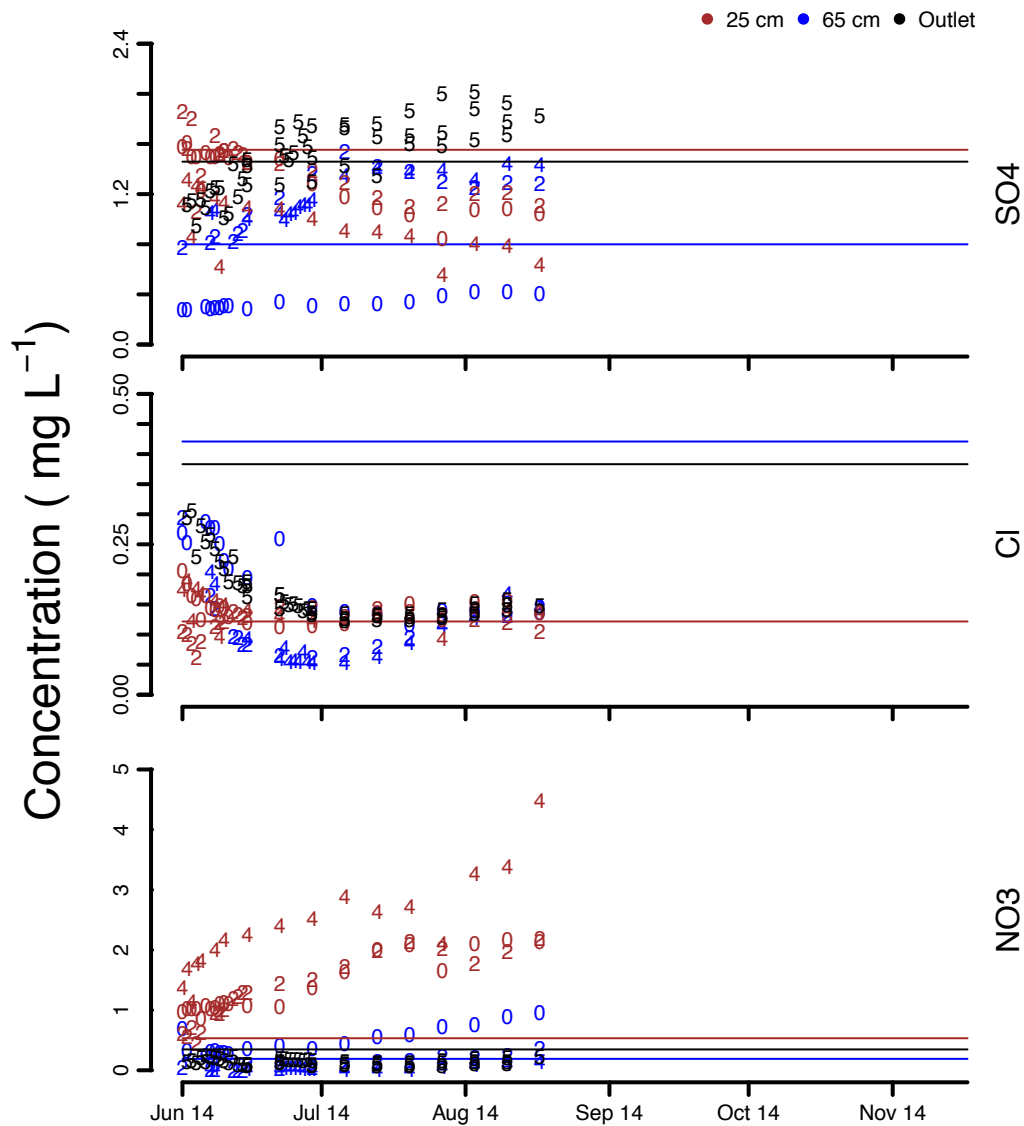
In Chapter 4, I aimed to answer the following research questions: Where (e.g., litter, soil, outflow) is the added  $^{15}\text{NO}_3^-$  tracer recovered? What is the timing and quantity of export of the pulse of  $^{15}\text{NO}_3^-$  added on a hillslope? What implications does this have for  $\text{NO}_3^-$  export at the watershed scale? I presented additional data from the dual tracer ( $^{15}\text{NO}_3^-$  and  $^2\text{H}$ ) experiment, including the mass balance and solid-phase recovery of the  $^{15}\text{NO}_3^-$  tracer. The soil microbial community at the surface soil and litter horizons in a devegetated hillslope, without influence from roots, could retain  $\text{NO}_3^-$  inputs at rates similar to other systems that contain plants because of a highly active soil microbial community. Of the  $^{15}\text{NO}_3^-$  tracer that passed through this retentive soil layer, there was a significant lag in breakthrough relative to the  $^2\text{H}$  tracer across a relatively short hillslope distance. I conjectured that this lag would be extended considerably for a longer, more typical hillslope length. The  $\delta^{15}\text{N}$  peaked in outflow 46 d after moving 5 m downslope of the tracer addition. Therefore, it would require roughly 1,130 d to travel the distance of a typical hillslope (120 m) in the basin, assuming roughly 1-D slope transport and similar retention rates observed in this study. Although, considering that half of the tracer mass exited much later (after 108 d) than when  $\delta^{15}\text{N}$  peaked, the travel time of  $\text{NO}_3^-$  may be over 2,600 d (7 y). These results may help explain delayed export of  $\text{NO}_3^-$  from watersheds that have increased availability of  $\text{NO}_3^-$  in hillslope soils but no concomitant export in stream water.

Together, the studies presented in this dissertation add to our understanding of the timing and quantity of moving water and solutes in forested hillslopes and watersheds. They also shed light on possible impacts from forecast increased climate variability and anthropogenic loading of  $\text{NO}_3^-$ .

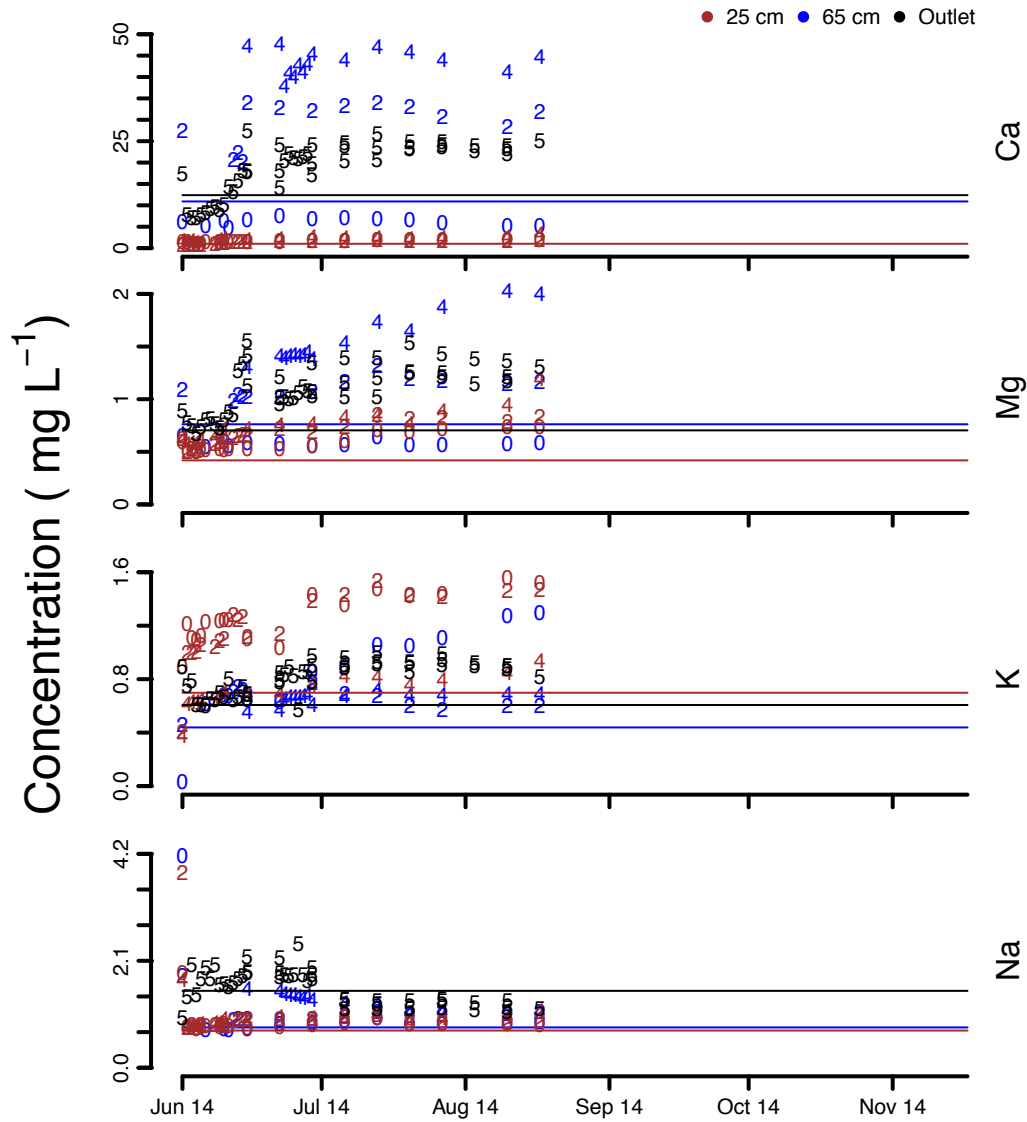




Appendix A2. Boxplots of DOC for shallow and deep soil lysimeters (brown) and outflow (blue). Background concentrations are in black.



Appendix A3. Timeseries of anion concentrations at lysimeters and outlet. Numbers indicate the downslope distance (m) away from the tracer addition; “5” indicates the outlet. Samples are color-coded by depth (i.e., shallow lysimeters at 25 cm depth, deep lysimeters at 65 cm depth, and outlet). A colored band shows the range of background concentrations taken before the tracer addition; the colored line inside the band indicates the median concentration.



Appendix A4. Timeseries of cation concentrations at lysimeters and outlet. Numbers indicate the downslope distance (m) away from the tracer addition; “5” indicates the outlet. Samples are color-coded by depth (i.e., shallow lysimeters at 25 cm depth, deep lysimeters at 65 cm depth, and outlet). A colored band shows the range of background concentrations taken before the tracer addition; the colored line inside the band indicates the median concentration.